Thèse de doctorat

de l'Université Sorbonne Paris Cité

Préparée à l'Université Paris Diderot

Ecole doctorale BioSPC (562)

Institut Jacques MONOD-UMR

Equipe Nanomanipulation de biomolécules

Dissecting enzymatic features of Reverse Gyrase and hyperthermophilic Topoisomerase III through a single-molecule perspective

Par Xi YANG

Thèse de doctorat de Biologie Moléculaire et Biophysique

Dirigée par Marc NADAL

Présentée et soutenue publiquement à Paris le 12 septembre 2019

Président du jury : Dr POMMIER, Yves, NCI-NIH Bethesda, USA

Rapporteurs : Dr BENSIMON, David, ENS, Paris

Rapporteurs : Pr RIOU, Jean-François, MNHN, Paris

Examinateurs : Dr LAMOUR Valérie, Université de Strasbourg, Strasbourg

Directeur de thèse : Pr NADAL Marc, Université Paris-Diderot, Paris

Membre invité : Pr STRICK, Terence, ENS, Paris

Titre : Analyse des caractéristiques enzymatique de la reverse gyrase et d'une topoisomerase III hyperthermophile en molecule unique.

Résumé :

Les ADN topoisomerérases sont des enzymes présentent chez tous les organismes vivant et elles résolvent les problèmes topologique de l'ADN grâce à des réactions de clivage et de religation. Ces enzymes ubiquitaires jouent un rôle essentiel dans de nombreux processus du métabolisme de l'ADN tel que la réplication et la reparation de l'ADN, la transcription, la recombinaison, la séparation des chromatides et la stabilité des génomes. Les topoisomérases sont classées en famille de type I et de type II selon leur structure et leur méchanisme. Parmi les topoisomérases de type I, une sous-famille a une structure en forme de cadenas et une reaction fondamentale de passage de brin qui supprime les surenroulement négatif un par un. Elles sont divisées en trois groupes : les Topo I, les Topo III et les reverse gyrase (RG). Les TopoI sont très efficace pour relaché les ADN sous-enroulés alors que les Topo III sont plus apte à traiter les problèmes de caténation de l'ADN. La reverse gyrase est une enzyme chimérique composé d'une hélicase de type RecQ et d'une Top IA. L'interaction helicase–topoisomérase confère à la reverse gyrase une nouvelle fonctionnalité lui permettant d'augmenter l'enchevêtrement des deux brins d'ADN en s'opposant à la torsion. Nous avons effectué des expériences en molécule unique pour disséquer le mécanisme de RG2 (TopR2) de *Sulfolobus solfataricus* dont l'activité est strictement dépendante de la présence d'ATP. Nous avons observé que la fixation initiale de TopR2 génère une bulle d'ADN de 20 paires de base et que la fixation de l'ATP referme l'ADN sur 10 paires de base. L'hydrolyse d'ATP entraine ensuite le passage de brin d'ADN et la reformation de la bulle initiale d'ADN de 20 paires de base aboutissant à une augmentation de l'enchevêtrement des brins d'ADN de un. Nous avons également décrit une caractéristique unique de TopA de *S. solfataricus*, une Topo III hyperthermophile. Cette enzyme peut séparer efficacement des caténanes fermés covalement et cette activité tire parti de la présence de régions d'ADN simple brin qui est favorisée haute température et qui peut être également stabilisée par des protéines liant l'ADN simple brin.

Mots clefs :

Topoisomérase, reverse gyrase, hélicase, pinces magnétiques, topologie de l'ADN, surenroulement de l'ADN, hyperthermophile, archée, étude en molécule unique.

Title: Dissecting enzymatic features of Reverse Gyrase and hyperthermophilic Topoisomerase III through a single-molecule perspective

Abstract :

DNA topoisomerases are present among all the living organisms and they resolve DNA topological problems through strand cleavage and re-ligation reactions. These ubiquitous enzymes play crucial roles in plenty of processes of DNA metabolism such as DNA replication and repair, transcription, recombination and chromatid segregation. Topoisomerases are categorized into type I and type II families concerning their differences in protein structure and mechanism. Among type I topoisomerases, Top IA sub-family enzymes share a padlock shape and a strand-passage core reaction which removes DNA negative supercoils one by one. They are subdivided into three groups: Topo I, Topo III and reverse gyrase (RG). Topo I is efficient at relaxing underwound DNA while Topo III is more adept at dealing with DNA catenation issues. RG is a chimera composed of a RecQ-like helicase and a Top IA. The helicase-topoisomerase interplay provides new functionality to RG which allows it to increase DNA linking number against torque. We applied single-molecule experimentation to dissect the mechanism of a *Sulfolobus solfataricus* RG (TopR2) which catalysis is strictly dependent on the presence of ATP. We observed that the initial binding of TopR2 on DNA generates a 20 base pair DNA bubble and ATP binding rewinds about 10 base pair within the bubble. The following ATP hydrolysis leads to DNA strand-passage and reforming of the initial 20 base pair DNA bubble, resulting in one unit increase of DNA linking number. We also describe the unique functionality of *S. solfataricus* TopA, a hyperthermophilic Topo III, to efficiently unlink covalently closed DNA catenanes. This activity is found benefited from the single-strand DNA region generated with high thermal energy and also promoted by single-strand DNA binding proteins.

Keywords:

Topoisomerase, reverse gyrase, helicase, magnetic tweezers, DNA topology, DNA supercoiling, hyperthermophile, archaea, single-molecule study.

Contents

Introduction

1. DNA—Structural and Topological Basics

It has been 150 years since the first discovery of the deoxyribonucleic acid (DNA) by Friedrich Miescher, a Swiss physiological chemist, who extracted this new substance from human white blood cells. The definition of this new cellular component had been given extensive attention for the next several decades, which went through Phoebus Levene's "polynucleotide" model, Chargaff's rule “A = T and C = G,” the X-ray structure by Rosalind Franklin and Maurice Wilkins, and the milestone proposal of the double-helix model by Watson and Crick (Pray, 2008). Great discoveries had been made in the follow-up studies of this genetic material which allow us to systematically describe its structure and functionality.

1.1 Major Primary Conformations of DNA

The structural feature of a DNA molecule is commonly known as two complementary polynucleotides intertwining each other, generating a double helix with hydrogen bonds formed via pairing of nitrogen-containing nucleobases between two polymer chains. The conformation of a double-stranded DNA molecule varies depending on its surrounding physical environment (ex. ionic and hydration conditions), DNA sequence, and interaction with other macromolecules. Three major acknowledged conformations are A-DNA, B-DNA, and Z-DNA.

B-DNA is the most typical right-handed DNA double helical conformation proposed by Watson and Crick (Fig 1, middle). Under the standard condition, a single helical turn of B-DNA comprises 10.4-10.5 base pairs with a diameter of 2 nm and it extends 3.4 nm along its helix-axis (Mirkin, 2001).

Compared with B-DNA, A-DNA is shorter and wider (Fig 1, left), with a larger number (~11) of base pairs per helical turn and a tilted base-pair plane instead of perpendicular to the helix axis. B-DNA tends to transform into A-DNA during

dehydration (Arnott & Hukins, 1972; Langridge *et al.*, 1960) and this transformation is also influenced by DNA sequences as it is found favored by certain stretches of purines (GAGGGA) (Mirkin, 2001). Additionally, the structure of DNA-RNA hybrids is reported to resemble an A-DNA conformation which can form during biological processes such as replication and transcription (Suresh & Priyakumar, 2014).

Z-DNA is a left-handed double helix and the narrowest (1.8 nm in diameter) among all three types (Fig 1, right). It contains 12 base pairs (6 dimers) in each helical turn (Wang, 1979). Z-DNA is formed with alternating purine-pyrimidine sequences. Its formation is favored in high salt solutions or coexists with divalent cations (Berg *et al.*, 2002).

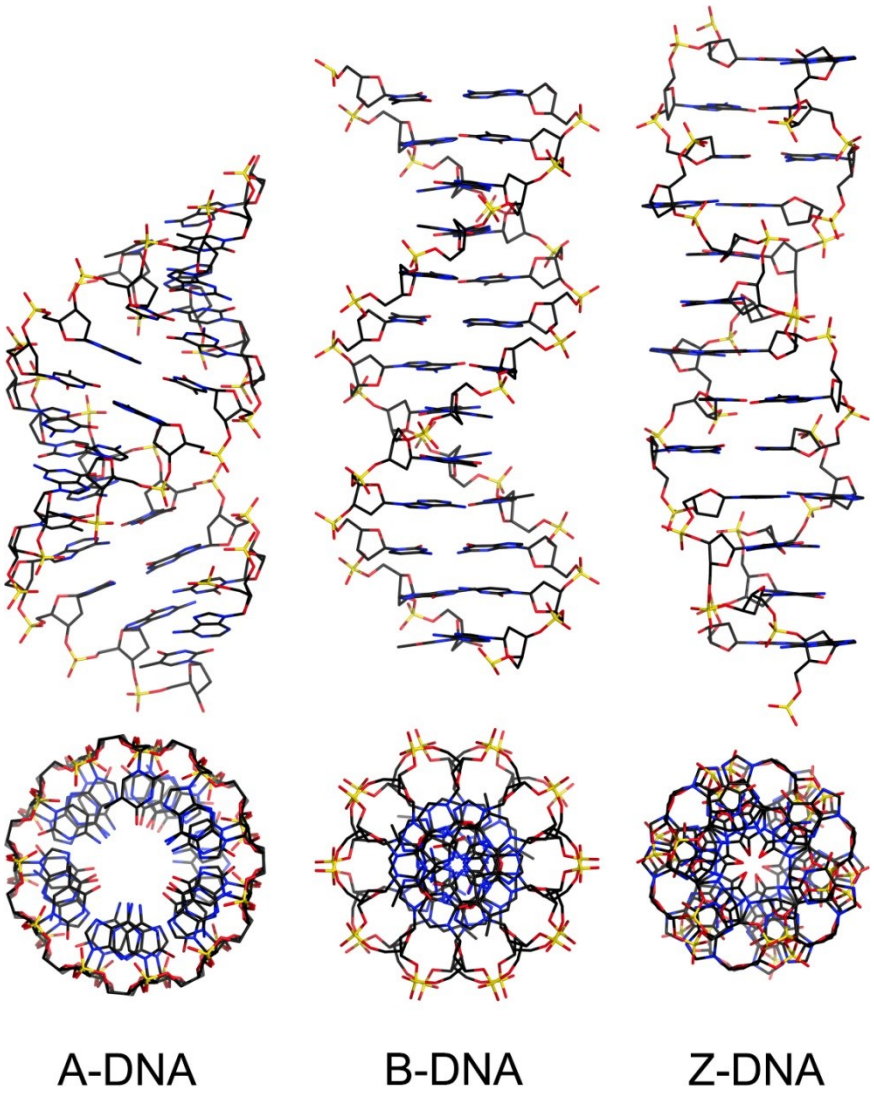

Figure 1. Models of three major conformation of double-strand DNA. From left to right: A-, B- and C-form DNA. Top views are presented below the side views (image by Mauroesguerroto, from Association of Inclusionist Wikipedians).

1.2 Topology of DNA

Despite its delicate primary double-helix structure discussed above, the overall geometry of a long DNA molecule can be treated as a semi-flexible polymer and modeled as a worm-like chain (Marko *et al.*, 1994). An ideal relaxed linear DNA in solution exhibits a simplest B-DNA form which minimize its free energy. In reality, deformations such as bending, twisting and compression create diversity in the geometric shape of DNA. In order to characterize these features, topological terms such as supercoiling, knot and link (catenane), had been introduced to study the morphology and dynamics of DNA.

1.2.1 DNA as a topological ribbon: linking number and supercoiling

A long DNA molecule *in vivo* is often constrained by multiple proteins such like histones or histone-like proteins and appears as a circular (covalently closed) form with a curved helical axis (Vos *et al.*, 2011). A DNA segment in these scenarios is defined as a DNA topological domain, without free rotation ends. In topology, the Linking number (Lk) is used to describe two parallel edges of a topological ribbon twisting around each other in three-dimensional space. When treating the two DNA backbones as the ribbon edges, DNA Lk is used to define a DNA topological domain as the number of times one DNA twin backbone winds around the other (Buck, 2009). Two geometric variables, twist (Tw) and Writhe (Wr), are also introduced to combine DNA geometry to DNA topology. Tw is the number of DNA helical turns and it describes the tightness of the two backbones wrap around each other in 3D space. Wr is the amount of coiling of the DNA double helix winding around itself (Mirkin, 2001).

The Lk of a circular DNA or a torsionally constrained linear DNA stays unchanged without strand breakage, while the values of Tw and Wr compensate each other and their sum remains constant according to the equation below (Bauer & Vinograd, 1968; Fuller, 1978; White & Bauer, 1987):

$$L_{\mathrm{k}} = T_{\mathrm{w}} + W_{\mathrm{r}}$$

For a relaxed DNA topological domain (10.5 base pairs per turn), Lk = Tw. Torsional energy on DNA generated upon strand twisting tends to convert to bending energy and is observed as DNA buckling. This structural transition is chiral:

When Lk > Tw (Wr > 0), the DNA molecule is positively supercoiled, with a right-handed torque on the DNA which causes left-handed double-strand plectonemes; When Lk < Tw (Wr < 0), the DNA molecule is negatively supercoiled and forms right-handed double-strand plectonemes (Mirkin, 2001).

In vivo, DNA supercoiling can be generated by protein complexes during genome replication, recombination and gene transcription (Vos *et al.*, 2011).

1.2.2 DNA Knots and Catenanes

Except supercoiling, DNA catenanes and knots have also been found existing in the biological system, often as intermediates or by-products during genome transactions and packaging. A covalently closed DNA molecule is defined knotted when it cannot be transformed into a simple circle through continuous deformation (without cleavage and resealing). If similar entanglement occurred between multiple DNA molecules, the interlocked DNA nanostructure is called a catenane (Witz, 2009). DNA knots and catenanes are frequently generated through cellular events and usually affect to genome stability and transactions. They can be efficiently removed by special enzymes called DNA topoisomerases, which are discussed in the next section.

2. DNA Topoisomerases

2.1 Definition and Classification

Topoisomerases are enzymes capable of modifying DNA topology, through DNA strand cleavage, shuffling and re-ligation. They all share a conserved nucleophilic tyrosine in their active centers to perform a transesterification reaction, in which the Tyrosine residue acts as a nucleophile and attacks the phosphodiester bond on the DNA backbone (Wang, 1971). It generates a covalent 5' or 3' phosphor-tyrosyl bond (Fig. 2.1) depending on the type of enzyme. This transient DNA break allows further topological modifications on the DNA substrate and these modifications are finally locked by DNA re-ligation which reforms the broken phosphodiester bond.

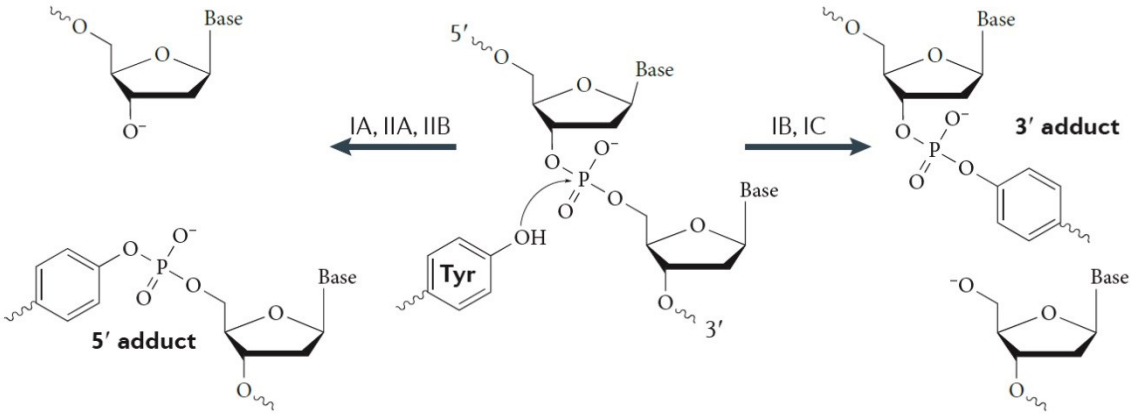

Figure 2.1. DNA cleavage reaction by topoisomerases. Nucleophilic attack by the catalytic tyrosine (middle) of top IA, IIA and IIB generates a 5' phosphor-tyrosyl bond which covalently links the enzyme and DNA (left). Nucleophilic attack by top IB and top IC forms a 3' phosphor-tyrosyl bond on the DNA (right) (Vos *et al.*, 2011).

Topoisomerases are classified into two major families, type I and type II, according to their difference in DNA strand-cleavage strategy. Type I topoisomerases cleave a single strand on a DNA duplex while type II enzymes cleave both strands. Further classifications are also applied for both of these two categories concerning their diversities in protein sequence, 3-D structure, and detailed mechanisms (Vos *et al.*, 2011).

2.1.1 Type I topoisomerases

Type I family is divided into three sub-families: Type IA, IB, and IC. Type IA topoisomerases with a padlock shape are known for their “strand passage” mechanism during supercoiling activity, in which the enzymes cleave one DNA single-strand and pass the second strand through the gap before resealing the broken strand (Fig 2.2a), thus remove one negative DNA supercoil at a time (Dekker *et al*., 2002). Further segmentation divides type IA sub-family into three groups concerning their differences in structure and functionality: topo I (in bacteria), topo III (in bacteria, archaea and eukaryote) and reverse gyrase (in bacteria and archaea) (Garnier *et al.*, 2018).

Type IB topoisomerases differ from type IA in their core mechanism of supercoil removal. After strand-cleavage, the cleaved end of the broken DNA single strand rotates around its intact counterpart to release the topological tension (Koster *et al.*, 2005) and the friction within the DNA-protein complex controls the rate of rotation (Fig 2.2b). Thus they are also called ”swivelases”. These enzymes can relax positive as well as negative DNA supercoils using the torsional energy stored in their DNA substrates (Vos *et al.*, 2011).

Type IC topoisomerase has only have been found in one archaea and is named Topo V. Although they share a similar DNA strand rotation mechanism and relaxation activity with Type IB, comparison of these two types show little structural resemblance in their active sites (Taneja *et al.*, 2006)

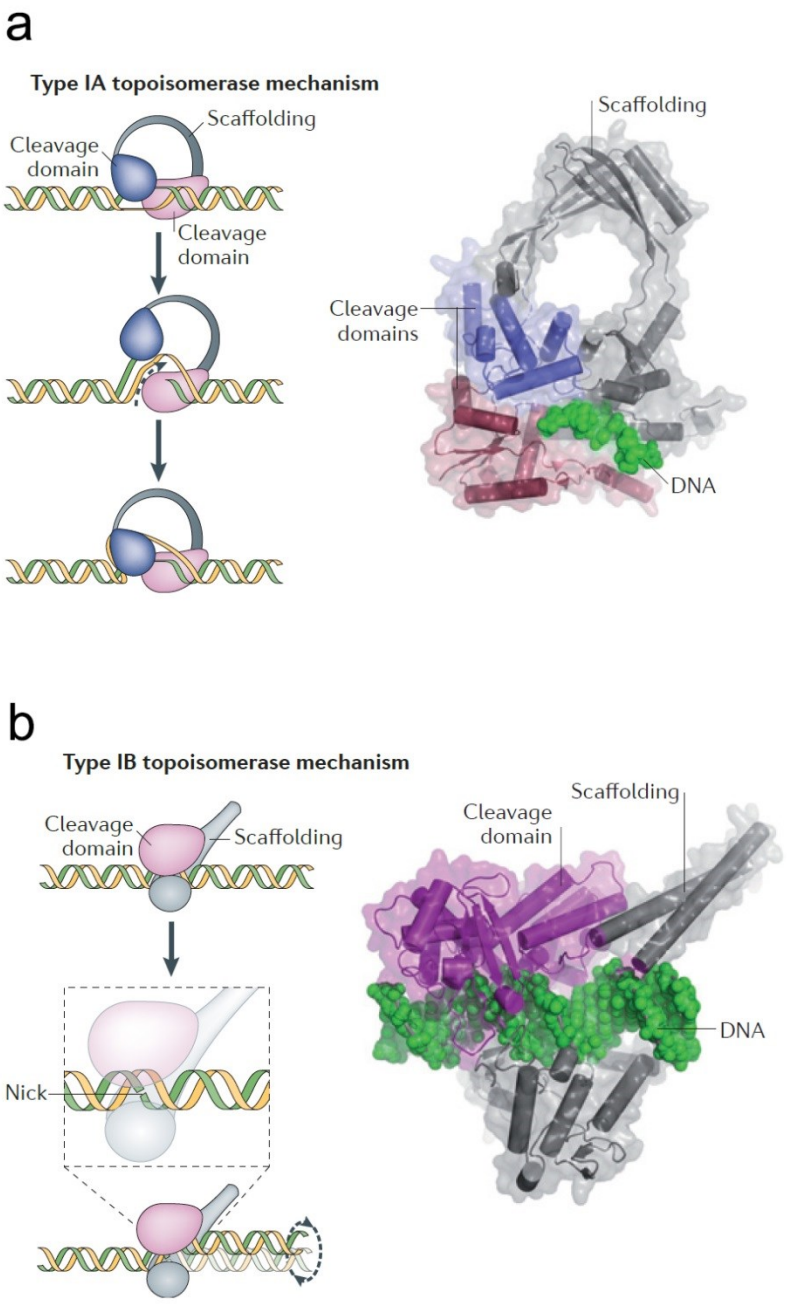

Figure 2.2. Mechanisms of type IA and type IB DNA topoisomerases. (a) Strand-passage reaction of type IA enzymes. Top IA cleaves one DNA strand (shown in green) and passes the other strand (yellow) through the broken gap. 3-D structure of *E. coli* topo III bound with ssDNA is shown on the right. (b) Mechanism of type IB DNA relaxation. Top IB releases DNA topological tension via rotating the intact DNA strand (yellow) after the cleavage of one DNA strand (green). The protein structure on the right represents a human topo IB bound with a DNA duplex (Vos *et al.*, 2011).

2.1.2 Type II topoisomerases

All the type II enzymes share a similar DNA cleavage site with topo IA, while they cut and re-ligate a DNA duplex rather than single-strand DNA. The type II topoisomerases catalysis requires energy from nucleotide hydrolysis. Type II family is divided into two sub-families: Type IIA and type IIB. During a typical type IIA reaction cycle, the enzyme wraps its DNA substrate around the C-terminal domains (CTDs) and then introduces a DNA double-strand break to one of the crossing DNA duplexes (G-segment). The enzyme then passes the adjacent DNA duplex (T-segment) through the gate on the G-segment before resealing the latter (Fig 2.3a) (Basu *et al.*, 2012; Gubaev & Klostermeier, 2014; Papillon *et al.*, 2013; Lamour *et al.*, 2002). Sub-families of type IIA topoisomerases include gyrase (in bacteria and archaea), topo II (in eukaryotes) and topo IV (in bacteria) (Vos *et al.*, 2011). In terms of functionality, these three sub-families share a common DNA break-resealing mechanism but differ in cellular responsibility. For example, gyrase is efficient at both relaxing DNA positive supercoils and introducing negative but hardly capable of resolving DNA catenation (Zechiedrich & Cozzarelli, 1995); By comparison, Topo IV enzymes are proficient decatenases (Charvin, *et al.*, 2003) and can also remove DNA supercoils (Bergerat *et al.*, 1994).

Type IIB topoisomerases, the other type II sub-family, include topo VI and a newly classified topo VIII. They share similar ATPase and DNA cleavage sites with type IIA family while varies in protein sequence and overall structure (Fig 2.3b). These sub-families also participate in DNA decatenation and supercoil removal using DNA double-strand break and strand-passage mechanism while details remain to be discovered (Wendorff & Berger, 2018; Gadelle *et al.*, 2014).

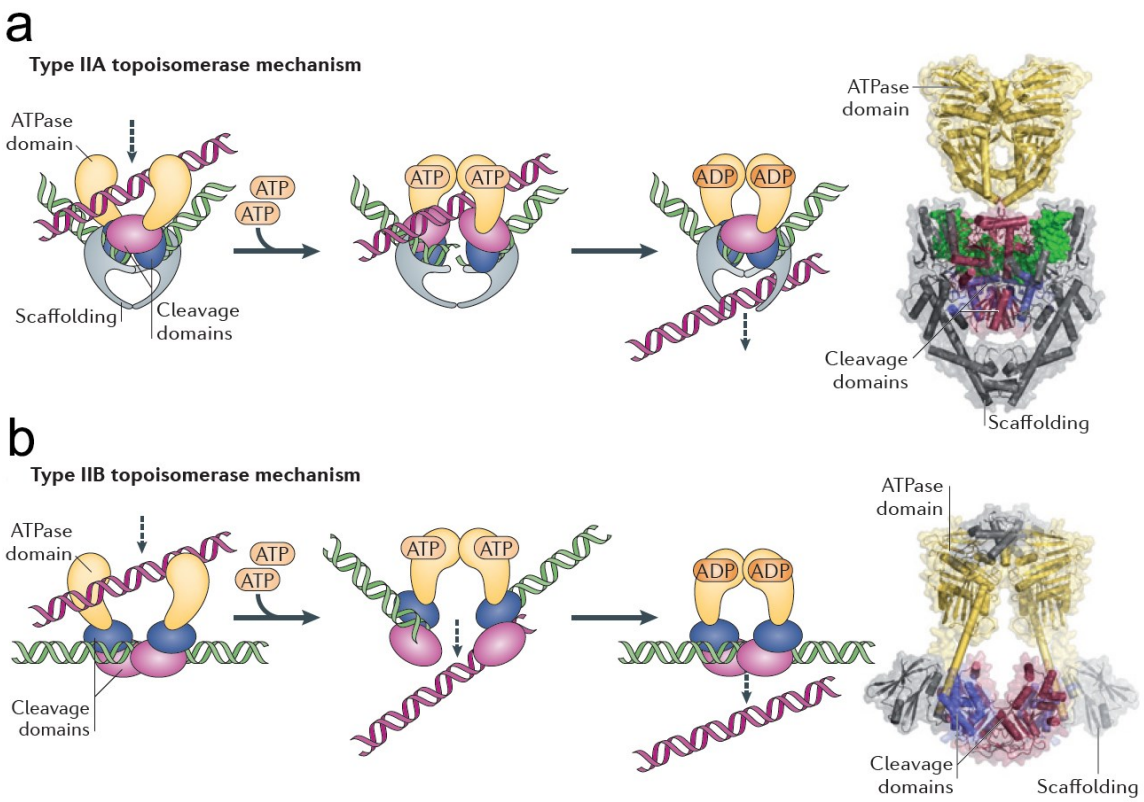

Figure 2.3. Mechanisms type IIA and type IIB DNA topoisomerases. (a) DNA strand passage of type IIA enzymes. Top IIA cleaves both strands on a DNA duplex (green) and pass an intact double strand (pink) through the broken ends. Strand passage requires ATP hydrolysis. The structure on the right shows the ATPase and DNA cleavage domains of the *Saccharomyces cerevisiae* topo II. (b) Similar DNA duplex strand passage mechanism of type IIB enzymes (left) and the protein structure of *Methanosarcina mazei* topo VI (Vos *et al.*, 2011).

2.2 Biological Roles of DNA Topoisomerases

DNA topoisomerases play crucial roles in all living cells, participating in many biological processes such as chromatin compaction, DNA replication, transcription, and recombination. Due to their presence, problems caused by DNA entanglements can be resolved to maintain a stable and functional genome.

2.2.1 Chromosome Organization and Participation of Topoisomerases

In eukaryotes, the lowest level of genome packaging includes an ~147 bp of DNA double helix wrapping around a histone octamer with ~1.8 left-handed turns, forming

a nucleosome core particle and introducing about -1 unit change of DNA linking number within this constrained region (Corless & Gilbert, 2016 & 2017). This change of DNA topology can be transmitted to the histone-free DNA linkers between each two core particles and assists the formation of higher-level DNA structures. Further packaging contains the alignment of the nucleosome-level structure and then compressing this nucleosome array to solenoid coils and loop structures until forming a more compacted chromosome during interphase, and ultimately a metaphase/anaphase chromosome before cell division (Kschonsak & Haering, 2015). During chromosome compaction and cell division in mitosis and meiosis, structural maintenance of chromosomes (SMC) complexes play important roles by providing topological constraints between two or more DNA strands, regulating various chromosomal activities such as chromosome condensation, sister chromatid cohesion and segregation. These are ATP-driven machineries conserved in both eukaryotic and prokaryotic, including condensin, cohesion, and SMC5–SMC6 complex (Uhlmann, 2016).

Unlike eukaryotes, bacteria usually lack histones to wrap DNA during chromosomal DNA packaging and their genome condensing highly depends on DNA supercoiling (mostly negative supercoiling). In *E. coli*, several protein families participate in this process to maintain supercoiled DNA and facilitate the formations of higher-level architectures (Griswold, 2008), such as H-NS (histone-like nucleoid-structuring protein), HU (histone-like protein) and IHF (integration host factor) (Shindo *et al.*, 1995; Johnson *et al.*, 2005).

Topoisomerases are found participating in the process of chromatin compaction by interacting with SMC complexes. As reported, Topo II α is immunolocalized with 13S condensing within a radially restricted scaffold during chromosome assembly (Maeshima & Laemmli, 2003). Moreover, direct interactions between SMCs and type II topoisomerases like TOP2 (in *D.melanogaster*) and topo IV (in *E. coli*) have also been confirmed and both of these interactions induce these topoisomerases to relax negatively supercoiled DNA (Bhat *et al.*, 1996; Hayama & Marian, 2010). On the other hand, researchers discovered the enzymatic feature of yeast Top2 during mitosis in which positive supercoiling on the chromosome DNA (mimicked by catenated plasmid) promotes decatenation of Top2. This provides a proof for the importance of Topoisomerase II in chromatid segregation (Baxter *et al.*, 2011).

Genetic evidence also supports the involvement of topo II in chromosome formation, in which both topo II inactivation (Uemura, 1987) or deletion (Adachi, 1991) results in the failure of chromosome formation.

A second way involving topoisomerases to genome organization is to cooperate with cellular transaction proteins. During cellular activities involving the unwinding/rewinding of DNA all have the potential to modify the supercoiling level on the genome. One example is transcription, in which RNA polymerase generates DNA positive supercoils ahead of the transcription complex and negative supercoils behind (Liu & Wang, 1987) (see 2.2.2). Cooperation between topoisomerases and RNA polymerase are necessary to regulate the local/overall genome topology, leaving negative supercoils within the regulatory regions, and remove obstacles on the DNA during transcription elongation (Kouzine *et al.*, 2014).

2.2.2 Transcription and Role of Topoisomerases

Transcription requires RNA polymerases to transfer genetic information from chromosome DNA to messenger RNA. During this process, conformational changes occur within the RNA polymerase (RNAP)-DNA complex. For example, RNAP in *E. coli* initiates transcription by unwinding ~10 bp of promoter DNA. Multiple cycles of abortive short-RNA synthesis happen before RNAP successfully extends RNA to ~9-11 bp, after which the enzyme escapes the promotor region and enters the following elongation stage. It holds a ~9 bp transcription bubble during this productive RNA synthesis stage until the encounter of a terminator DNA sequence, which releases the polymerase from its template DNA, causing a rewinding of the transcription bubble (Howan *et al.*, 2014; Revyakin *et al.*, 2006).

When an RNAP is traversing through a template DNA coding sequence, the topology on the DNA can be dynamically reorganized when the genomic DNA and RNAP are not free to rotate in the intricate cellular environment (eg., when they are anchored on a stable cellular structure). In this case, RNAP continually unwinds DNA in front, generating positive supercoils ahead and leaving underwound DNA behind (known as the twin-supercoiled-domain model) (Liu & Wang, 1987; Wu *et al.*, 1988). The consequent torque-accumulation on the DNA increases the possibility of a pause during elongation. In eukaryotes, RNA polymerase II (Pol II) faces a similar pausing

situation after extending the nascent RNA to 9-10 nt. It often experiences a second pausing when the RNA transcripts reach 20-50 nt (Pol II pausing) and going further into the productive elongation requires pause release by positive transcription elongation factor b (P-TEFb) (Gaertner & Zeitlinger, 2014; Zhou *et al.*, 2012). Genome-wide detections show a frequent appearance of RNAP pausing throughout the transcription regions including both the promoter and ORP segment (Mayer *et al.*, 2017).

Except for the pausing risk induced by positive supercoiling which prevents the continuity of RNA synthesis, negative supercoils generated behind RNAP also increases the potential of forming RNA-DNA hybrids (R-loops) (Drolet *et al.*, 1994). Both of these supercoiling related obstacles affect global cellular activities and genome stability (Blot *et al.*, 2006).

Topoisomerases are powerful tools to debug DNA topological troubles during transcription. For example, in bacteria, topo IV and gyrase are reported to participate in the positive supercoil removal events (Zechiedrich *et al.*, 2000), while the R-loop formation is supposed to be inhibited by the Topo I recruited by *E. coli* RNAP due to the direct protein-protein interaction reported between them (Cheng *et al.*, 2003; Sordet *et al.*, 2010).

During RNA Pol II transcription initiation in human, the cleavage activity of TOP1 is required but not its supercoil removal activity, which can be explained by the remaining of DNA negative supercoils to enhance the double-strand melting at the promoter region (Merino *et al.*, 1993). However, TOP1's relaxing activity is essential for RNA Pol II pause release and this activity is activated by bromodomain-containing protein 4 (BRD4) mediated RNA Pol II phosphorylation (Baranello *et al.*, 2016). Researchers also found Top2 β activity during transcription initiation, as they observed the Top2 β introduced DNA double-strand break (DSB) at the promoter region in an estrogen-induced cell (Williamson & Lees-Miller, 2010). One of the reasons to utilize Top2 β instead of nuclease to introduce DSB might be the re-ligation activity of the former to avoid causing permanent DNA lesions after DNA nicking (Pommier *et al.*, 2016).

Topoisomerases are also indispensable during transcription elongation. For example, transcription of long genes in yeast is interrupted as a consequence of Top2

inactivation (Joshi *et al.*, 2012). And inhibition of human TOP1 using camptothecin or topotecan also reduces transcription elongation in cancer cells (Ljungman & Hanawalt, 1996). More recently, a single-molecule assay reviewed a reduced DNA relaxation rate of human Top IB upon binding topotecan, especially its activity to remove positive DNA supercoils. This inhibition effect of topotecan *in vivo* led to an accumulation of DNA positive supercoiling in yeast cells which was generated during transcription/replication (Koster *et al.*, 2007). R-loop formation is another challenge for transcription as well as genome stability, in which the nascent RNA hybridizes with the complementary DNA single strand (Aguilera, 2002). R-loops can be efficiently removed by RNases and RNA-DNA helicases, and their formations are also inhibited by topoisomerases (Santos-Pereira & Aguilera, 2015). For example, R-loop accumulates in yeast cells lacking Top1 and Top3 due to the reduced control of local DNA negative supercoils during transcription that facilitates the RNA-DNA hybridization (Pommier *et al.*, 2016). In human cells lack TOP1 activity, DNA breaks are found at transcriptionally active gene sequences and they can be suppressed by overexpression of RNase H (Sordet *et al.*, 2010).

2.2.3 Replication and Role of Topoisomerases

DNA replication is initiated by the assembly of the replication protein complex which causes an unwinding on the template DNA within the replication origin area, forming a replication fork. When the replication fork is elongating on the DNA template, helicases ahead unwinds DNA in front and the DNA polymerase performs semi-conservative DNA synthesis (Wang, 2009). Replication finishes when two replication forks approach each other, defined as fork convergence, leading to the disassembly of the replication complex (Dewar & Walter, 2017). Most replication termination processes in eukaryotic cells are believed to be sequence nonspecific, while replication in bacteria is arrested at a certain termination region (*Ter* sites in *E. coli*), where the termination factor *Tus* interrupts the progression of replicative helicase DnaB and ends replication (Valjavec-Gratian *et al.*, 2005).

Like in transcription, elongation of the replication fork causes the built-up of overwound DNA in front of the fork and generates underwound DNA behind the fork. This underwound region behind the fork can lead to the formation of pre-

catenane/catenane between the two replicated daughter DNA duplexes (Vos *et al.*, 2011; Pommier *et al.*, 2010). During termination, replication fork convergence generates high topological stress on the non-replicated DNA double strands between two converging forks which has to be removed to promote the completion of DNA synthesis. Details of this replication fork encounter and the mechanisms of replisome disassembly still need to be discovered in future studies (Dewar & Walter, 2017).

Both prokaryotes and eukaryotes require topoisomerases for their replication initiation. For example, *E. coli* topo IAs and gyrase perform a bidirectional regulation in supercoiling at the oriC region (Hiasa *et al.*, 1994; Kaguni & Korngerg, 1984). Replication initiation in eukaryotes includes activities of topoisomerases such as human topo IIα，topo IB and topo IIβ (Abdurashidova *et al.*, 2007; Yang *et al.*, 2000), although their certain responsibilities remain undefined. One possible reason for topoisomerases to participate in replication initiation is due to their capability to stop aberrant replication initiations, *e.g.*, starting at R-loop sites rather than replication origin sites (Pommier *et al.*, 2016).

During replication elongation, positive supercoils accumulated in front of the replisome require the activity of type II topoisomerases, *e.g.*, DNA gyrase in bacteria and topo IB in eukaryotes (Zechiedrich & Cozzarelli, 1995). On the other hand, pre-catenation behind the fork is also resolved by type II enzymes (Baxter & Diffley, 2008) together with topo III (Nurse *et al.*, 2003) to prevent daughter strands from abnormal segregation. During fork convergence, the unreplicated DNA duplex between the two converging replication forks goes through a hemicatenane stage. Studies have shown the participation of type IA enzymes in removing hemicatenane. For example, in eukaryotes, topo III is well known to cooperate with RecQ family helicases in resolving hemi-catenation, along with RecQ-mediated genome instability protein 1 (RMI 1) and RMI 2 (Vos *et al.*, 2011; Dewar & Walter, 2017). In human cells lack BLM helicase, ultrafine DNA bridges persist in anaphase and cause difficulty in sister-chromatid separation which is known as a Bloom's syndrome (Chan *et al.*, 2007).

Replication termination also requires topoisomerases. For example, absence of topo IAs in *E. coli* disrupts the ability of termination factor (*Tus*) to arrest replicative helicase (DnaB), possibly due to the accumulation of negative supercoils that

increases the DNA unwinding activity of DnaB at the termination site and decreases the *Tus*-DnaB interaction lifetime (Valjavec-Gratian *et al.*, 2005 ; Vos *et al.*, 2011).

2.2.4 DNA Recombination and Role of Topo III

Genetic recombination allows living organisms to exchange genomic information and generate diversity within their offspring. In eukaryotes, recombination commonly takes place during the pairing of homologous chromosomes in meiosis, with an elevated rate at genome regions called “hotspots”. A special enzyme named Spo11 is responsible for generating a DNA double-strand break (DSB), using the similar mechanism of Archaeal topo VI, and covalently links to the DNA with a tyrosine induced phosphodiester bond (Bergerat *et al.*, 1997). The DSB ends are then treated to ssDNA overhangs and captured by recombinases. These protein-coated DNA ends then invade their homologous DNA strands and go through a crossover or non-crossover pathway, depending on either one or two DSB ends involved in the invasion (Wright *et al.*, 2018; Brick *et al.*, 2018).

In the non-crossover pathway, ligation of two synthesized DNA single strands after strand invasion leads to the formation of a double Holiday junction (dHJ). Topo III is well known to dissolve double Holiday junctions (dHJs) through cooperation with RecQ helicase (Plank *et al.*, 2006; Wu & Hickson, 2003; Chen *et al.*, 2014). Details will be discussed in the next section.

3. Type IA Family Topoisomerases—Similarities and Diversities

Among all topoisomerases, only type IA family members are present in all living organisms. They share a general toroidal or padlock shape and a conserved enzyme core. They also present a common mechanism known as “strand passage” in DNA supercoiling modification. Nevertheless, members of this large family differ in protein sequence and biological function (Garnier *et al.*, 2018). They are thus divided into three sub-families—topo I, topo III and reverse gyrase—based on discoveries and current understandings of these enzymes.

3.1 Structure of Type IA Topoisomerases

3.1.1 Overall Structure of Classical Top IAs

The overall composition of a Top IA topoisomerase includes two parts: a conserved enzyme core and a variable C-terminal region. The enzyme core contains four (five for some members) conserved motifs which form a toroidal structure of all the Top IAs, also known as a padlock structure (Zhang *et al.*, 2011; Nadal, 2007).

Domain I, also named TOPRIM domain, contains three to five β-sheets inserted among α-helices and it belongs to the Rossmann fold super-secondary structure (Fig 3.1), commonly found in proteins interacting with nucleic acids. Conserved residues in domain I include ExxK (in motif 1) and DDE (in motif 3) (Fig 3.1) which face to the catalytic tyrosine (located in the domain III) in 3-D space. They are also involved in binding Mg(II), a crucial cation for the transesterification reaction (Garnier *et al.*, 2018).

The arch-shaped domain II is composed of two head-to-tail folds and is named Topo fold (Fig 3.1). It joins domain III and IV together, forming a toroidal structure as a whole (Fig 3.1). The inner surface of the toroid is covered with positively charged amino acid residues, giving it potential to trap a polynucleotide chain. As only hydrogen bonds but no direct covalent constraint existing between domain III and domain I or IV, the toroidal structure has the freedom to open like a gate (Viard & de la Tour, 2007). This gate-opening has been observed in a single-molecule

experiment, in which the enzyme holds two single-strand DNA ends after DNA cleavage and the conformational change related to gate opening generates a 6.6 nm gate within the enzyme (Mills *et al.*, 2018). A flexible peptide linking domain II and domain IV together (called hinge II-IV) is suggested critical to the switch between gate-closing and gate-opening states (Garnier *et al.*, 2018).

The C-terminal region of type IA topoisomerases is variable throughout the family and it often contains one or multiple Zinc-binding folds such as 4-Cys zinc ribbon domains. While this part is missing in the reverse gyrase sub-family and also absent for some of the classical top IAs (Nadal, 2007). Zn(II) ions were found present in the Zinc-binding motifs of *E. coli* topoisomerase I. Either removal of these Zn(II) ions or substitution of the Zinc-binding cysteine residue affects the ability of the enzyme to remove negative DNA supercoils (Tan *et al.*, 2015).

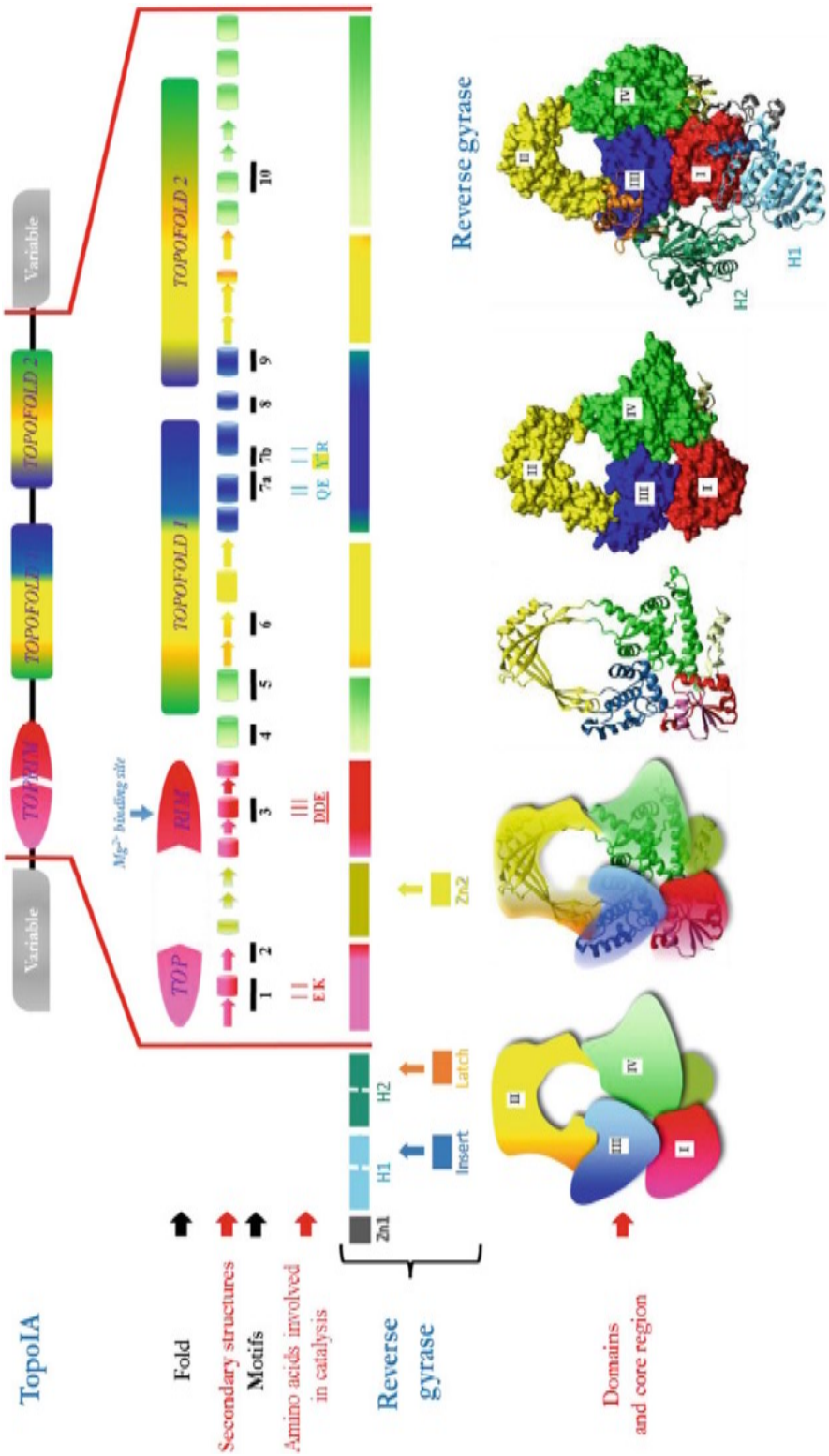
TopoIA
Fold
Secondary structures
Motifs
Amino acids involved in catalysis
Reverse gyrase
Domains and core region
Variable
TOPRIM
TOPOFOLD 1
TOPOFOLD 2
Variable
TOP
RIM
TOPOFOLD 1
TOPOFOLD 2
Mg2+ binding site
EK
DDE
QE
YGR
Zn1
H1
H2
Insert
Latch
Zn2
Reverse gyrase
H1
H2

Fig 3.1 Overall perspective of type IA domain architecture and 3-D structures.

Top row: Schematic representation of an overall top IA domain structure. Conserved domains of the enzyme core are color coded. N- and C- terminal variable domains are painted with neutral gray. Middle-upper row: domain architecture of the top IA enzyme core with detailed motif information. Functional protein motifs are numbered down below. Reserved residues for catalysis are labeled and the catalytic tyrosine is highlighted in yellow and marked with "*". Middle-lower row: alignment of the structure of reverse gyrase. N-terminal insertions and a Zn2 motif located in the Toprim domain are indicated below. Bottom row: presentation of four 3-D structures of *E. coli* top IA (PDB ID: 3PX7) in different display models on the left and the structure of *T. maritima* reverse gyrase on the right (PDB ID: 4DDU). Domain I-IV are labeled with Roman numerals (Garnier *et al.*, 2018).

3.1.2 Structure of Reverse Gyrase, A Special Top IA Family Member

Among the type IA topoisomerase family, hyperthermophilic reverse gyrase (RG) is a special family member. It has been initially found in hyperthermophilic and later in thermophilic Archaea and Bacteria, crucial for the survival of species living in extremely hot environments. RG is a chimera which comprises a C-terminal domain belonging to a classical type IA topoisomerase and an N-terminal part related to the RecQ family helicases (Super Family 2 group) (Nadal, 2007; Perugino *et al.*, 2009). Crystallographical analyses have attained structures of RG in *A. fulgidus* (*Afu*) and *T. maritima* (*Tma*) (Rodríguez & Stock, 2002; Rudolph *et al.*,2013).

Like a typical SF2 helicase, the N-terminal unit of RG consists of two RecA fold, named H1 and H2, and each of them harbors a variable insertion (Fig 3.2a). The architecture of H1 insertion varies throughout the family, with a β-hairpin in *Afu* RG and a helix-loop in *Tma* RG. The H2 domain insertion is called the latch domain, which length varies from 10 to 120 residues. The latch domains of *Afu* and *Tma* RGs each forms an independent protein folding within the H2 domain and communicates with the topoisomerase segment (Lulchev *et al.*, 2014).

Although sharing little similarity in length and protein sequence, removal of these latch domains leads to significant functional defects, *e.g.*, decrease of their DNA binding affinity at all the ATP hydrolysis states, disability of DNA unwinding and loss

of positive supercoiling activity (Ganguly *et al.*, 2010 ; Ganguly *et al.*, 2013 ; del Toro Duany *et al.*, 2014).

Most reverse gyrases adopt two zinc fingers, with one located at the N-terminal region ahead of H1 domain (Zn1) and the other inserted into the TOPRIM domain (Fig 3.2b), within the topoisomerase segment (Zn2). Zn1 is presented as an extension of the helicase domain and forms a second attachment with the topoisomerase domain in *Tma* RG except for the latch attachment. Zn2 of *Tma* RG is spatially adjacent to the catalytic tyrosine and ionically interacts with Zn1 (Fig 3.2b) (Lulchev *et al.*, 2014). The importance of the two zinc fingers in DNA-binding has been proved in the study of *Tma* RG, in which deleting the two zinc fingers or mutating the zinc-binding cysteines disables the catalysis of the enzyme (both DNA overwinding and negative plectoneme removal) (Rudolph *et al.*, 2013). Study on *Thermoanaerobacter tengcongensis* RG also sustains the indispensability of these zinc fingers that mutating either of them significantly reduces the DNA binding affinity of RG and also disrupts the introduction of DNA positive supercoils (Li *et al.*, 2011).

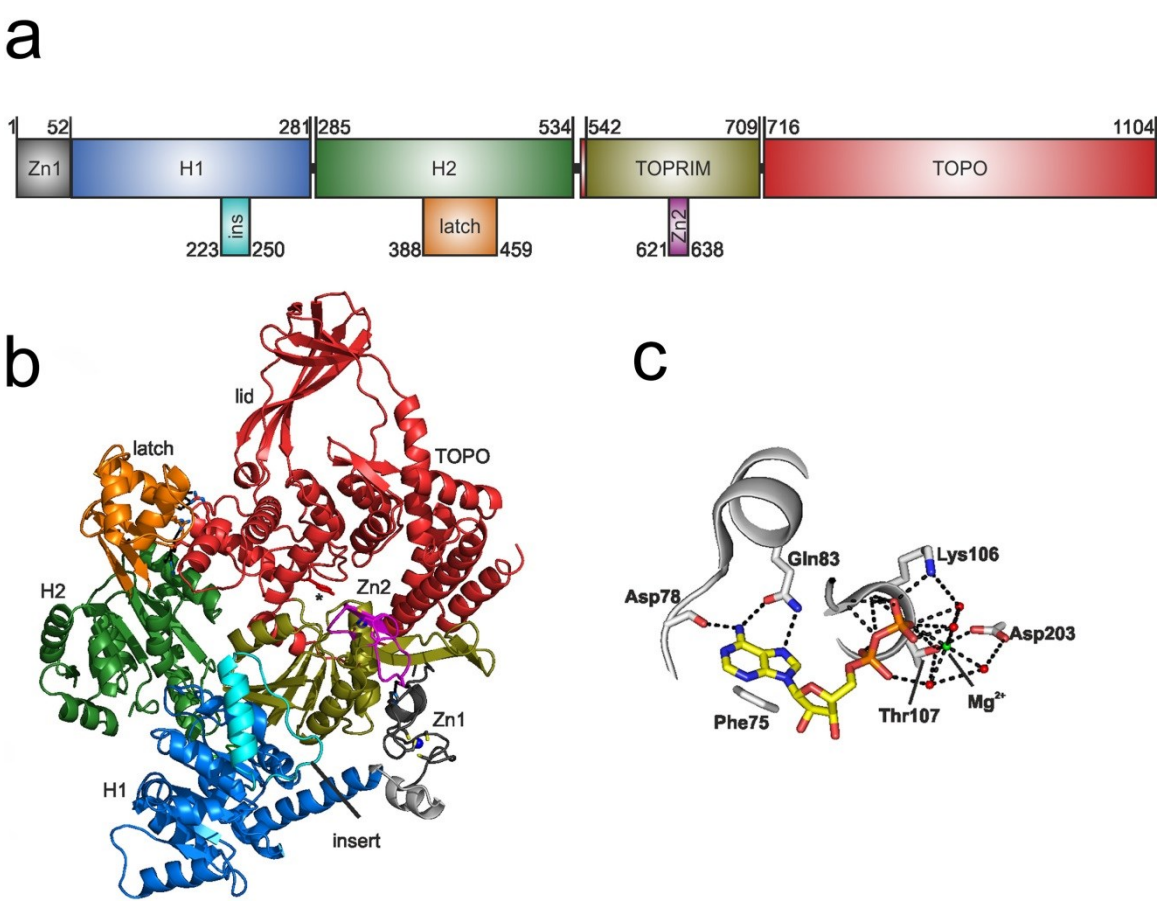

Fig 3.2 Structures of *T. maritima* (*Tma*) RG. (a) Domain structure of *Tma* RG. Conserved protein domains are drawn with rectangles and filled with colors. Start/end positions of amino acid residues are labeled with numbers. Three protein insertions are indicated down below. (b) 3-D structure of *Tma* RG (PDB ID: 4DDU). Conserved protein motifs and features are labeled and painted with the same colors as shown in (a). The catalytic tyrosine is marked with "*". (c) 3-D structure of RG ATPase bound with ADP (PDB ID: 3P4X). Conserved amino acid residues which interact with ADP are indicated with sticks. Adenine base and two phosphate groups are presented with yellow and orange sticks. Dotted lines represent the hydrogen bonds between protein residues and ADP (Lulchev *et al.*, 2014).

Only RG in the top IA family can benefit from the free energy stored in the nucleotides through hydrolysis, which supports the DNA positively supercoiling activity. The ATPase domain of RG is located in the N-terminal helicase part and it shares the conserved Walker A and Walker B motifs with all the DEAD-box helicases

within the SF2 helicase family (Rudolph *et al.*, 2013; Byrd & Raney, 2012). Details of the nucleotide-binding site are obtained with a crystal of the *Tma* RG helicase domain bound with ADP (PDB ID: 3P4X) (Fig 3.2c). Within the ATP-binding pocket, the adenine base of ADP is recognized by Gln83 in the nucleotide binding pocket and they interact through a bidentate hydrogen bond. Meanwhile, Asp78 and Phe75 also participate in stabilizing the adenine base with a hydrogen bond and a hydrophobic interaction respectively. The α- and β-phosphoryl groups of ADP form hydrogen bonds with conserved residues in the Walker A motif, *e.g.*, two Gly, one Lys and two Thr. Also, the ATP binding pocket traps an Mg^{2+} which plays an essential role in stabilizing the nucleotide by ionically contacting its β-phosphate (del Toro Duany *et al.*, 2011; Rudolph *et al.*,2013).

3.2 Structural Analysis Illustrates Type IA-DNA Interaction

Crystallographic analyses also obtained Top IA crystals bound with DNA which elucidate the model of Top IA-DNA interaction. Firstly, a Top IA enzyme core was crystallized with a 13-base single-strand DNA oligo at the strand-cleavage intermediate state, in which the *E. coli* Topo I (with D111N mutation to slow down strand religation) covalently links to the DNA through the catalytic tyrosine (Fig 3.3a). A well-defined nine-base oligonucleotide interacts with the enzyme through an arginine-enriched binding pocket at the interface of the domains I, III and IV, with seven bases located in the 5’ DNA segment upstream the cleavage site and the 3’ DNA segment contains the rest two bases (Fig 3.3b) (Zhang *et al.*, 2011).

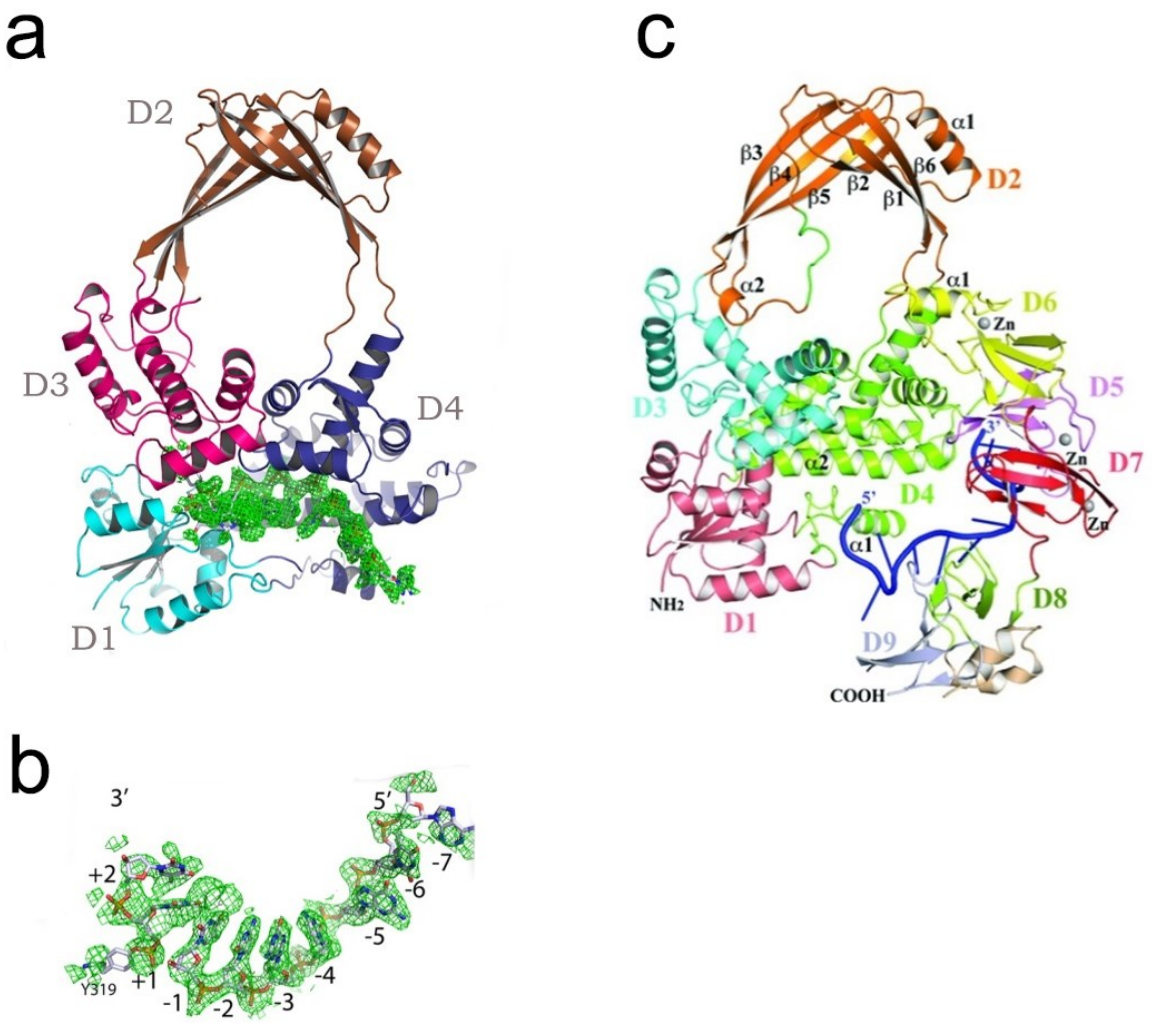

Fig 3.3 Structures of *E. coli* topo I bound with ssDNA. (a) N-terminal structure of *E. coli* topoisomerase I interacting with 9-base ssDNA. 3-D ribbon stands for refined four conserved domains (D1-4) and the ssDNA is represented with an electron density map in green (Zhang, 2011). (b) Details of the 9-base ssDNA in the enzyme active site. Protein residues in the 5' and 3' fragments upstream/downstream the cleavage site are labeled with numbers. The catalytic tyrosine (Y319) is covalently linked to the 3' fragment (Zhang, 2011). (c) Full-length structure of *E. coli* topo I with ssDNA bound on the C-terminal region. Domains and structural feathers are labeled and the ssDNA is shown in blue (Tan *et al.*, 2015).

A more recent crystallographic study of *E. coli* Topo I acquired the full-length enzyme structure and also obtained the structural information of an ssDNA fragment interacting with the enzyme C-terminal flexible protein region (Fig 3.3c). Researchers

then blended these two structures to combine the ssDNA interaction with both the N-terminal and the C-terminal domains (Fig 3.4a).

With this theoretical structure of the protein-DNA complex, they proposed two potential models which provide a general perspective of how the enzyme binds an unwound DNA throughout strand-passage reaction (Fig 3.4a, b). These two models are termed single-chain and double-chain model according to the conformation of the DNA when trapped by the protein. In the single chain model, the G-strand (cleaved strand) is bent greatly in the middle to interact with both the enzyme core and C-terminal segments (Fig 3.4b); in the double chain model, the enzyme core and C-terminal segments each separately holds the G-strand or the T-strand (Fig 3.3c). When concerning the total length of a single ssDNA fragment wrapping around the enzyme, the single chain model requires at least 18 bp and is much longer than that in the double chain model which only requires 8-9 bp (Tan *et al.*, 2015).

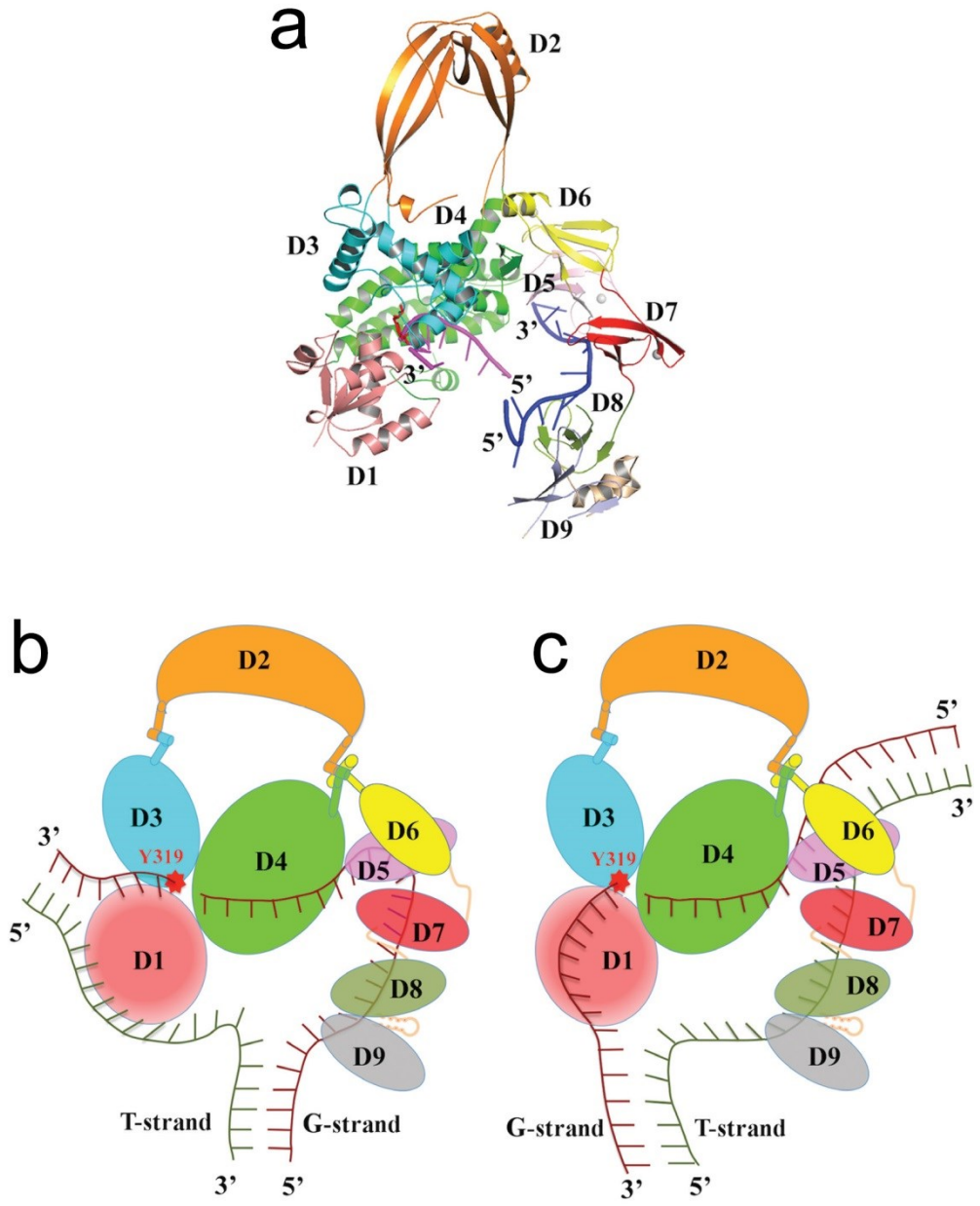

Fig 3.4 3-D structure and theoretical models of ssDNA binding on the full-length *E. coli* topo I. (a) 3-D structure of topo I bound with ssDNA generated by blending two structural files presented in Fig 3.2a and 3.2c (Tan *et al.*, 2015). Protein is shown with color-coded ribbon and ssDNA fragments are presented with pink/blue sticks (b) Single-chain DNA binding model. The enzyme interacts with the DNA Gate-strand (G-strand) only. Domains are numbered (D1-9) and DNA T-/G-strand is presented with green/red string. The catalytic tyrosine is marked with a red star (Y319). (c) Double-chain DNA binding model. The N-terminal domains interact with G-strand and the C-terminal domains interact with T-strand. Protein domains and ssDNA strands are presented as described in (b) (Tan *et al*., 2015).

So far, no solid structural information has been achieved concerning RG-DNA interaction. While a three-dimensional electron microscopy study provided some clues by presenting an image of *Sulfolobus tokodaii* RG binding on a circular DNA duplex, in which the DNA duplex goes through a 10–20 A wide cleft within the RG helicase-like domain and interacts with the inner surfaces of the cleft (Matoba *et al.*, 2002). However, the relatively low resolution of the image prevents researchers from a deeper look into the structural details.

3.3 Diversities in Top IA Functionality

Divergences in enzymatic activities exist among Topo I, Topo III and RG such as their preferences in manipulating different DNA topologies and their nucleotide dependences.

3.3.1 Topo I is Adept at Removing Negative DNA Supercoils

The initial understanding of top IA was its ability to relax DNA negative supercoils and to balance the reverse activity performed by gyrase. Topo I, such as well-defined *E .coli* TopA (ω protein), only exists in bacteria and is characterized by its high efficiency of removing DNA negative supercoils (Viard *et al.*, 2007). Top IA requires a ssDNA bubble to perform strand passage, thus it relaxes negatively rather than positively supercoiled DNA (Dekker *et al*., 2002; Kirkegaard & Wang, 1985). This feature had been perceived to be important for chromosome organization such as preventing R-loop formation during transcription and stabilizing DNA double helixes for organisms living at high temperatures. Interactions between Topo I and the β-subunit of RNA polymerase have also been reported to support this point (Cheng *et al.*, 2003). Another role of topo I suggested *in vivo* is to inhibit ssDNA formation at vulnerable sequences. This has been supported by an *E. coli* topA mutant which is sensitive to the increase of temperature (Qi *et al.*, 1999).

3.3.2 Topo III is Proficient in Manipulating DNA Catenation

Topo III enzymes, such as *E .coli* TopB, yeast Topo III and human Topo IIIα/β, are well known for their high efficiency to catenate/decatenate and knot/unknot nicked or gapped DNA substrates (Garnier *et al.*, 2018). Compared with Topo I, a Topo III enzyme relaxes DNA negative supercoils more slowly and in a distributive manner (Goulaouic *et al.,* 1999). However, the actual role of these enzymes is still controversial due to their ambiguous activities observed both *in vivo* and *in vitro*. For example, *in vitro* experiments show that a topo III has both decatenation and catenation activities (in the presence of RecQ helicase) (DiGate & Marians, 1988; Harmon *et al.*, 1999) and also capable of removing DNA precatenanes (Mondragón *et al.*, 1994; Hiasa & Marians, 1994). *In vivo* studies indicate that topo III prefers to generate catenanes and knots on nicked/gaped DNA circles rather than to decatenate DNA (Rybenkov, 1997; Perez-Cheeks, 2012).

One of the unique features of Topo III enzymes is their ubiquitous cooperation with SF2 helicases in all domains of life, such as RecQ in *E. coli*, Sgs1 in yeast, Hel112 in *Sulfolobus* and BLM and WRM in human (Garnier *et al.*, 2018). These cooperations are essential for the maintenance of a proper genome structure to facilitate busy cellular transactions. In *E. coli*, interaction with RecQ improves the DNA catenation activity of Topo III (Harmon *et al.*, 1999). In eukaryotes, the activity of topo III-RecQ complex is further modified by regulatory protein Rmi1 (in yeast) or Rmi1-Rmi2 (in human) and all of these components work together as a “dissolvasome” to solve DNA topological puzzles during replication, homologous recombination repair (HRR) and mitosis (Hickson & Mankouri, 2011; Cejka *et al.*, 2012). Both yeast and human Rmi1 improves decatenation performed by RecQ-Topo III during double Holiday junction (dHJ) dissolution (Bocquet *et al.*, 2014). Numerous human RecQ-like proteins, such as BLM and WRN helicases, interact with Topo III enzymes and abnormal cross-talks between them lead to major molecular disorders. For example, mutation in BLM or WRN gene implicates in Bloom or Werner syndrome respectively, and a mutated RecQ4 gene is responsible for the Rothmund-Thomson syndrome. Defect in each of these RecQ-like genes can cause excessive chromosomal disorder, predisposing patients to cancer (Amor-Guéret & Riou, 2012; Wu & Hickson, 2001; Temime-Smaali, *et al.*, 2008; Ellis *et al.*, 1995; Brosh Jr, 2013). Interestingly, recent studies reveal a new partner of human topo III, Plk1-interacting checkpoint

helicase (PICH), which belongs to the SNF2 family (Baumann *et al.*, 2007). PICH binds on the DNA and creates a loop as an independent DNA topological domain. PICH translocating on the DNA overwinds DNA within the loop, generating negative DNA supercoils outside the loop due to topology redistribution. Removal of negative DNA supercoils by topo IIIα-Rmi1-Rmi2 complex then achieves an overall positively supercoiled DNA (Bizard *et al.*, 2019). This overwound DNA is believed to be essential for the chromatid separation in anaphase (Baxter *et al.*, 2011).

3.3.3 Comparative Studies Between Topo I and Topo III

Recent single-molecule techniques such as magnetic tweezers provide single-DNA/enzyme resolution which are suitable for tracking enzymatic activities on a DNA substrate. Comparative studies using magnetic tweezers illustrate diversity in mechanisms between topo I and topo III. On a negatively supercoiled DNA, Topo I relaxes DNA negative supercoils in a more processive way and with a much faster overall rate, while topo III relaxation undergoes multiple bursts with long pauses between these bursts (Terekhova *et al.*, 2012). Researchers also compared DNA decatenation activity between them using DNA braids as substrate. Both topo I and topo III can remove DNA catenanes with DNA duplexes containing a bulged, but with different pausing lengths. Topo III reaction contains shorter pauses thus it achieves a higher overall decatenation rate (Terekhova *et al.*, 2014).

Comparison in 3-D structure between Topo I and Topo III shows some major differences which are suggested to explain the functional diversities between these enzymes. Firstly, the C-terminal domain of topo I is larger compared with topo III. This protein segment containing Zinc fingers is responsible for topo I DNA interaction and also controls the specificity of its DNA cleavage site for some of the family members (Ahumada & Tse-Dinh, 1998; Tan Viard *et al.*, 2004). Another difference is that an additional peptide about 17-amino-acids is inserted into domain III of topo III in *E.coli* but not Topo I. It is close to the catalytic tyrosine within the topo III active center and its deletion causes lose of decatenation activity (Li *et al.*, 2000). However, this insertion is not conserved in all the Topo III family members, e.g., absent in topo III enzymes in *Sulfolobus solfataricus*, yeast and human (Viard *et al.*, 2001; Garnier *et al.*, 2018).

3.3.4 Reverse Gyrase Adds Positive Supercoils to DNA

RG is the only top IA family member which works independently to stepwise introduce positive supercoils to DNA, with one unit increase of Lk in each enzymatic cycle (Forterre *et al.*, 1985). At least one RG gene is presented in each of the hyperthermophiles while absent in mesophilic organisms. This makes the unique topoisomerase a marker for hyperthermophilic organisms (Nadal, 2007; Forterre, 2002). Compared with topo III, which cooperate with SF2 helicases, almost all RGs naturally combine a topo IA with a helicase in the genomic level (Nadal, 2007), rather than building up a protein complex after protein expression.

Most organisms living under moderate temperature, like mesophilic bacteria, require an overall negative supercoiled genome to facilitate chromosome assembly and cellular transactions. In contrast, DNA underwinding of thermophile and hyperthermophile is reduced to protect their genomes from thermal denaturation at higher temperatures. Reverse gyrase, which works efficiently *in vitro* to overwind DNA, is believed useful in these organisms. For example, DNA of SSV1, a virus induced into *Sulfolobus,* is highly positively supercoiled (Nadal *et al.*1986). Moreover, analysis on plasmids in several hyperthermophiles and thermophiles indicates that they are generally less underwound (with a superhelical density from −0.015 to 0.013), than that in mesophiles (between −0.048 and −0.068) (López-García *et al.*, 1999; Lulchev *et al.*, 2014). More evidence of RG participation in DNA protection and repair have been reported, including its activity in annealing ssDNA, supercoiling ssDNA bubbles (Hsieh *et al.*, 2006) and involvement in DNA repair process after DNA damage (Valenti *et al.*, 2009; Napoli *et al.*, 2004).

3.3.5 Two Types of Reverse Gyrase

Although similar in protein sequence and architecture, differences in the RG family still exist. Within the Archaea domain, for example, each Crenarcheota like *Sulfolobus solfataricus* (*S.so*), encodes two RGs: TopR1 and TopR2. Comparison between these two *S.so* RGs reviewed their great differences in enzymatic feature such as nucleotide and temperature dependences. Firstly, TopR1 can relax DNA

negative supercoils without burning ATP. TopR2 is a different type of reverse gyrase which has been studied in depth more recently. One of their major differences is that the catalysis of TopR2 is strictly dependent on the presence of ATP. Moreover, concerning their temperature dependence and cellular functions, both *in vivo* and *in vitro* experiments demonstrate that TopR1 is more active at higher temperatures and it is required during cell division. TopR2 is active in a wider temperature range and it participates throughout the entire cell cycle (Bizard *et al.*, 2011; Couturier *et al.*, 2014).

Although numerous protein structures have been obtained and their activities in DNA topology modification unveiled by *in vitro* and *in vivo* studies, the perplexing mechanisms of type IA topoisomerases and their functional diversities within the family need further elucidation. Also, a deeper understanding of the enzymatic kinetics requires powerful tools like single-molecule experimentations to achieve data with better spatial and temporal resolution. The principles and applications of these newly invented approaches will be discussed in the next section.

4. Technologies and Applications — Practicable to Study DNA Topoisomerases

As mentioned in the last chapter, studying DNA topoisomerases requires experimental tools with high resolutions which can sensitively identify DNA topological features during an assay, important for the determination of the mechanisms of an enzyme. Multiple approaches have been developed and proven useful, such as traditional one/two-dimensional gel electrophoresis and single-molecule experiments. Combination of the latter and contemporary fluorescence microscopies, such as total internal reflection fluorescence, also provides more opportunities to observe the behavior of individual components in a reaction system.

Characteristics and applications of these traditional and modern technologies are discussed below.

4.1 Conventional One/two-dimensional Electrophoresis

Agarose gel electrophoretic analysis is among the most commonly used and easily accessible approaches. One-dimensional gel electrophoresis (1-D electrophoresis) allows the separation of DNA topoisomers (closed circular DNA) at different supercoiling levels. During a standard agarose gel electrophoresis, DNA topoisomers with different linking numbers migrate with different velocities and they appear as a DNA ladder on the gel. Between each two adjacent DNA bands, there is one unit difference in linking number (Keller, 1975).

One of the defects of this method is the lack of resolution for highly supercoiled DNA topoisomers (*e.g.*, superhelical density greater than 0.05 as an absolute value), as they usually migrate as a single band on the gel. A solution to properly separate negatively supercoiled DNA topoisomers is the addition of DNA intercalators such as ethidium bromide and chloroquine, in which the intercalators insert between stacked DNA base pairs, affecting the helical repeat of the DNA double helix. As a result, the Tw value of the closed circular DNA increases which transfers to the growth of DNA Wr. Thus the introduction of intercalators transforms a highly negative supercoiled DNA to a less supercoiled form, which supercoiling level falls into the detectable range and can be well separated (Mirkin, 2001). On the contrary, to resolve the highly positively supercoiled DNA, netropsin is introduced which has the opposite effect of chloroquine (Nadal *et al.*, 1988; Bell *et al.*, 1998).

Another disadvantage of 1-D electrophoresis is its inability to segregate topoisomers with same superhelical density but different signs or with structural transitions. The solution is to introduce intercalators after a standard agarose gel electrophoresis and followed by a second electrophoresis in the perpendicular direction (2-D electrophoresis). The intercalators unwind DNA and make the positively supercoiled topoisomers more compact (migrate faster in the second electrophoresis) and the negatively supercoiled ones less compact (fall behind) (Fig 4.1a) (Peck & Wang, 1983).

One example of applying 2-D electrophoresis is a study of reverse gyrases, in which researchers incubated negatively supercoiled DNA substrates with TopR1 at various concentrations of ATP and then separately loaded the DNA products on an agarose gel. By performing 2-D electrophoresis in the gel and followed by ethidium bromide staining, they obtained the overall topological features of the DNA products at different ATP levels (Fig 4.1b). The result shows that the degree of DNA positive supercoiling introduced by the enzyme is increasing from low to high ATP concentrations applied in the assay, illustrating the nucleotide-dependent character of TopR1 positive supercoiling activity (Bizard *et al.*, 2011).

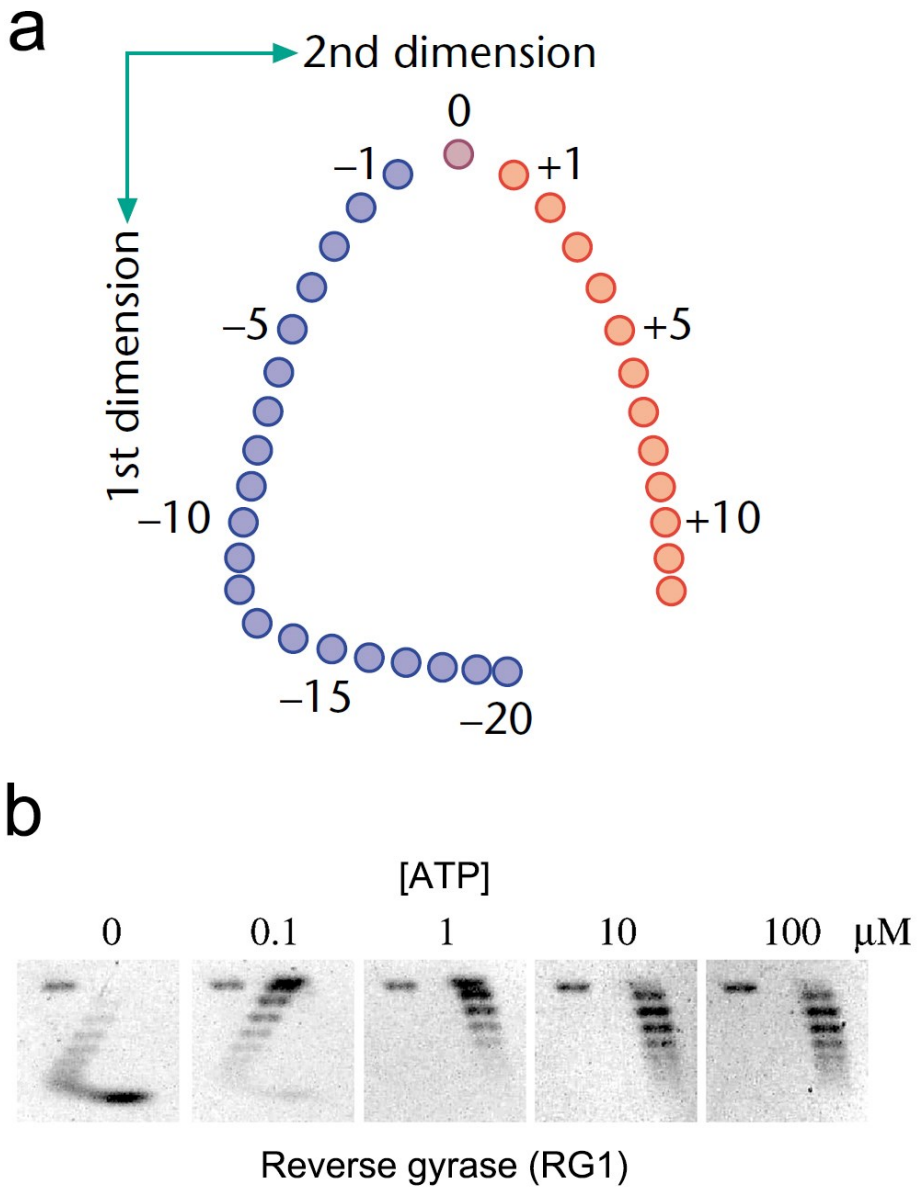

Fig 4.1 Schematic of the DNA supercoiling patterns after 2-D electrophoresis on an agarose gel. (a) A theoretical pattern of DNA topoisomers separated by 2-D electrophoresis. The experimental

process is described in the main text. Arrows indicate the directions of the first and second electrophoresis. Negatively supercoiled DNA topoisomers are presented with blue dots and positively supercoiled DNA in red. Supercoiling levels of the corresponding topoisomers are marked with numbers (Mirkin, 2001). (b) Result of TopR1 DNA positive supercoiling assay performed with five different ATP concentrations. 2-D electrophoresis result shows that the enzyme slightly relaxes highly underwound DNA without ATP. Increasing ATP concentration promotes the activity of TopR1 to remove negative DNA supercoils and overwind DNA. Single bands at top-left positions represent nicked DNA circles as a control (Bizard *et al.*, 2011).

4.2 Single-molecule Experimentations and Applications

4.2.1 Classical Magnetic Tweezers (MT)

Among all the single-molecule approaches, MT has been used most frequently to study enzymes transacting on DNA due to its convenience in directly observing and manipulating DNA topology (Strick *et al*., 2012). In a classical MT assay, a DNA molecule with a proper length is constrained by attaching one end to a glass surface and the other end to a magnetic bead via affinity interactions between biomolecules (Fig 4.2a). The DNA tether linked to the magnetic bead is then extended in the magnetic field formed by a pair of magnets on top of the reaction chamber. Swiveling of the magnets results in the rotation of the magnetic bead along with the torsionally constrained DNA molecule, introducing DNA supercoils. Adding supercoils to a relaxed DNA tether increases its torsional energy which can be further transformed to buckling energy via formation of DNA plectonemes. This structural modification on the vertically extended DNA leads to a significant change of the DNA end to end extension (the distance between the magnetic bead and the glass surface). Using a conventional inverted microscope connected to a video camera, one can monitor the DNA extension in real-time by measuring the diameter of the diffraction ring of a magnetic bead. To convert the change of DNA extension to the change of DNA supercoiling, an “extension *vs* supercoiling” curve is also recorded (Fig 4.2b) before starting the assay, which is used to measure the amplitudes of the enzymatic steps in the assay (Strick *et al.*, 1996; Lionnet *et al.*, 2012).

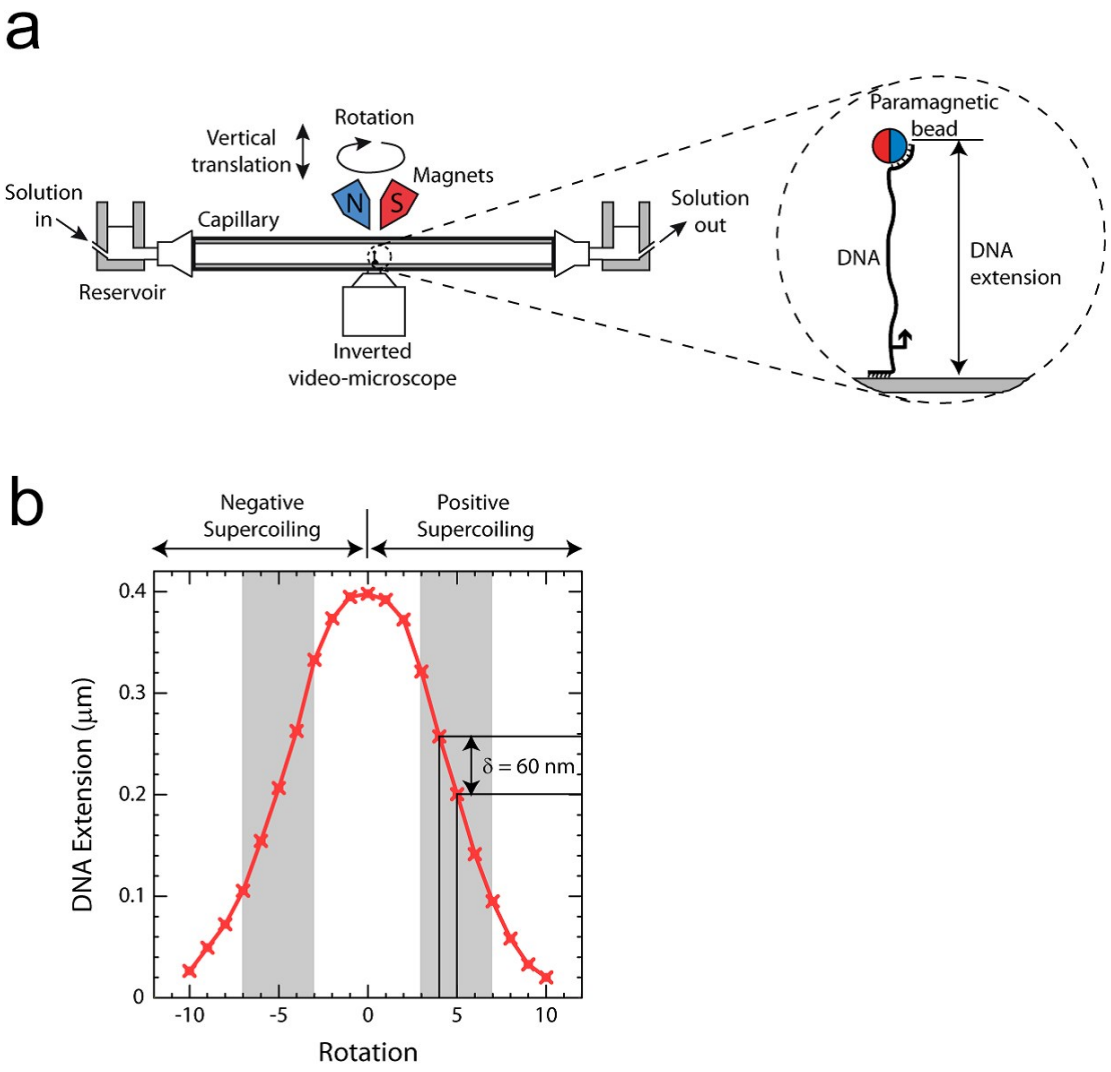

Fig 4.2 Schematic presentation of the magnetic tweezers assay. (a) MT experimental setup using capillary as a reaction chamber. The surfaces of the capillary are coated with anti-digoxigenin to capture one of the DNA ends labeled with digoxigenin. The other end of the DNA tether is attached to a magnetic bead through biotin-streptavidin interaction. Two reservoirs are connected at both sides of the capillary to inject reaction solution from left to right. A pair of magnets are placed above the capillary to extend the DNA tether and introduce rotation to the bead-coupled DNA. The diffraction ring of the magnetic bead is collected with an inverted objective below the bottom surface of the capillary connected to CCD camera. Computer software is applied to measure the diameter of the diffraction ring to achieve the relative position of the bead from the surface. Magnets and magnetic beads are shown with north (N, in blue) and south (S, in red) poles. (b) An "extension vs. supercoiling" calibration curve recorded for at 34°C (stretching force F = 0.3 pN). The recording is started by -10 DNA supercoils and ended with +10 supercoils. Each rotation step adds +1 DNA supercoil by rotating the magnets 360° clockwise (bottom view). DNA extension is recorded at each supercoiling state and plotted as a function of magnet rotation (red crosses). Grey areas indicate the linear regimes on both negatively and positively supercoiled states, in which DNA extension increases/decreases linearly with the number of supercoils (~60 nm/supercoil) (Lionnet *et al.*, 2012).

4.2.2 Combining MT with Single Fluorescent Particle Tracking

Combinations of MT and other advanced technologies have been applied which provide new features for specificities in various projects. One example is the combination of MT and fluorescent microscopy in the rotor bead tracking (RBT) assay, in which a fluorescent-labeled bead is attached to the DNA tether. Instead of topologically fixing a double-strand DNA tether, introducing DNA site-specific nicking (Gore *et al.*, 2006) or a free swivel (Basu *et al.*, 2012) to link DNA and the magnetic bead both allow the DNA tether rotate freely to prevent torque generation (Fig 4.3a). Rotation of the DNA tether can be observed via measuring the swivel angle of the fluorescent bead. By combining the fluorescent and bright-field microscopy, researchers can achieve in real-time both the change in DNA extension and DNA rotation to analyze DNA wrapping/bending and DNA supercoiling separately. An application of this method is to study the mechanism of negative DNA supercoiling by gyrase. During the catalytic cycle, gyrase wraps the double-strand DNA around itself and performs strand passage. Both the change in DNA extension due to DNA wrapping and the change of DNA rotation due to supercoiling can be recorded simultaneously to generate an integrative view of the enzyme activity (Fig 4.3b) (Basu *et al.*, 2012).

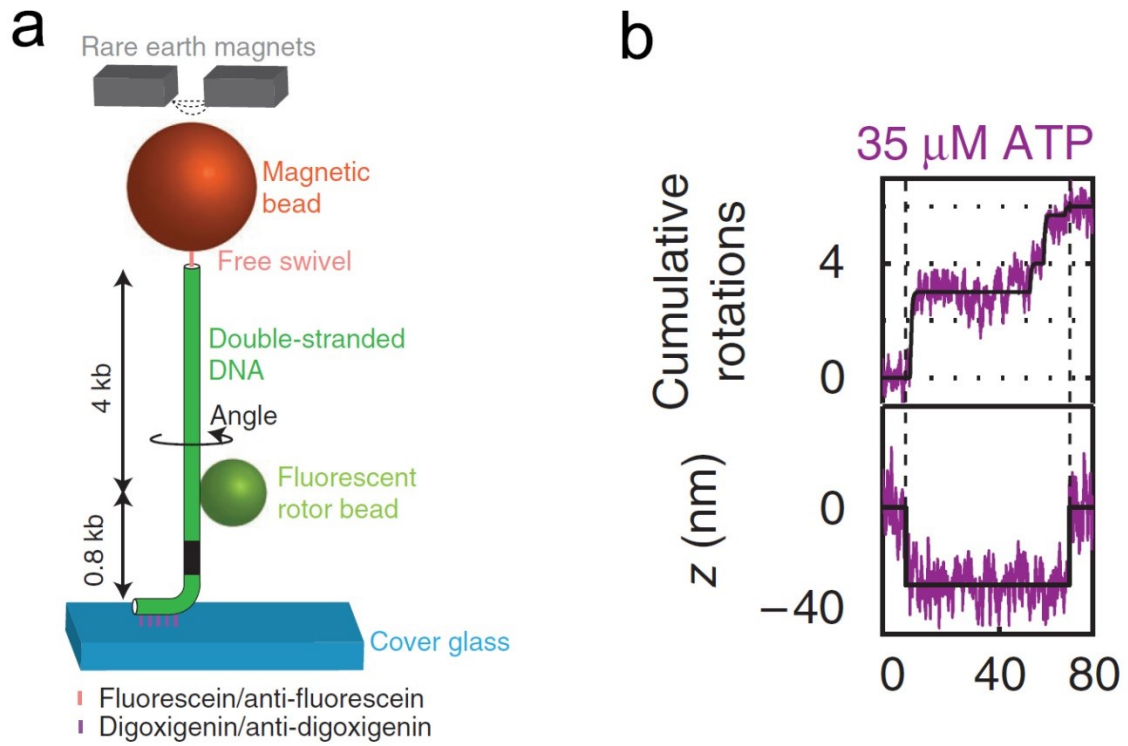

Figure 4.3 Single-molecule experiment combining MT and fluorescent bead tracking. (a) Schematic representation of the experimental setup used to study DNA gyrase. A 4.8-kb DNA tether (shown as a green tube) is extended in the magnetic field with one end fixed on the cover glass via digoxigenin/anti-digoxigenin coupling. The other DNA end labeled with fluorescein is captured by an anti-fluorescein coated magnetic bead (red), which allows the DNA to rotate freely along its long axis. The fluorescent bead (green) is attached to the DNA tether through biotin-neutravidin interaction. The position of the fluorescent bead on the DNA is indicated in numbers. (b) Alignment of the tracking of DNA rotation angle (top) and DNA extension (below). Two datasets are collected simultaneously and plotted as a function of time. The cumulative rotation presents the change of DNA supercoils during catalysis and the tracking of z (DNA extension) shows the size of DNA wrapping by gyrase. ATP concentration applied in the assay is shown on top (Basu *et al.*, 2012).

4.2.3 Introducing TIRF to MT Assays

Total internal reflection fluorescence (TIRF) field microscopy is based on an evanescent wave created by the total internal reflection of a laser beam, to excite the fluorophores close to the reflection surface. When applied in biology, the exponential decay of the evanescent field allows the excitation within only a shallow layer into a biological sample to improve the signal-to-noise ratio of the fluorescence (Axelrod *et al.*, 1981). Researchers applied TIRF microscopy in a single-molecule assay studying the mechanism of Mfd translocase displacing RNAP during transcription-coupled

repair (TCR) (Fig 4.4a). They obtained the presence/absence of the fluorescent-labeled proteins on the DNA tether by collecting and analyzing fluorescent signal emitted in the TIRF field with an EMCCD camera. At the same time, the DNA extension information is attained by tracking the magnetic bead position described above. Therefore, this method couples both of the information of DNA topological change and also the participation/position of the interest protein components in the complex (Fig 4.4b) (Graves *et al.*, 2015).

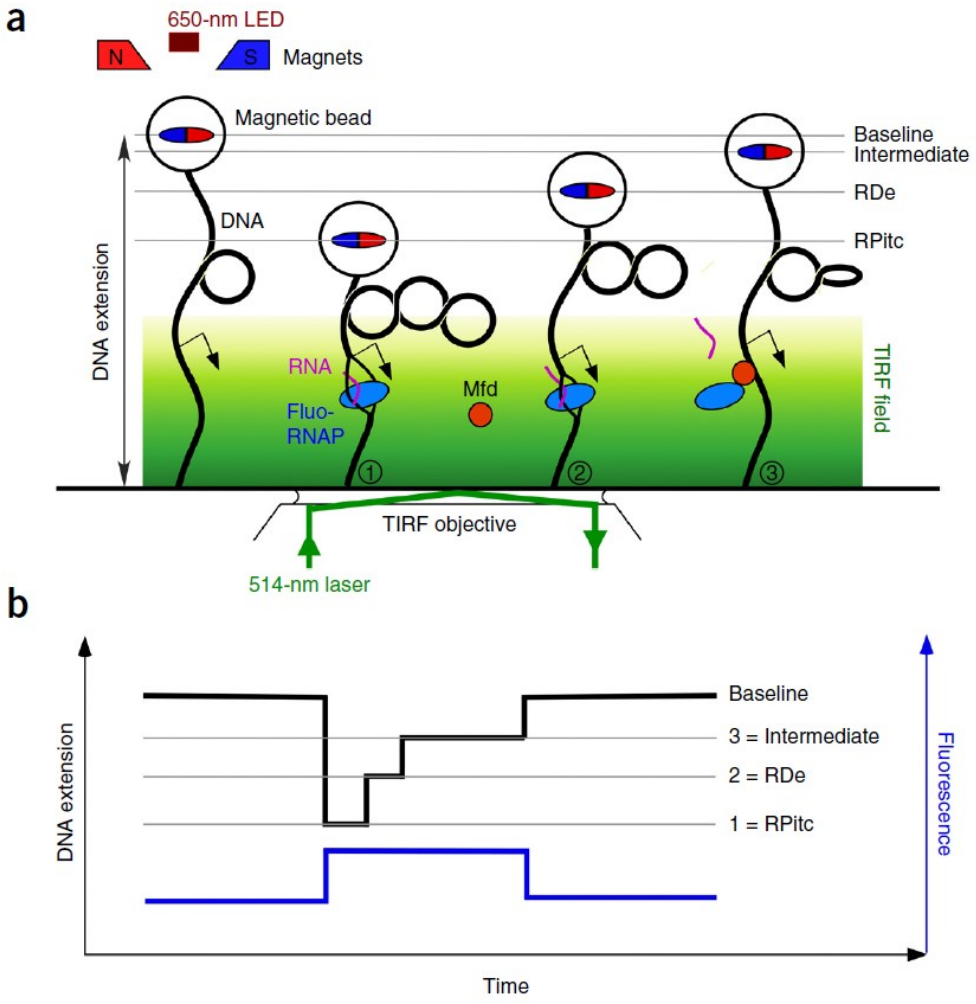

Figure 4.4 Illustration of the MT experiment combined with TIRF microscopy. (a) MT assay is performed under the TIRF field created by a laser beam (green lines and arrows) traveling through the objective below the cover-slip. The evanescent field is coated with gradient color (green to yellow) above the surface. The DNA tether is prepared using the same method described before and adding positive supercoils. The fluorescence-labeled RNAP (blue ellipses) unwinds the DNA promoter region and transcribes DNA template into RNA (purple curves) before stalled by a DNA lesion (① & ②). Mfd (red circles) displaces stalled RNAP and translocates with it on the DNA (③). "RP_{itc}", "RD_e",

“Intermediate” and dotted lines indicate different stages of transcription (see details in the reference paper) and their corresponding DNA extensions. The direction of transcription on the DNA is indicated with arrows. Hollow circles with small ellipses filled in blue and red represent magnetic beads. Permanent magnets are shown on top with north (N, in blue) and south (S, in red) poles. (b) Schematic describes the alignment of the tracking of DNA extension collected with the bright field signal and the intensity of the fluorescence emitted from the fluorescently labeled RNAP. Dotted lines represent DNA extensions in different transcription stages with the same marks labeled in (a). A LED light emitting 650 nm light is shown above the magnets with a dark red rectangular (Graves *et al.*, 2015).

4.2.4 Combining MT-TIRF with PIFE

Protein-induced fluorescence enhancement (PIFE) is a technique based on the behavior of the carbocyanine dye Cy3, which fluorescence emission is enhanced in the vicinity of a protein molecule due to the decay of photoisomerization (Stennett *et al.*, 2015). A recent research project studying the mechanism of *E. coli* Topo III was reported combining MT and TIRF and also included PIFE measurement to detect the presence/absence on the DNA and the conformational change of the enzyme interacting with DNA. A single-strand DNA bulge was introduced to the DNA tether and labeled by a Cy3 group which is adjacent to the topoisomerase binding site. During the experiment, binding of the enzyme on the bulge leads to a significant increase in the overall fluorescence intensity (Fig 4.5a,b). Local fluorescent spikes with higher peak values were also detected within the protein binding time windows which are highly correlated to but more frequent than the supercoiling events (decrease of DNA extension measured with white field signal) (Fig 4.5b). These results indicate that the enzyme constantly performs DNA strand-passage activities during a relaxation pause before successively increasing one unit of DNA linking number (Gunn *et al.*, 2017).

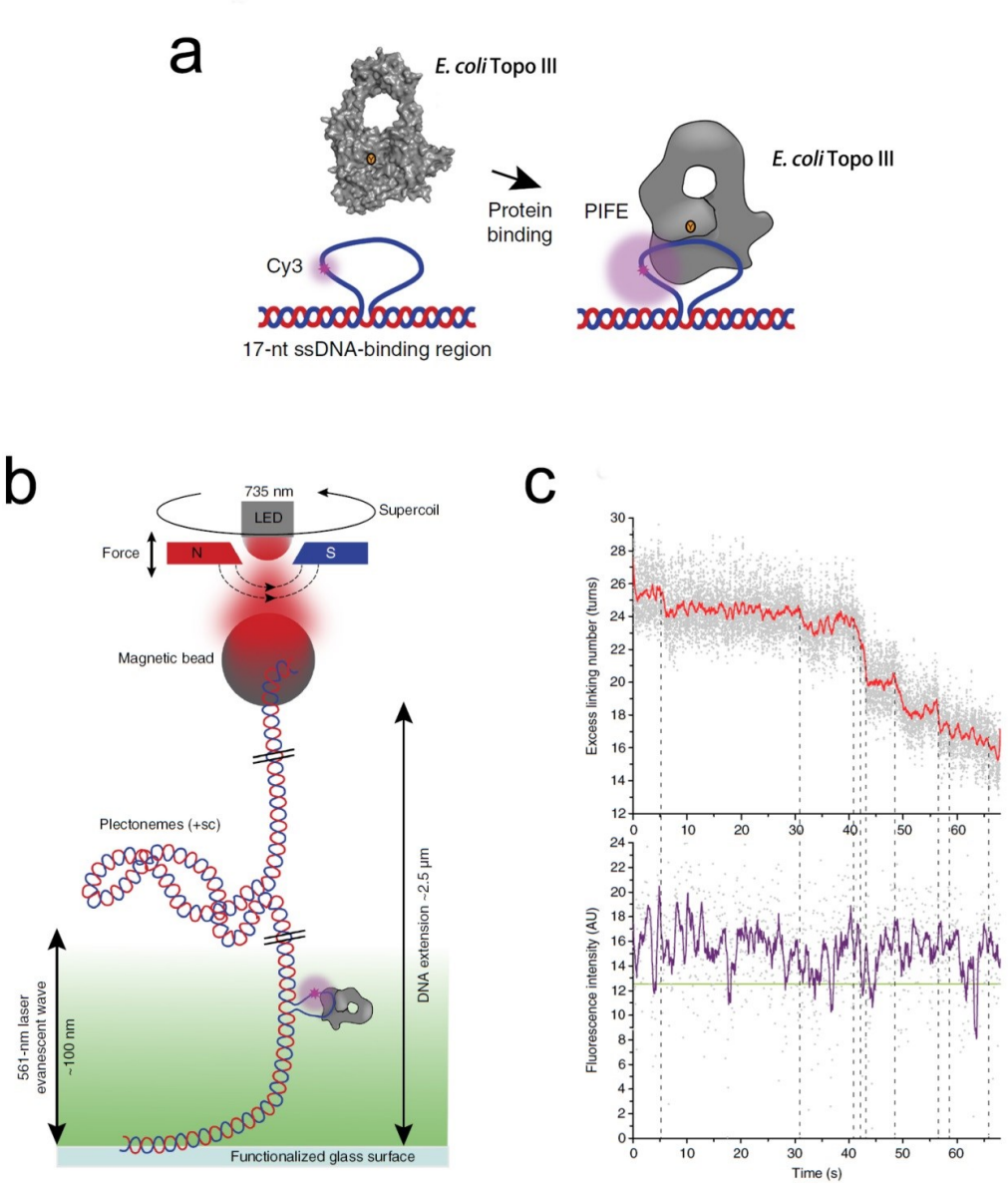

Fig 4.5 Graphical representation of MT-TIRF-PIFE assay. (a) Experimental design of protein binding induced PIFE. An ssDNA bulge labeled with Cy3 (containing a 17-base enzyme binding site) is inserted into the DNA tether for binding of *E. coli* Topo III. Enzyme binding on the DNA bulge causes an increase of the fluorescent intensity due to the PIFE effect (explained in the main text). (b) Illustration of the MT-TIRF setup. DNA tether containing the Cy3 labeled bulge is extended and positively supercoiled in the magnetic field (as described earlier in this chapter) with a TIRF field applied close to the surface to excite Cy3 group. The depth of the TIRF field and the DNA extension are labeled with arrows. LED light, magnets and magnetic beads are indicated in the figure. (c) Alignment of simultaneously recorded DNA extension (red) and fluorescence signal containing PIFE spikes (purple). Each dotted line indicates a supercoiling change on the DNA (Δ Lk +1) (Gunn *et al.*, 2017).

As proofed above, MT-based techniques are useful in studying the mechanisms of DNA-associating enzymes including topoisomerases. We apply MT assay to study the kinetic features of two type IA topoisomerases in *Sulfolobus solfataricus*: one reverse gyrase (TopR2) and one classical type IA enzyme TopA. TopR2 is the first reverse gyrase discovered which catalysis strictly linked to the existence of nucleotides (Bizard *et al.*, 2011). TopA is found as a DNA decatenase and capable of untangling covalently closed DNA catenanes without the help of a DNA helicase (Bizard *et al.*, 2018). We investigate the enzymatic features of TopR2 catalysis, including its DNA interaction and nucleotide cycle. We also describe the kinetics of TopA in DNA supercoiling with a single-molecule resolution and combine it with the *in bulk* assays to further illustrate the decatenation mechanism of the enzyme.

Objectives

Type IA topoisomerase family includes three members: Topo I, Topo III and Reverse gyrase. Topo IIIs exist in all domains of life and they universally cooperate with RecQ helicases. This partnership *in vivo* plays a key role in maintaining genome stability by solving DNA tangling problems (Garnier *et al.*, 2018). For example, in the presence of RecQ and SSB proteins, *E. coli* Topo III can efficiently catenate covalently closed circular DNA without a nick or an ssDNA region (Harmon *et al.*, 1999). In eukaryotes, similarly, the Top3-RecQ-Rmi1 protein complex is found efficient in decatenating genomic DNA, crucial in the process of double Holliday junctions dissolution (Cejka *et al*., 2010; Cejka *et al*., 2012; Bocquet, *et al*., 2014). In archaea, the TopoIII collaborate with Hel112 and regulate the activity of the latter (Valenti *et al*., 2012). Reverse gyrase (RG) binds together a RecQ-like helicase and a classical type IA (Nadal, 2007). Direct coupling between these two functional domains achieves a unique ability of RG to introduce DNA positive supercoils in steps of +1 (Forterre *et al.*, 1985). Although important in numerous cellular transactions, mechanisms of these Top III-RecQ collaborations and helicase-Top IA direct coupling in RG have not been fully understood.

Sulfolobus solfataricus possesses three type IA enzymes, one Topo III (TopA), and two RGs (TopR1 and TopR2). We adopt single-molecule experimentation together with classical in bulk assays to characterize detailed catalytic features of RG supercoiling and TopA catenation. We stepwise dissect the ATP cycle of RG, including its DNA binding, ATP association and ATP hydrolysis; and also investigate the manner of TopA manipulating DNA during its catenation. Comparison between RG and TopA in DNA topological modification provides new insights for understanding both helicase-topoisomerase direct coupling in RG and RecQ-Topo III collaboration.

Results

A manuscript and a published article are provided in this section to show the research outcomes:

1. Manuscript on reverse gyrase mechanism titled “Direct observation of Helicase-topoisomerase coupling within reverse gyrase”.

2. Published article on the hyperthermophilic Topo III titled “TopA, the *Sulfolobus solfataricus* topoisomerase III, is a decatenase”.

1. Direct observation of Helicase-Topoisomerase coupling within Reverse Gyrase

Direct observation of Helicase-Topoisomerase coupling within Reverse Gyrase

Xi Yang[1], Florence Garnier[1,2], Hélène Débat[1,2], Terence Strick[1,3,4,*], Marc Nadal[1,*]

[1]Institut Jacques Monod, CNRS, UMR7592, Université de Paris F-75205 Paris, France
[2]Université de Versailles St. Quentin-en-Yvelines, France
[3]Institut de Biologie de l'Ecole normale supérieure, 75005 Paris France
[4]Programme Equipes Labellisées, Ligue Nationale Contre le Cancer 75013 Paris, France
*to whom correspondence should be addressed : strick@ens.fr; marc.nadal@ijm.fr

Reverse gyrases (RGs) are the only topoisomerases capable of generating positive supercoils in DNA. Members of the type IA family, they do so by generating a single-strand break in substrate DNA and then manipulating the two single strands to generate positive topology. Here we use single-molecule experimentation to reveal the succession of steps which make up the catalytic cycle of reverse gyrase. In the initial state RG binds to DNA and unwinds ~2 turns of the double-helix in an ATP-independent fashion. Upon nucleotide binding RG then appears to rewind approximately ~1 turn of DNA. Nucleotide hydrolysis and/or product release leads to an apparent increase in linking number of 2 units, for a net change of topology of +1 turn in the next iteration of the initial state. Final dissociation of RG from DNA results in rewinding of the 2 turns of DNA which were initially disrupted. Taken together these results provide new insight into the functioning of these unique molecular motors which tightly couple helicase and topoisomerase activities.

Introduction

Reverse gyrase is a unique ATP-consuming topoisomerase which can generate positive supercoils in DNA [1, 2, 3, 4]. Absolutely essential to maintenance in its niche for the hyperthermophilic archaea in which it was discovered [5], it consists of a single polypeptide chain which contains two major domains: an N-terminal RecQ-like helicase domain and a C-terminal topoisomerase domain [6, 7]. The exact role of positive supercoiling in hyperthermophilic life is not fully understood – nor is it fully established. Positive supercoiling could maintain DNA under double-strand form despite elevated temperature, allowing for regulation of gene expression during transcription initiation [8, 9]. Maintaining DNA in the double-strand form can also make it more resistant to various damage-inducing processes [10, 5, 11]. Reverse gyrase could also generate positive supercoiling to regulate Holiday junctions. In eukaryotes for instance, the transient association of the RecQ-like BLM helicase with hsTop3 has been found to modulate numerous DNA transactions including resolution of double-Holiday junctions (dHJ) [12, 13, 14, 15]. Despite the importance of this system for genome stability, the detailed molecular mechanisms which couple helicase and topoisomerase activities and result in formation of positive supercoiling remain poorly understood. Single-molecule methods have recently provided estimates for the turnover rate and torque-dependence of a few reverse gyrases working simultaneously [16, 17]. Here we describe observations of discrete catalytic turnovers by single molecules of reverse

gyrase, as well as discrete substeps in the cycle, and parse these for mechanistic insights [18, 19, 20, 21, 22, 23].

High-resolution single-molecule magnetic trapping experiments have proven useful for the study of topoisomerases as they allow one to easily control and monitor DNA supercoiling [24, 25, 26, 27, 28, 29]. As depicted in Figure 1a, a single linear DNA molecule is torsionally constrained by the magnetic trap when it is tethered by multiple attachments to a magnetic bead at one end and to a glass surface at the other. The trap allows one to control the rotation and extending force applied to the DNA via the magnetic bead. The position of the bead above the surface can be monitored in real-time using videomicroscopy, allowing one to directly observe the end-to-end extension of the DNA resulting from the interplay of DNA topology and extension [30, 31]. Rotating the magnets by one full turn allows one to impose a unit change in the DNA linking number, Lk, which is normally constant for a topologically closed system. Lk is the sum of twist (Tw, the number of times the two single-strands cross intramolecularly) and writhe (Wr, the number of looped plectonemic supercoils in the molecule): Lk = Tw + Wr [32, 33, 34]. When DNA is gently extended by a sub-picoNewton force and supercoiled in the magnetic trap, every additional unit rotation (i.e. a change in DNA linking number ΔLk = 1) causes a unit change in DNA writhe (ΔWr). As a result the bead's position changes by an amount reflecting the DNA contour length consumed by formation of a plectonemic supercoil [30] (Supp. Fig 1). For a constant extending force F = 0.2 pN (1 pN = 10^{-12} N) this corresponds to a change in DNA extension of approximately 60 nm. If for instance a supercoiled DNA comes to be unwound e.g. as in promoter melting by RNA polymerase [8], this results in a local decrease in Twist (ΔTw = -1) and a concomitant increase, at fixed linking number, of Writhe (ΔWr= +1); this results in an increase in extension for negatively supercoiled DNA but a decrease in extension for positively supercoiled DNA.

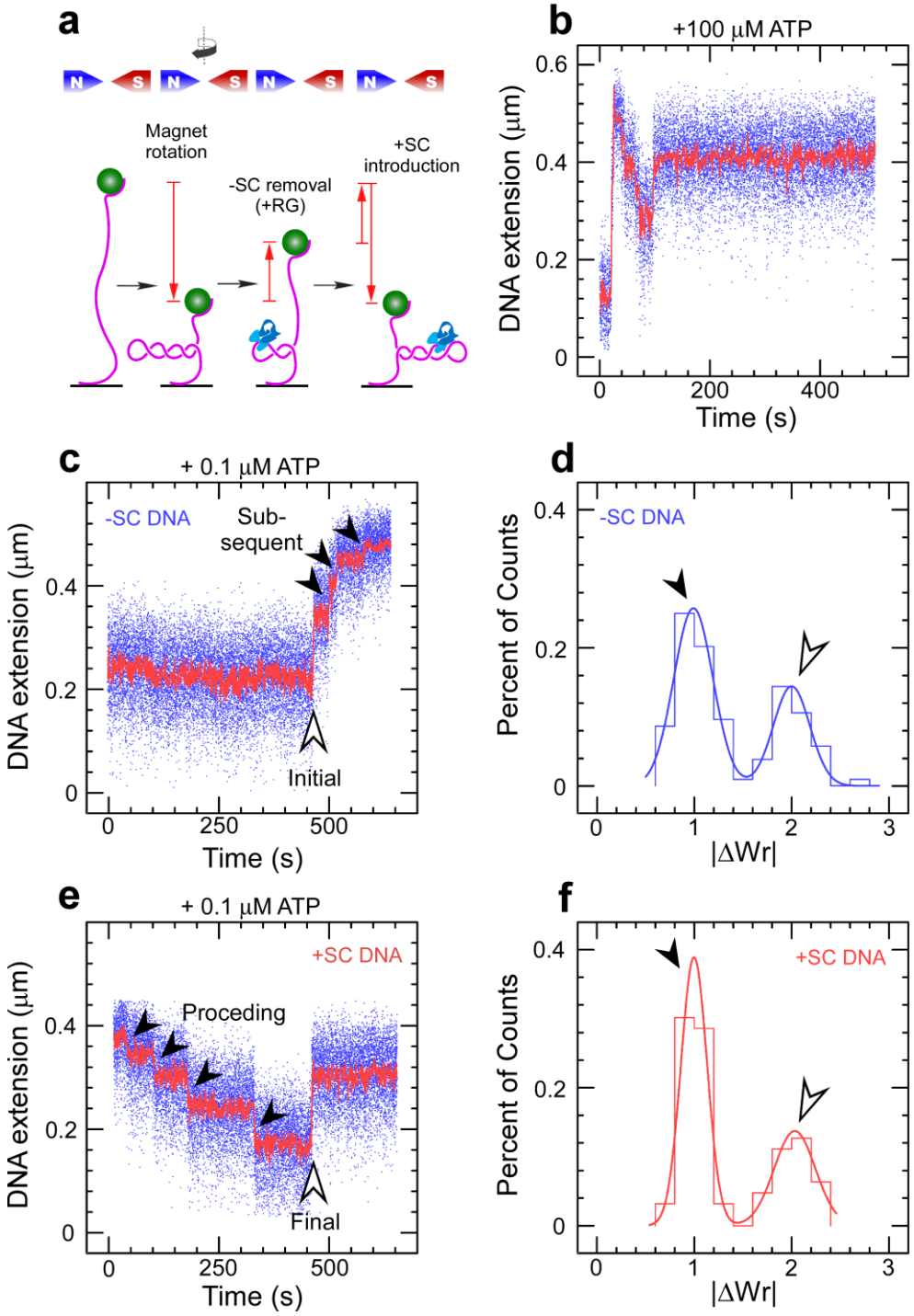

Figure 1. Catalytic introduction of positive supercoils by RG. a, Sketch of the assay showing DNA tethered between a glass surface and a magnetic microsphere which can be manipulated with a magnetic trap. Clockwise rotation of the magnets (as seen from above) results in negative DNA supercoils which reduce DNA extension. RG first removes the negative supercoils before introducing net positive supercoiling. **b**, Time-trace for the extension of a negatively supercoiled DNA exposed to RG and 100 μM ATP. **c**, Time-trace for the extension of a negatively supercoiled DNA exposed to RG and 0.1 μM ATP. Light arrow highlights the initial interaction, filled arrows the subsequent interactions. **d**, Histogram of change in DNA extension observed in c, taking into account both the initial and subsequent interaction observed between RG and DNA. Data are fit to a double-Gaussian (solid line), with means $\Delta Wr^{initial}$ = 2.00 ± 0.01 and $\Delta Wr^{subequent}$ = 1.00 ± 0.01 (SEM, n = 104). **e, f**, are as with the prior two panels but for positively supercoiled DNA, and with means $\Delta Wr^{preceding}$ = 1.00 ± 0.01 and ΔWr^{final} = -2.00 ± 0.01 (SEM, n = 63).

Catalytic properties of reverse gyrase: steps of 2, steps of 1

If one provides *S. solfataricus* TopR2 reverse gyrase (RG) with a gently extended, negatively supercoiled DNA substrate and 0.1 mM ATP at 45°C, the DNA's extension first rapidly increases and reaches a maximum before slowly decreasing in a stepwise fashion (Fig. 1b). This reflects generation of positive supercoiling by a highly processive enzyme, first rapidly annihilating negative supercoils and then slowly introducing net positive supercoils into the DNA. The reaction appears to end with dissociation of RG from DNA. Discrete steps corresponding to catalytic turnover by a single RG are readily observed even at 0.1 μM ATP (Fig. 1c,e), allowing one to characterize single turnover events more readily for both negatively and positively supercoiled DNA.

The change in extension of the first step observed on negatively supercoiled DNA is approximately twice as large as that of successive steps (Fig. 1c,d). Converting step sizes to changes in writhe (plectonemic supercoils, as discussed earlier) indicates the first DNA transaction imposed by RG results in $\Delta Wr = +2$ whereas successive transactions on negatively supercoiled DNA are characterized by $\Delta Wr = +1$ (Fig. 1d). Similarly, the change in extension at the last step observed on positively supercoiled DNA is, likewise, twice as large as that of the preceding steps, although it is of opposite sign (Fig. 1e,f). Again the preceding steps are characterized by $\Delta Wr = +1$ while the last DNA transaction imposed by RG mirrors the first ($\Delta Wr = -2$) (Fig. 1f).

Repeated steps of $\Delta Wr = +1$ are consistent with the expectation from biochemical experiments that reverse gyrase is a type I topoisomerase which introduces a single unit of positive topology ($\Delta Lk=+1$) at each catalytic turnover [2, 35]. Dwell-time measurements for this state performed at different ATP concentrations allow determination of reaction kinetics as defined by the Michaelis-Menten model (see Fig. 2 and Supp. Fig. 2). Comparison of results obtained for negatively or positively supercoiled DNA substrate gives $K_M = 1.0 \pm 0.06$ μM (SEM) and $1/Vmax = 2.4 \pm 0.2$ s (SEM) for the former and $K_M = 7.1 \pm 0.5$ μM (SEM) and $1/Vmax = 2.7 \pm 0.2$ s (SEM) for the latter. The greatest difference between the two reactions thus appears to reside in a roughly seven fold difference in affinity for nucleotide.

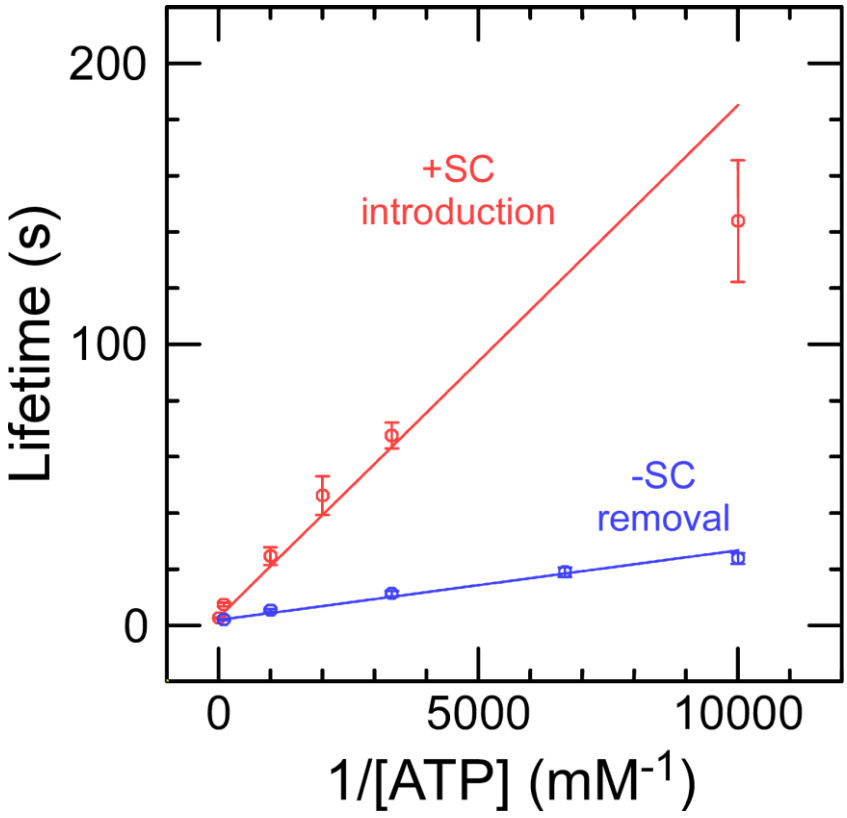

Figure 2. RG catalysis as a function of NTP concentration and sign of supercoiling. Dwell-times reflect average values ± SEM obtained from ~65-269 individual events for removal of negative supercoils (blue) and introduction of net positive supercoils (red). Linear fits are to the Michealis-Menten model (see text for details), returning for negative supercoiling $1/V_{max}$ = 2.4 ± 0.2 s and K_M = 1.0 ± 0.06 μM and for positive superociling $1/V_{max}$ = 2.7 ± 0.2 s and K_M = 7.1 ± 0.5 μM.

Analysis of step amplitudes in the absence of ATP: step of 2

To understand the significance of the initial and final steps of $|\Delta Wr| = 2$. We sought to detect binding and dissociation of RG to DNA in the absence of ATP. Binding of RG to negatively supercoiled DNA resulted in a stable increase in DNA extension (Fig. 3a) which could be reversed upon positive supercoiling, with amplitude corresponding to $|\Delta Wr| = 2$ for binding/dissociation (Fig. 3b). This indicates that the initial step of $\Delta Wr = +2$ reflects the initial DNA transaction imposed by RG on DNA prior to ATP usage and processive catalysis by the motor.

The changes described above are consistent with formation of a significant unwound DNA region by RG in its initial interaction with its substrate. Indeed, unwinding of negatively supercoiled DNA upon/after initial RG-DNA binding ($\Delta Tw^{bind} = -2$) will titrate out two negative supercoils ($\Delta Wr^{bind} = +2$), resulting in an increase in DNA extension for negatively supercoiled DNA. Rewinding of positively supercoiled DNA prior to/upon RG dissociation ($\Delta Tw^{unbind} = +2$) will titrate out two positive supercoils ($\Delta Wr^{bind} = -2$) and thus result in an increase in DNA extension for positively supercoiled DNA. From this analysis we propose that RG unwinds the equivalent of two turns of DNA upon binding. Although a change in DNA topology under similar conditions had been reported previously, the bulk assays used had not provided information on the precise nature or extent of the modification [36].

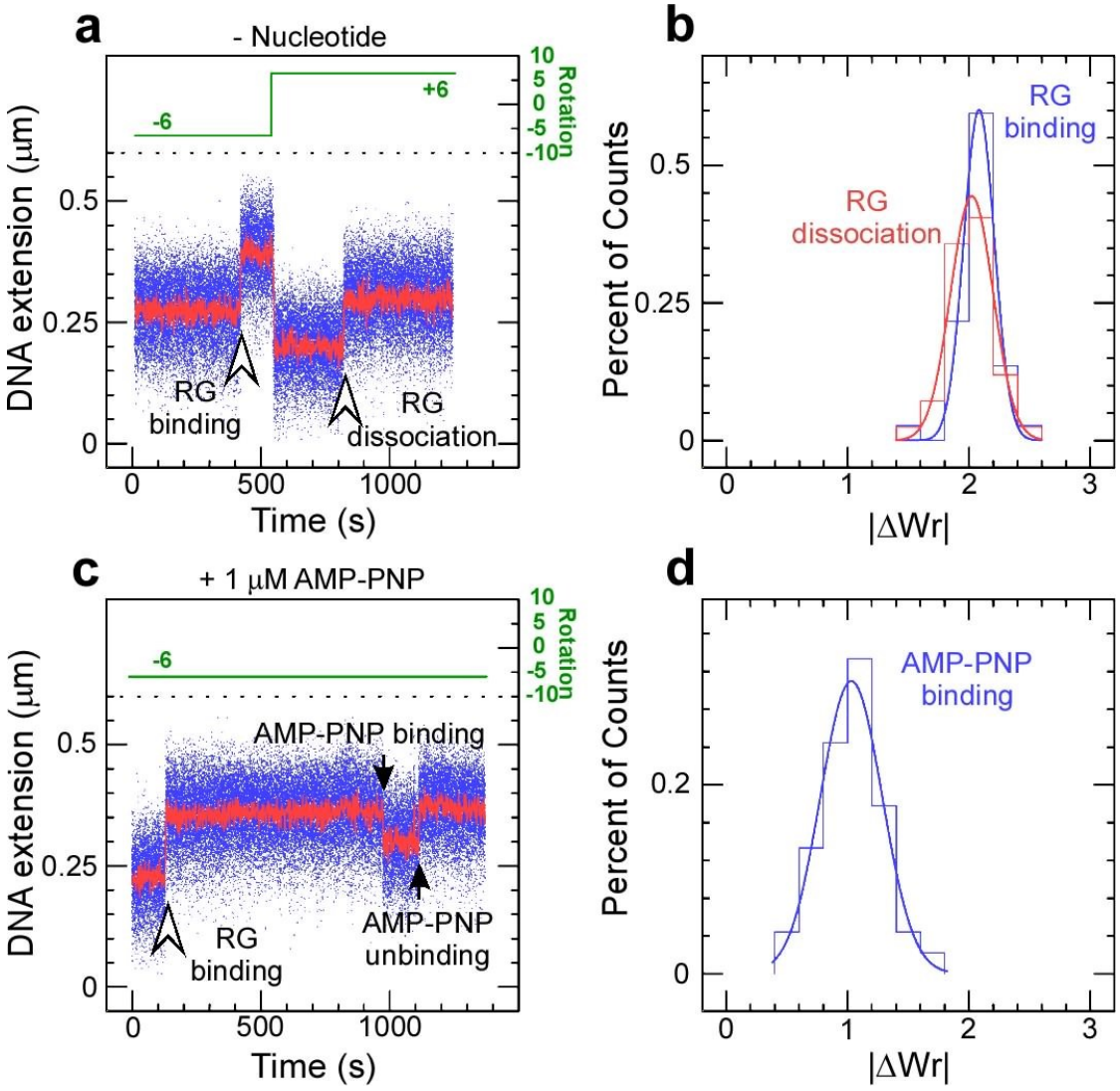

Figure 3. RG-DNA interactions in the absence and presence of AMP-PNP. **a**, Time-trace obtained in the absence of nucleotide cofactor shows RG binding to negatively supercoiled DNA results in an increase in DNA extension. This interaction can be reversed upon positive supercoiling, as evidenced by an increase in DNA extension observed in these conditions. **b**, Histograms of change in DNA extension observed for negatively and positively supercoiled DNA, corresponding, respectively, to the DNA unwinding step (blue) and DNA rewinding step (red). Solid lines are Gaussian fits, indicating that unwinding involves a mean of 2.08 ± 0.02 turns of DNA (SEM, n =37) and rewinding involves a mean of 2.02 ± 0.03 turns of DNA (SEM, n=42). **c**, Extension time-trace obtained in the presence of 1 μM AMP-PNP shows RG binding to negatively supercoiled DNA and then binding nucleotide analog. This interaction spontaneously reverses. **d**, Histogram of reversible extension changes observed in the presence of AMP-PNP. Solid line is a Gaussian fit giving a mean of 1.03 ± 0.04 (SEM, n=45).

Unwinding of a DNA substrate containing a bubble: reverse gyrase as a molecular ruler

Further evidence for the idea that RG unwinds DNA in its initial interaction was obtained by providing the reverse gyrase with a negatively supercoiled DNA substrate engineered to contain a mismatched bubble of either 5 bases or 10 bases. When provided with the 5-base or 10-base bubbles but no ATP, RG binds and apparently unwinds the DNA (Supp. Fig.3), albeit to a progressively smaller extent. Analysis of the DNA extension changes indicate that this reverse gyrase unwinds approximately 1.4 turns of DNA when provided with a 5-base bubble and 0.9 turns of DNA when provided with a 10-base bubble, in a roughly linear relation with respect to what is observed on regular B-DNA. These results suggest that RG unwinds a total of approximately 20 base pairs upon binding DNA and before binding ATP.

Decoupling nucleotide binding and hydrolysis using AMP-PNP

To proceed along its reaction pathway, reverse gyrase must next bind nucleotide. We carried out experiments using negatively supercoiled DNA and RG in the presence of 1 μM AMP-PNP. We now observe the initial unwinding interaction discussed above, followed by a new transition corresponding to an abrupt decrease in DNA extension. Converting into writhe as before indicates the resulting state has Wr^{NTP} = +1 relative to the initial state without RG (ΔWr^{NTP}=-1, where the change is relative to the prior state with RG bound to DNA) (Fig. 3c,d). Because RG is not able to hydrolyze this analog, it ultimately will release it back into solution, and this is observed as a return of the DNA extension to the initial state. We find that the dwell-time prior to observing the analog-induced transition decreases with analog concentration, although the concentration-dependence of the transition rate suggests the analog does not bind as well as ATP and furthermore displays complex association kinetics (Supp. Fig. 4). The overall behavior nevertheless supports the idea that nucleotide binding causes reverse gyrase to rearrange DNA topology as the next step of the catalytic cycle, and we tentatively propose it involves topological rewinding of DNA, leading to a state with one remaining unit of topological unwinding Tw^{NTP}=-1 relative to the initial state without RG (ΔTw^{NTP}=+1, where the change is relative to the prior state with RG bound to DNA). The remaining experiments aim to demonstrate this, first by ruling out the possibility of strand passage using a catalytic tyrosine mutant, and second by mixing ATP and AMP-PNP to observe reactions on positively supercoiled DNA.

In the presence of AMP-PNP, the catalytic tyrosine mutant $TopR2^{Y903F}$ recapitulated the same initial steps of DNA unwinding (ΔTw^{bind} =-2) and nucleotide binding (ΔWr^{NTP} = -1)/unbinding (ΔWr^{NTP} = +1) (Supp. Fig . 5). As $TopR2^{Y903F}$ lacks the ability to cleave DNA, we conclude that the DNA extension changes ΔWr^{NTP} observed upon nucleotide binding are reversible DNA topological transitions independent of DNA strand cleavage and transport, and involve no change in linking number. Thus also nucleotide binding alone on wild-type enzyme does not permit for even a single round of stable DNA strand passage, which must take place at a later step of the reverse gyrase catalytic cycle. However, because observing AMP-PNP binding to reverse gyrase on positively supercoiled DNA was technically challenging due to rapid dissociation of the topoisomerase, we were not able at this stage to specify the nature of the topological rearrangement imposed on DNA by RG in the nucleotide-bound state (eg DNA bending/wrapping vs. DNA rewinding).

To overcome this difficulty, we next combined AMP-PNP with a very low amount of ATP, increasing the lifetime of the nucleotide-bound state prior to hydrolysis while slowly allowing reverse gyrase to complete its cycle after exchanging AMP-PNP for ATP. After binding to negatively supercoiled DNA (ΔTw^{bind}=-2), RG generated a slow, multi-state staircase pattern clearly displaying a succession of steps alternating between decreases in extension (ΔWr^{NTP} = -1 relative to prior state) followed by two-fold larger increases in extension ($\Delta Wr^{ADP\cdot Pi}$ = +2 relative to prior state) for a net change of ΔWr=+1 per cycle (Fig. 4a,b). As per prior results for AMP-PNP binding to RG on negatively supercoiled DNA, we propose that the decrease in DNA extension corresponds to nucleotide binding, and the increase in writhe $\Delta Wr^{ADP\cdot Pi}$ = +2 reflects both ATP hydrolysis (or subsequent steps such as ADP and/or Pi release) and the strand passage reaction itself.

On positively supercoiled DNA with wild-type RG, the AMP-PNP + ATP combination resulted in a symmetric, slow, multi-state staircase pattern clearly displaying a succession of steps alternating between increases in extension (ΔWr = -1 relative to prior state) and two-fold larger decreases in extension (ΔWr = +2 relative to prior state) for a net change of ΔWr=+1 per cycle (Fig. 4c,d).

The mirror symmetry of the time-traces obtained on negative and positively supercoiled DNA implies that i) the step corresponding to nucleotide binding is the increase in DNA extension observed on positively supercoiled DNA (ΔWr^{NTP} = -1 relative to prior state), ii) that this step corresponds to partial rewinding of the RG:DNA bubble state and not DNA bending/wrapping ($\Delta Tw^{NTP} = -\Delta Wr^{NTP}$ = +1, a consequence of conservation of linking number absent strand transport and cleavage), and iii) that nucleotide hydrolysis is coupled to the strand passage reaction and coupled to an increase in writhe of $\Delta Wr^{ADP\cdot Pi}$ = +2.

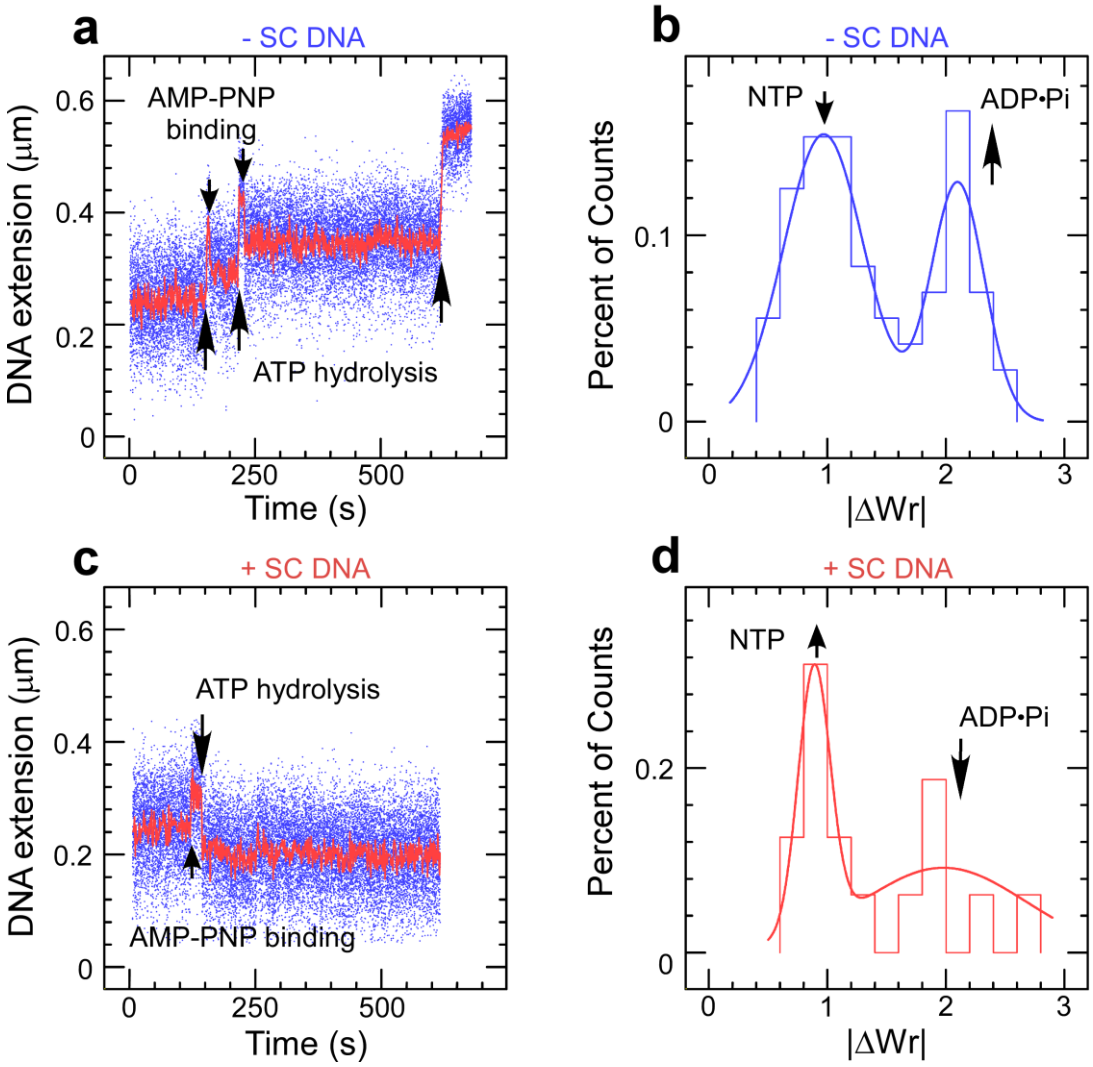

Figure 4. RG-DNA interactions in the presence of a mixture of AMP-PNP and ATP. **a**, Time-trace obtained on negatively supercoiled DNA. Smaller steps with decrease in DNA extension correspond to AMP-PNP binding and the subsequent extension rebounds relate to ATP hydrolysis and Pi/ADP release. **b**, Histogram of extension changes observed on negatively supercoiled DNA. Data are fit to a double-Gaussian, giving means ΔWr^{NTP} = -0.97 ± 0.13 turns and $\Delta Wr^{ADP\cdot Pi}$ = +2.10 ± 0.13 (SEM, n = 72). **c**, Time-trace obtained on positively supercoiled DNA mirror-symmetric with that on negative. **d**, Histogram of extension changes observed on positively supercoiled DNA. Data are fit to a double-Gaussian (solid line), giving ΔWr^{NTP} = -0.89 ± 0.06 and $\Delta Wr^{ADP\cdot Pi}$ = +1.98 ± 0.48 (SEM, n = 16).

Model for the catalytic cycle of reverse gyrase and perspectives

These observations lead to the following model which considers the different manipulations observed in the DNA (Fig. 5). Because RG contains a helicase domain it is reasonable to interpret a part of the topological changes observed as fundamentally connected to twist deformations of DNA, simply manifest as changes in DNA writhe in the magnetic trap. Thus upon binding to DNA, RG unwinds the equivalent of two turns of DNA, reaching a state with Tw^{bind} = -2 relative to the initial, protein-free state Tw=0. When RG binds nucleotide it partially rewinds the DNA, leading to a state with Tw^{ATP}= -1 relative to the initial one. The

nucleotide-bound state leads to an undetected transient state corresponding to a nucleotide-hydrolysis-dependent state (e.g. ADP·Pi or related states with partial or complete product release). This transient state separating catalytic cycles includes a net increase in linking number $\Delta Lk = +1$ via strand cleavage and transport ($\Delta Tw=+1$, returning twist to the initial state $Tw^{ADP\cdot Pi} = 0$) yet requiring no further change in writhe. It further leads to a state where RG is free of NTP, i.e. in which the RG-DNA bubble has been reset from $Tw^{ADP\cdot Pi} = 0$ to $Tw^{bind} = -2$ and linking number and writhe have both increased by one unit relative to the prior cycle.

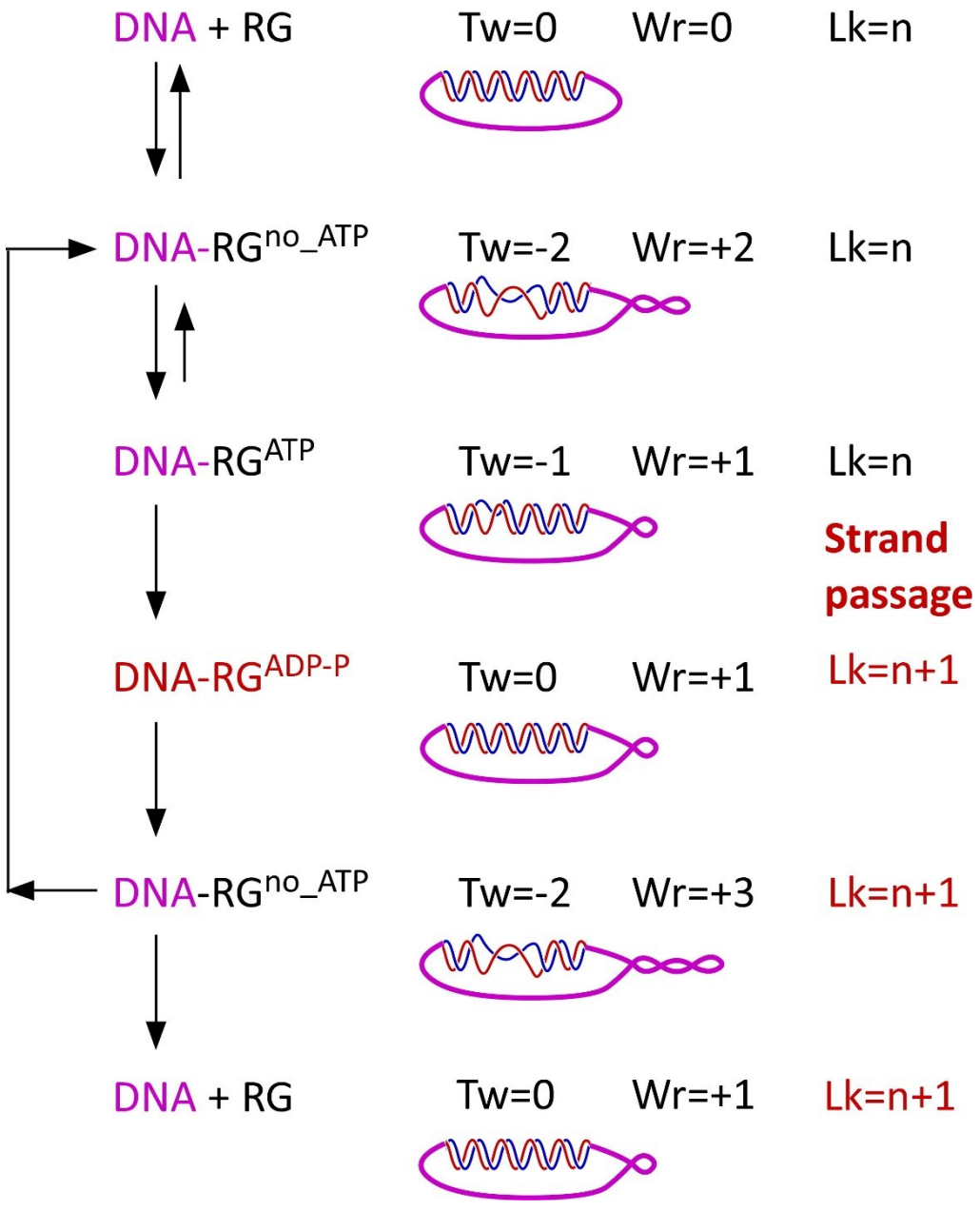

Figure 5. Model for reverse gyrase cycle. The enzyme is viewed as a topological state machine, manipulating DNA twist in an ordered reaction, first via its helicase domain and then via its topoisomerase domain. ATP hydrolysis is absolutely required for strand passage, and linking number increases by +1 at each catalytic cycle.

Finally, these results also indicate that reverse gyrase may be able to positively supercoil DNA until it reaches a natural "set point." Indeed, the fact that affinity for nucleotide is seven-fold lower for positively supercoiled DNA than for negatively supercoiled DNA suggests that the enzyme's overall reaction rate progressively decreases as positive supercoiling increases. We are not aware of other DNA-processing enzymes for which nucleotide affinity depends on DNA supercoiling. Although the total ATP concentration *in vivo* may be much higher than the micromolar affinities determined here, it should be kept in mind that also *in vivo* countless enzymes compete for this ATP. The tight affinity of TopR2 reverse gyrase for ATP means that it is likely to compete effectively against other enzymes for ATP, and the supercoiling-dependence of this affinity suggests that a single topoisomerases species may be sufficient to regulate topological homeostasis of the nucleoid.

Acknowledgements

X.Y. was supported during doctoral training by a scholarship from the China Scholarship Council. Research was supported in part by the Ligue Nationale Contre le Cancer "Equipe Labellisée" program. Further core funding was provided by the Institut Jacques Monod, the University of Paris Diderot (University of Paris), INSERM, CNRS, and Ecole normale supérieiure (Paris Sciences et Lettres).

Bibliography

[1] A. Kikuchi and K. Asai. Reverse-gyrase - a topoisomerase which introduces positive superhelical turns into DNA. *Nature*, 309:677–681, 1984.
[2] P. Forterre, G. Mirambeau, C. Jaxel, M. Nadal, and M. Duguet. High positive supercoiling in vitro catalyzed by an ATP and polyethylene glycol-stimulated topoisomerase from Sulfolobus acidocaldarius. *EMBO J.*, 4:2123–2128, 1985.
[3] S. Nakasu and A. Kikuchi. Reverse gyrase; ATP-dependent type I topoisomerase from Sulfolobus. *EMBO J.*, 4:2705–2710, 1985.
[4] M. Nadal, G. Mirambeau, P. Forterre, W.D. Reiter, and M. Duguet. Positively supercoiled DNA in a virus-like particle of an archaebacterium. *Nature*, 321:256–258, 1986.
[5] H. Atomi, R. Matsumi, and T. Imanaka. Reverse gyrase is not a prerequisite for hyperthermophilic life. *J. Bacteriol.*, 186:4829–4833, 2004.
[6] M. Nadal. Reverse gyrase: an insight into the role of DNA-topoisomerases. *Biochimie*, 89:447–455, 2007.
[7] F. Garnier, H. Debat, and M. Nadal. Type IA DNA Topoisomerases: A Universal Core and Multiple Activities. *Methods in molecular biology (Clifton, NJ)*, 1703:1–20, 2018.
[8] A. Revyakin, R.H. Ebright, and T.R. Strick. Promoter unwinding and promoter clearance by RNA polymerase: detection by single-molecule DNA nanomanipulation. *Proc. Natl. Acad. Sci (USA)*, 101:4776–4780, 2004.
[9] A. Revyakin, C.-Y. Liu, R.H. Ebright, and T.R. Strick. Abortive initiation and productive initiation by RNA polymerase involve DNA scrunching. *Science*, 314:1139–1143, 2006.
[10] M. Kampmann and D. Stock. Reverse gyrase has heat-protective DNA chaperone activity independent of supercoiling. *Nucleic Acids Res.*, 32:3537–3545, 2004.
[11] A. Valenti, G. Perugino, T. Nohmi, M. Rossi, and M. Ciaramella. Inhibition of translesion DNA polymerase by archaeal reverse gyrase. *Nucleic Acids Res.*, 37:4287–4295, 2009.
[12] S.-H. Lee, G.E.-L. Siaw, S. Willcox, J.D. Griffith, and T.-S. Hsieh. Synthesis and dissolution of hemicatenanes by type IA DNA topoisomerases. *Proc. Natl. Acad. Sci. (USA)*, 110:E3587–E3594, 2013.
[13] S. H. Chen, J.L. Plank, S. Willcox, J.D. Griffith, and T.-S. Hsieh. Top3alpha is required during the convergent migration step of double holliday junction dissolution. *PLoS One*, 9:e83582, 2014.
[14] N. Bocquet, A.H. Bizard, W. Abdulrahman, N.B. Larsen, M. Faty, S. Cavadini, R.D. Bunker, S.C. Kowalczykowski, P. Cejka, I.D. Hickson, and N.H. Thomä. Structural and mechanistic insight into holliday-junction dissolution by Topoisomerase IIIalpha and RMI1. *Nat. Struct. Mol. Biol.*, 21:261–268, 2014.
[15] L. Wu, S.L. Davies, P.S. North, H. Goulaouic, J.-F. Riou, H. Turley, K.C. Gatter, and I.D. Hickson. The Bloom's syndrome gene product interacts with topoisomerase III. *J. Biol. Chem.*, 275:9636–9644, 2000.
[16] T. Ogawa, K. Yogo, S. Furuike, K. Sutoh, A. Kikuchi, and K. Kinosita. Direct observation of DNA overwinding by reverse gyrase. *Proc. Natl. Acad. Sci. (USA)*, 112:7495–7500, 2015.
[17] T. Ogawa, K. Sutoh, A. Kikuchi, and K. Kinosita. Torsional stress in dna limits collaboration among reverse gyrase molecules. *The FEBS journal*, 283:1372–1384, 2016.
[18] T.R. Strick, V. Croquette, and D. Bensimon. Single-molecule analysis of DNA uncoiling by a type II topoisomerase. *Nature*, 404:901–904, 2000.
[19] G. Charvin, T.R. Strick, D. Bensimon, and V. Croquette. Topoisomerase IV bends and overtwists DNA upon binding. *Biophys. J.*, 89:384–392, 2005.
[20] G. Charvin, A. Vologodskii, D. Bensimon, and V. Croquette. Braiding DNA: experiments, simulations, and models. *Biophys. J.*, 88:4124–4136, 2005.
[21] G. Charvin, T.R. Strick, D. Bensimon, and V. Croquette. Tracking topoisomerase activity at the single-molecule level. *Annu. Rev. Biophys. Biomol. Struct.*, 34:201–219, 2005.
[22] D.A. Koster, K. Palle, E.S.M. Bot, M.-A. Bjornsti, and N.H. Dekker. Antitumour drugs impede DNA uncoiling by topoisomerase I. *Nature*, 448(7150):213–217, Jul 2007.

[23] A. Basu, M. Hobson, P. Lebel, L.E. Fernandes, E.M. Tretter, J.M. Berger, and Z. Bryant. Dynamic coupling between conformations and nucleotide states in DNA gyrase. *Nat. Chem. Biol.*, 14:565–574, 2018.
[24] N.H. Dekker, T. Viard, C.. Boutier de La Tour, M. Duguet, D. Bensimon, and V. Croquette. Thermophilic topoisomerase I on a single DNA molecule. *J. Mol. Biol.*, 329:271–282, 2003.
[25] J. Gore, Z. Bryant, M.D. Stone, M. Nöllmann, N.R. Cozzarelli, and C. Bustamante. Mechanochemical analysis of DNA gyrase using rotor bead tracking. *Nature*, 439:100, 2006.
[26] A. Basu, A.J. Schoeffler, J.M. Berger, and Z. Bryant. ATP binding controls distinct structural transitions of Escherichia coli DNA gyrase in complex with DNA. *Nat. Struct. Mol. Biol.*, 19:538, 2012.
[27] M.J. Szafran, T. Strick, A. Strzaka, J. Zakrzewska-Czerwinska, and D. Jakimowicz. Á highly processive topoisomerase I: studies at the single-molecule level. *Nucleic Acids Res.*, 42:7935–7946, 2014.
[28] K.H. Gunn, J.F. Marko, and A. Mondragón. An orthogonal single-molecule experiment reveals multiple-attempt dynamics of type IA topoisomerases. *Nat. Struct. Mol. Biol.*, 24:484–490, 2017.
[29] M. Mills, Y.-C. Tse-Dinh, and K.C. Neuman. Direct observation of topoisomerase IA gate dynamics. *Nat. Struct. Mol. Biol.*, 25(12):1111, 2018.
[30] T. Strick, J.F. Allemand, D. Bensimon, A. Bensimon, and V. Croquette. The elasticity of a single supercoiled DNA molecule. *Science*, 271:1835 –1837, 1996.
[31] T. Lionnet, J.-F. Allemand, A. Revyakin, T.R. Strick, O.A. Saleh, D. Bensimon, and V. Croquette. Single-molecule studies using magnetic traps. *Cold Spring Harbor Protocols*, 2012:pdb–top067488, 2012.
[32] W. Bauer and J. Vinograd. The interaction of closed circular DNA with intercalative dyes: I. the superhelix density of SV40 DNA in the presence and absence of dye. *J. Mol. Biol.*, 33:141–171, 1968.
[33] F.B. Fuller. Decomposition of the linking number of a closed ribbon: a problem from molecular biology. *Proc. Natl. Acad. Sci. (USA)*, 75:3557, 1978.
[34] J.H. White and W.R. Bauer. Superhelical DNA with local substructures. A generalization of the topological constraint in terms of the intersection number and the ladder-like correspondence surface. *J. Mol. Biol.*, 195(1):205–213, May 1987.
[35] M. Nadal, C. Jaxel, C. Portemer, P. Forterre, G. Mirambeau, and M. Duguet. Reverse gyrase of sulfolobus: purification to homogeneity and characterization. *Acta Chemica Scandinavica, Series B: Organic Chemistry and Biochemistry*, 27:9102–9108, 1988.
[36] C. Jaxel, M. Nadal, G. Mirambeau, P. Forterre, M. Takahashi, and M. Duguet. Reverse gyrase binding to DNA alters the double helix structure and produces single-strand cleavage in the absence of ATP. *EMBO J.*, 8:3135–3139, 1989.
[37] A. Bizard, F. Garnier, and M. Nadal. TopR2, the second Reverse Gyrase of Sulfolobus solfataricus, exhibits unusual properties. *J. Mol. Biol.*, 408:839–849, 2011.
[38] C. Jaxel, M. Duguet, and M. Nadal. Analysis of DNA cleavage by reverse gyrase from Sulfolobus shibatae B12. *European journal of biochemistry / FEBS*, 260:103–111, 1999.
[39] J. Fan, M. Leroux-Coyau, N.J. Savery, and T.R. Strick. Reconstruction of bacterial transcription-coupled repair at single-molecule resolution. *Nature*, 536:234–237, 2016.
[40] K. Howan, A.J. Smith, L.F. Westblade, N. Joly, W. Grange, S. Zorman, S.A. Darst, N.J. Savery, and T.R. Strick. Initiation of transcription-coupled repair characterized at single-molecule resolution. *Nature*, 490:431–434, 2012.
[41] E.T. Graves, C. Duboc, J. Fan, F. Stransky, M. Leroux-Coyau, and T.R Strick. A dynamic DNA-repair complex observed by correlative single-molecule nanomanipulation and fluorescence. *Nat. Struct. Mol. Biol.*, 22:452–457, 2015.

Materials and Methods

Materials

All restriction enzymes and DNA ligase were purchased from New England Biolabs; thermostable DNA polymerase and modified nucleotides for attachment of DNA to surfaces was purchased from Roche. Oligonucleotides were from Eurofins Genomics. BSA and Tween-20 was from Roche, ATP or non-hydroylzable analog AMP-PNP were from Jena Biosciences. All other chemicals (β-mercaptoethanol, glycerol) were purchased from Merck.

Protein expression and purification.

TopR2 reverse gyrase, the product of the *topR2* gene, was expressed as described previously [37]. To create the TopR2^{Y903F} catalytic mutant we used the QuikChange II Site-Directed Mutagenesis Kit (Agilent) to modify a codon-optimized version of the *topR2* gene inserted between the NdeI and XhoI sites of the pET28b expression vector (Novagen, USA). The TopR2 and TopR2^{Y903F} proteins were expressed and purified essentially as described previously [37] except that a gel filtration step was included. The proteins were dialyzed into the same storage buffer as described previously, however here the glycerol concentration was 50% (v/v). Protein was dispensed into single-use aliquots, snap-frozen in liquid nitrogen, and stored at -80°C.

Preparation of DNA tethers for single-molecule experiments

- **3 kb DNA tether.**

The 3 kbp DNA fragment used in these experiments corresponds to a part of the *Thermus aquaticus rpoC* gene (seq ID Y19223.3, from position 227 to 3190) cloned into the XbaI and SbfI sites of pUC18. The following oligonucleotides, designed for optimal TopR2 binding as per a prior study [38], were then annealed and inserted at the KpnI site of the 3 kbp fragment:

AT-T 5'TGTCAGCCCGTGATATTCATTACTTCTTATCCTAAGTAC
and
AT-B 5'TTAGGATAAGAAGTAATGAATATCACGGGCTGACAGTAC

The recombinant plasmid was cut with XbaI and SbfI and the 3 kbp fragment of interest purified by gel electrophoresis. The 3 kbp fragment was then ligated to 1 kbp biotin-labeled DNA at one end and 1 kbp digoxigenin-labeled DNA at the other end. These 1 kbp DNA fragments were labeled as described previously [9].

- **DNA tethers containing a mismatched bubble.**

For DNA containing a mismatched 10 bp bubble, we used a 2.2 kb DNA fragment that corresponds to a part of the *T. aquaticus rpoC* gene (from position 2103 to 4125) cloned into the XbaI and SbfI sites of pUC18. This DNA fragment was prepared as described above except that before the ligation with the 1 kb biotin-labeled or digoxigenin-labeled DNA fragments, the two following oligonucleotides, both bearing 5' phosphates, were annealed and then ligated into the 2.2 kb DNA between unique HindIII and SpeI sites:

5'-AGCTGGATACTTACAGCCATAT**CAGTTACGCC**TACTCCATCCCATATG
and
5'-CTAGCATATGGGATGGAGTA**TCAGCCGTGT**ATATGGCTGTAAGTATCC

where bases in bold correspond to the 10-bp mismatched bubble region.

For DNA containing a mismatched 5 bp bubble, the same procedure was used but with oligonucleotides

5′–AGCTGGATACTTACAGCCATAT**CAGTT**TACTCCATTCCATCCCATATG

and

5′–CTAGCATATGGGATGGAATGGAGTA**CGTGT**ATATGGCTGTAAGTATCC

- **Assembly in the magnetic trap**

The assembled DNA constructs were attached as described [39] first to streptavidin-coated magnetic beads (MyOne C1, ThermoFisher), then to anti-digoxigenin coated capillaries, and finally placed on a temperature controlled home-built magnetic trap running the PicoTwist software suite (PicoTwist SARL, http://www.picotwist.com).

Single-molecule DNA nanomanipulation.

In all experiments, enzymes with or without nucleotides are injected before introducing DNA supercoiling, and it is ensured that the DNA's mechanical properties are unchanged before and just after injection (i.e. before enzymes begin to act on the DNA).

- **Reverse Gyrase catalytic assays**

Reverse gyrase catalytic assays were performed at 45 ^{o}C in reaction buffer containing 40 mM Na·Hepes pH 8.0, 100 mM NaCl, 10 mM $MgCl_2$, 20 mM β-mercaptoethanol, 0.1% Tween 20 (v/v), 0.5 mg/ml BSA (w/v), and ATP or non-hydroylzable analog AMP-PNP as indicated. The detailed procedures for manipulation in the magnetic trap have been extensively described elsewhere [31, 40, 41, 39]. For these experiments DNA tethers were extended using a 0.2 pN force (1 picoNewton = 10^{-12} N) and reverse gyrase was at 50 pM. Then, we introduced six negative supercoils into the DNA using the magnetic trap to generate a substrate for reverse gyrase. After the reaction was complete, the DNA was once more negatively supercoiled to permit a new reaction round.

- **Reverse Gyrase-DNA unwinding/rewinding assays**

After addition of 50 pM RG but no ATP, we introduced six negative supercoils into the 3 kbp DNA (see Supplementary Fig. S1). After observing a change in DNA extension mediated by RG binding, the magnets were rotated by +12 turns so as to positively supercoil the DNA tethers with ~6 positive supercoils. Reversal of the RG-mediated change in DNA extension was observed before regenerating the initial supercoiling state on the DNA with ~6 negative supercoils.

- **Reverse gyrase unwinding assays on DNA containing a mismatched bubble**

In these assays the 2.2 kbp DNA tethers containing either a 5 base or a 10 base mismatched bubble were negatively supercoiled by six turns and then exposed to 10 pM RG. After observing the DNA unwinding events on the DNA, RG buffer with 0.1% SDS was injected to wash off enzyme bound to DNA. An extra wash step with RG buffer was applied to remove

SDS, and then a second round of RG addition could be carried out.

- **TopR2/TopR2^{Y903F} AMP-PNP binding assays**

Assays for AMP-PNP binding to reverse gyrase and its catalytically inactive mutant TopR2^{Y903F} were conducted in the same experimental conditions as the TopR2 DNA unwinding/rewinding assays conducted on the the 3 kbp DNA tethers.

- **Reverse gyrase catalysis in the presence of AMP-PNP and ATP mixes**

In attempts to optimize data collection we tested a range of ATP:AMP-PNP molar ratios (ranging from 1:1 to 1:20) and concentrations (ATP ranging from 1 to 100 μM), but no clear optimal condition emerged. As a result we present only step amplitude measurements obtained in the range of conditions explored, and not step dwelltime measurements.

Data collection and analysis

Real-time tracking of DNA extension and data analysis were carried out as described previously using the PicoTwist software package [41, 39]. All events for which step-amplitude or step-dwell time measurements were determined were within the linear regime of the extension vs. supercoiling curves as discussed above.

For the step-amplitude measurements, changes of DNA extension (in μm) between two unwinding/rewinding or catalytic steps were measured and then converted to changes in DNA writhe (Wr) according to the extension *vs* supercoiling curve (see Supp. Fig. S1). Histogram plots of step-amplitude distribution were then fitted to a Gaussian or double Gaussian function.

For step-dwell time measurements (including catalytic step-lifetime and AMP-PNP waiting-time measurements), histograms of dwell-time distribution were fitted to single-exponential functions, yielding average lifetime values and the associated standard error. Kinetic analysis was carried out using the linear form of the Michaelis–Menten equation [1].

$$t = \frac{K_M}{Vmax}\left(\frac{1}{[\mathrm{ATP}]}\right) + \frac{1}{Vmax} \qquad [1]$$

Average lifetimes obtained at different ATP concentrations were further plotted as a function of the inverse of ATP concentration. Points for -SC removal and +SC introduction were fitted separately by linear regression to obtain K_M and V_{max}. In the AMP-PNP binding analysis, an AMP-PNP concentration versus association rate scatter plot was created to show the AMP-PNP concentration dependence.

Supplementary Information

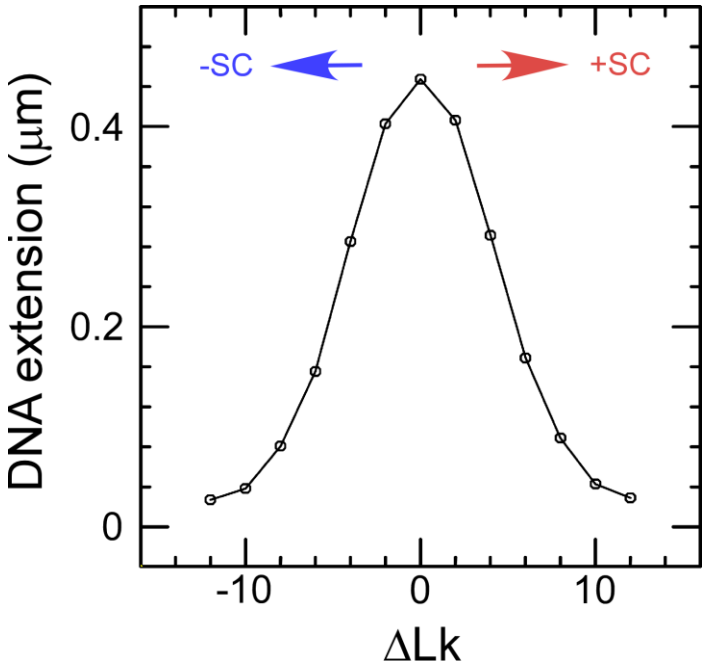

Supplementary Figure 1. Calibration of DNA supercoiling.
DNA extension vs. supercoiling curve for the 3 kb DNA used in these eperiments. Data were recorded for an extending force F = 0.2 pN and at 45°C in the standard reaction buffer (see Materials and Methods). Recording was started at -12 DNA supercoils and ended at +12 supercoils, incrementing the DNA linking number by two units (ΔLk = +2) in a stepwise fashion by rotating the magnets 720° counterclockwise (top view). DNA extension is measured and averaged for 10 seconds at each supercoiling step and plotted as a function of supercoiling number (black circles). In the linear regime for negative supercoiling (from -6 to -2 turns) the DNA extension increases linearly with increasing linking number at a rate of ~60 nm/turn. In the linear regime for positive supercoiling (from +2 to +6 turns) the DNA extension decreases linearly with increasing linking number at a rate of ~60 nm/supercoil. These changes in extension correspond to the formation of plectonemic supercoils as depicted Fig. 1.

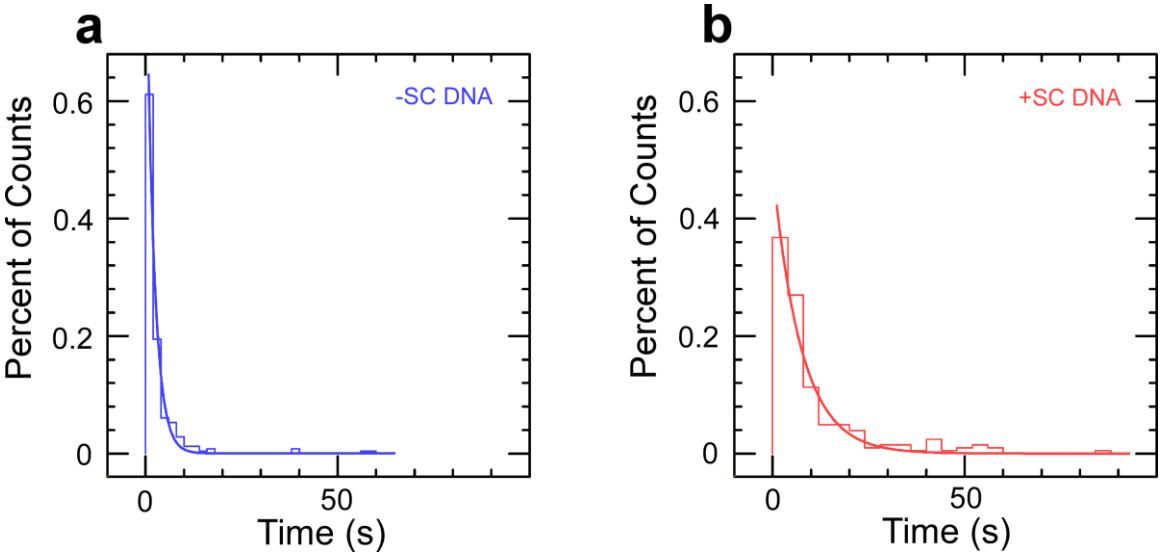

Supplementary Figure 2. Analysis of reverse gyrase catalytic rate by dwelltime measurements for positive or negative supercoiling. Both datasets were obtained at 10 μM ATP. Dwelltimes between successive catalytic events are represented in histogram form. For negatively supercoiled DNA (blue), fitting the dwelltime distribution to a single-exponential (solid blue line) gives a mean of 2.5 ± 0.2 s (SEM, n = 247). For positively supercoiled DNA (red), fitting the dwelltime distribution to a single-exponential (solid red line) gives a mean of 6.8 ± 0.7 s (SEM, n = 206).

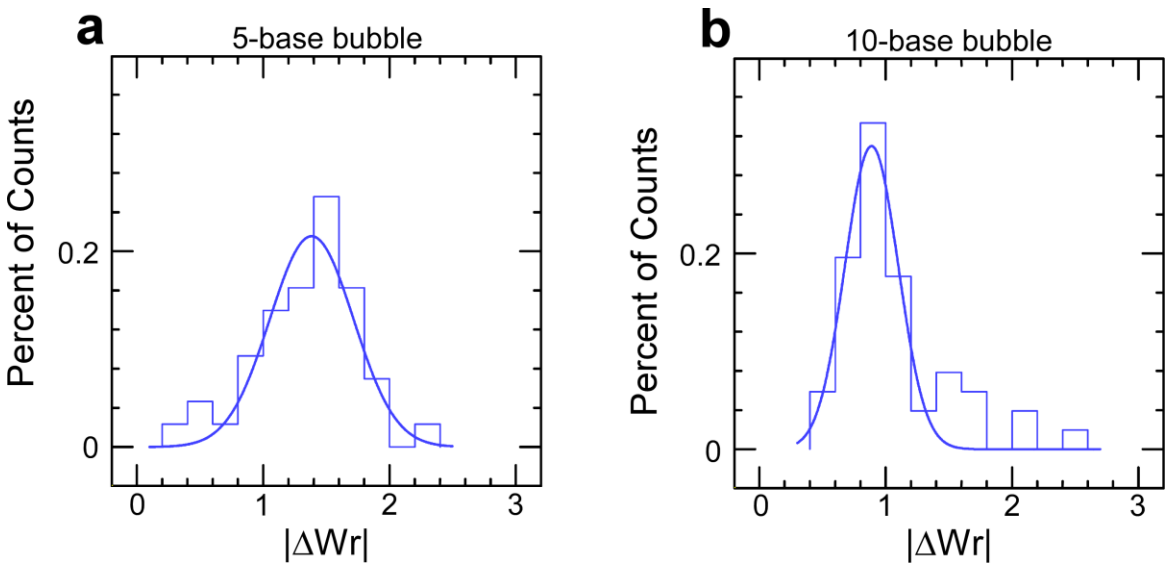

Supplementary Figure 3. DNA unwinding observed in the absence of nucleotide on DNA substrates presenting a region with non-complementary strands. a, ΔWr for initial unwinding by RG as observed on a 2 kbp DNA containing a 5-base mismatched bubble and plotted as a histogram. Fitting to a Gaussian (blue line) gives a mean value of 1.38 ± 0.07 (SEM, n = 43). **b**, ΔWr for initial unwinding by RG as observed on a 2 kbp DNA containing a 10-base mismatched bubble and plotted as a histogram. Fitting to a Gaussian (blue line) gives a mean value of 0.89 ± 0.04 (SEM, n = 51).

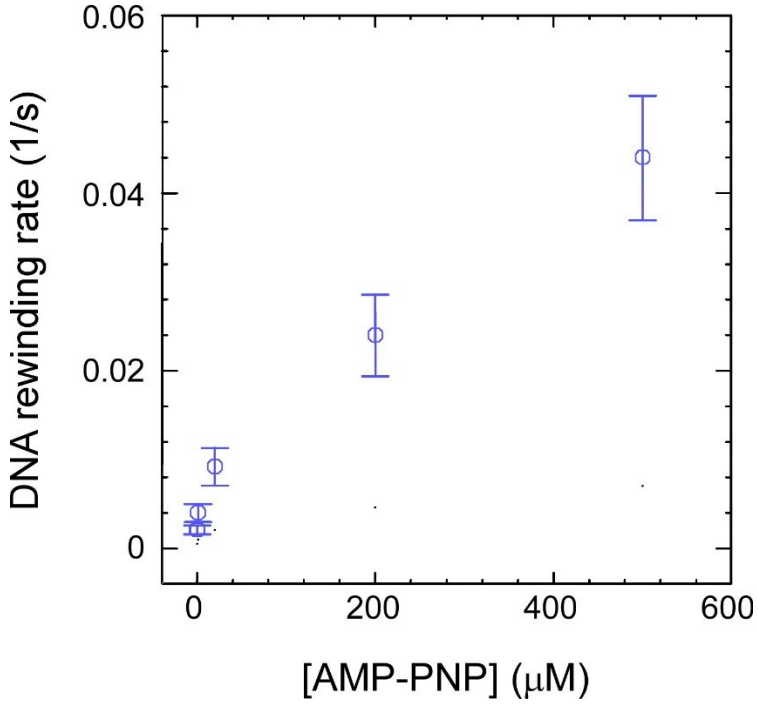

Supplementary Figure 4. Analysis of waiting times for AMP-PNP binding. Plot shows the inverse of the average time elapsed between initial unwinding of DNA by reverse gyrase and subsequent binding of nucleotide to reverse gyrase (as indicated by the observation of apparent partial rewinding upon AMP-PNP binding). For each AMP-PNP concentration we built a histogram representing the distribution of waiting times with 33-77 events collected, and fit to a single-exponential. Points represent inverse of mean values and error bars represent the standard deviation. DNA substrate is negatively supercoiled by ~6 turns in these experiments.

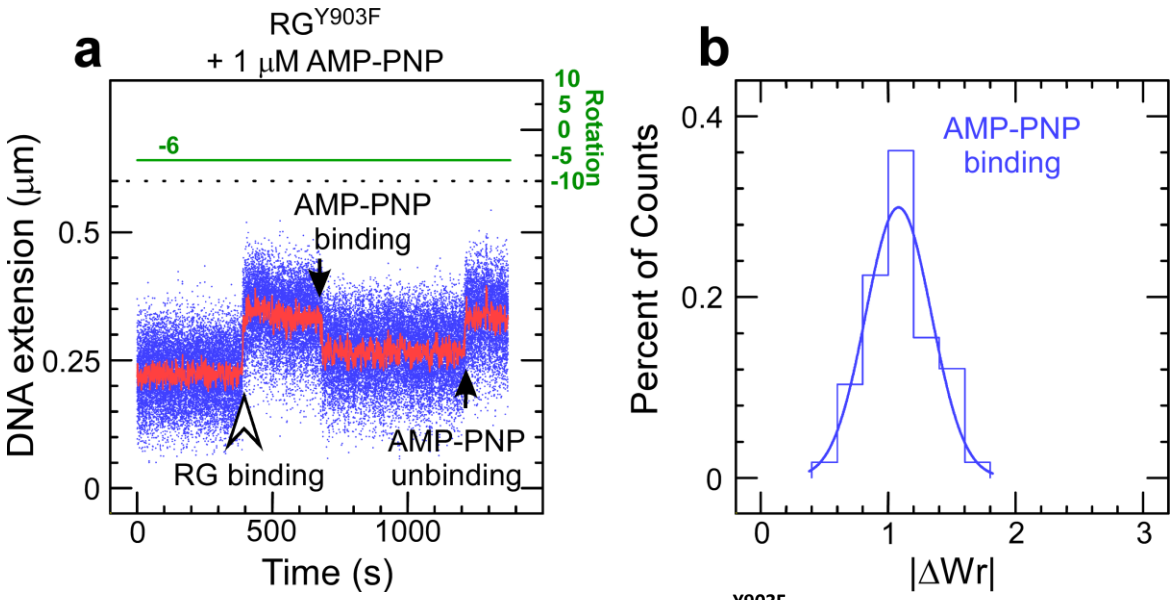

Supplementary Figure 5. Analysis of the TopR2^{Y903F} interactions with negatively supercoiled DNA in the presence of AMP-PNP. **a,** Time-trace showing initial unwinding of DNA by TopR2^{Y903F}, followed by partial rewinding/re-unwinding upon AMP-PNP binding/unbinding. **b**, Histogram showing the change in DNA writhe upon AMP-PNP binding. Fitting to a single-Gaussian (blue line) gives a mean absolute value $<|\Delta Wr|> = 1.08 \pm 0.04$ (SEM, n = 58).

2. TopA, the *Sulfolobus solfataricus* topoisomerase III, is a decatenase

Published online 14 December 2017

Nucleic Acids Research, 2018, Vol. 46, No. 2 ***861–872***
doi: 10.1093/nar/gkx1247

TopA, the *Sulfolobus solfataricus* topoisomerase III, is a decatenase

Anna H. Bizard[1,†], Xi Yang[2,3,†], Hélène Débat[3,4], Jonathan M. Fogg[5,6,7], Lynn Zechiedrich[5,6,7], Terence R. Strick[2,3,8], Florence Garnier[3,4] and Marc Nadal[2,3,*]

[1]Université Versailles St-Quentin, Institut de Génétique et Microbiologie, UMR 8621 CNRS-Université Paris-Sud, 91405 Orsay Cedex, France, [2] Univ Paris Diderot, Sorbonne Paris Cité, Institut Jacques Monod, UMR 7592 CNRS, 75013 Paris, France, [3]Programme Equipes Labellisées, Ligue Contre le Cancer, 75013 Paris, France, [4]Université Versailles St-Quentin, Institut Jacques Monod, UMR 7592 CNRS-Université Paris Diderot, 75013 Paris, France, [5]Department of Molecular Virology and Microbiology, Baylor College of Medicine, One Baylor Plaza, MS: BCM-280, Houston, TX 77030, USA, [6]Verna and Marrs McLean Department of Biochemistry and Molecular Biology, Baylor College of Medicine, One Baylor Plaza, MS: BCM-280, Houston, TX 77030, USA, [7]Department of Pharmacology and Chemical Biology, Baylor College of Medicine, One Baylor Plaza, MS: BCM-280, Houston, TX 77030, USA and [8]Ecole Normale Supérieure, Institut de Biologie de l'Ecole Normale Supérieure (IBENS), CNRS, INSERM, PSL Research University, 75005 Paris, France

Received July 21, 2017; Revised November 29, 2017; Editorial Decision November 30, 2017; Accepted December 12, 2017

ABSTRACT

DNA topoisomerases are essential enzymes involved in all the DNA processes and among them, type IA topoisomerases emerged as a key actor in the maintenance of genome stability. The hyperthermophilic archaeon, *Sulfolobus solfataricus,* contains three topoisomerases IA including one classical named TopA. *Sso*TopA is very efficient at unlinking DNA catenanes, grouping *Sso*TopA into the topoisomerase III family. *Sso*TopA is active over a wide range of temperatures and at temperatures of up to 85°C it produces highly unwound DNA. At higher temperatures, *Sso*TopA unlinks the two DNA strands. Thus depending on the temperature, *Sso*TopA is able to either prevent or favor DNA melting. While canonical topoisomerases III require a single-stranded DNA region or a nick in one of the circles to decatenate them, we show for the first time that a type I topoisomerase, *Sso*TopA, is able to efficiently unlink covalently closed catenanes, with no additional partners. By using single molecule experiments we demonstrate that *Sso*TopA requires the presence of a short single-stranded DNA region to be efficient. The unexpected decatenation property of *Sso*TopA probably comes from its high ability to capture this unwound region. This points out a possible role of TopA in *S. solfataricus* as a decatenase in *Sulfolobus*.

INTRODUCTION

DNA topoisomerases are the enzymes required to manage the topological constraints generated during all DNA transactions (1,2). Topoisomerases carry out this task by introducing transient breaks into DNA: type-II topoisomerases generate double-stranded breaks, whereas type-I topoisomerases generate single-stranded breaks. Type-I topoisomerases can be further subdivided into three subtypes, IA, IB and IC, the IA subtype being the only topoisomerase present in all three domains of life.

Structurally all type IA topoisomerases share a highly conserved toroidal architecture formed by two 'topofold' domains associated to a Toprim domain (3,4). Despite the structural similarities, it is possible to classify type IA enzymes into subfamilies based on their distinct catalytic activities (3,5,6). The subfamily corresponding to *Escherichia coli* protein ω (topoisomerase I, topo I) was the first described (7) and is principally responsible for relaxing negatively supercoiled DNA in mesophilic bacteria (8). The second subfamily of type IA topoisomerases, named topoisomerase III (topo III), was first described in *E. coli* and yeast (9–11). Unlike topo I, bacterial topo III is able to efficiently decatenates linked DNA (9,12–14), as long as one of the circles contains a break in one strand. The *E. coli* and yeast topoisomerase III enzymes are also able to act in coordina-

*To whom correspondence should be addressed. Tel: +33 01 57 27 80 21; Email: marc.nadal@ijm.fr
†These authors contributed equally to the paper as first authors.
Present address: Anna H. Bizard, University of Copenhagen, Institute of Cellular and Molecular Medicine (ICMM), Center for Chromosome Stability (CCS) and Center fo Healthy Ageing (CEHA), Blegdamsvej 3B, DK-2200 København N, Danmark.

tion with partner proteins; the helicase RecQ for *E. coli* or Sgs1 and Rmi1 for yeast, to catalyze catenation and decatenation of dsDNA (14,15). Catenation occurs under conditions where the partner proteins are in excess, decatenation occurs at lower protein concentrations (14). Some topo III enzymes also unlink RNA catenanes (16–18). These diverse *in vitro* activities reflect the fact that topoisomerases III enzymes are implicated in the processing of a wide variety of linked nucleic acids substrates *in vivo*, including double Holliday junctions, hemicatenanes R-loops and D-Loops (14,19–23). Topo III enzymes, and together with helicases in the SF2 group such as RecQ, Sgs1 or BLM, also play key roles in maintaining genome stability both in Bacteria and in Eukarya (24–26).

Finally, the third subfamily of type IA topoisomerases are the reverse gyrases (TopR), a particular topoisomerase unique to and ubiquitous in hyperthermophiles sequenced to date (27,28). Structurally, this enzyme is a chimera between a classical type IA topoisomerase and an SF2 helicase (28,29). This chimera is responsible for adenosinetriphosphate (ATP)-dependent positive supercoiling of the DNA, which is thought to help prevent DNA melting at high temperature (28). However, the precise role of reverse gyrase is not yet understood.

While several organisms, including hyperthermophiles, have two type IA topoisomerases, most of the Crenarchaeota, such as *Sulfolobus solfataricus* P2 (30), have three type IA topoisomerases: a classical type IA topoisomerase (TopA), and two reverse gyrases (TopR1 and TopR2). The few studies that have been carried out on *S. solfataricus* TopA revealed that its relaxation activity on negatively supercoiled DNA is relatively inefficient, suggesting that *S. solfataricus* TopA (*Sso*TopA) may be more similar to topo III than to topo I enzymes (31,32).

In the present study, we characterized *Sso*TopA using ensemble analysis and single molecule experiments. Our data demonstrate that *Sso*TopA belongs to the topoisomerase III subfamily of type IA because it unlinks DNA. Surprisingly, we demonstrated that *Sso*TopA disentangles supercoiled catenanes, without requiring either a gap/nick in one of the DNA circles or additional partner proteins. *Sso*TopA needs only a short single-stranded DNA region to efficiently catalyze the topological conversions.

MATERIALS AND METHODS

Materials

Ethidium bromide was purchased from Boehringer Mannheim. Dithiothreitol (DTT), polyethylenimine, chloroquine and agarose were purchased from Sigma. Ammonium sulfate was from Fisher. Toluene was purchased from VWR Intl. All other chemicals were purchased from Merck. Thermophilic SSB, T5 exonuclease, Nb. BbvCI, Nt. BspQI and all the restriction enzymes were purchased from New England Biolabs (NEB). S1 nuclease was purchased from Fermentas.

Purification of SsoTopA

Expression and purification of *Sso*TopA were performed as described previously (33). A gel filtration step was included to isolate highly pure enzyme for the single molecule experiments. Briefly, we used a 24 ml Superdex 200 prepacked column (GE Healthcare Life Sciences) equilibrated in a buffer containing 40 mM Tris–Cl pH 8.0, 1 M NaCl, 1 mM ethylenediaminetetraacetic acid (EDTA), 0.5 mM β-mercaptoethanol and 10% glycerol. The fractions corresponding to *Sso*TopA were pooled and stored at 4°C. The final preparation was pure, as judged by sodium dodecylsulphate-polyacrylamide gel electrophoresis (SDS-PAGE), with only a single band visible by Coomassie blue staining (Supplementary Figure S1).

DNA relaxation and kinetoplast DNA decatenation

The standard reaction mixture (10 μl) contained 50 mM Tris–HCl, pH 8.0, 0.5 mM DTT, 0.5 mM EDTA, 100 mM NaCl (TR buffer), 15 mM $MgCl_2$ and either 0.15 μg of negatively supercoiled plasmid pTZ18R DNA or 0.5 μg of kinetoplast DNA (from Topogen). After addition of the enzyme, the mixture was incubated at the indicated temperature for up to 30 min. The reaction was stopped by cooling the reaction mixture on ice and adding 0.1% SDS, 25 mg/ml bromophenol blue and 15% sucrose (final concentrations). The samples were loaded onto gels and analyzed by one-dimensional gel electrophoresis (1.2% agarose gel in TEP buffer: 36 mM Tris, 1 mM EDTA, 30 mM NaH_2PO_4) at room temperature and run at 3 V/cm for 6 h. The gel was washed in TEP buffer for 30 min and stained as described previously (34).

Nuclease assay

pTZ18R DNA was incubated with *Sso*TopA at 95°C for 8 min, then cooled at 4°C. DNA was extracted with chloroform/isoamyl alcohol (24:1), precipitated with ethanol, then resuspended in 10 mM Tris–HCl, pH 7, 0.1 mM EDTA and finally incubated with increasing amounts of S1 nuclease at 4°C overnight in the buffer provided by the manufacturer. The reaction products were analyzed by agarose gel electrophoresis as described above except that we used a 2% agarose gel.

T5 exonuclease assay

pTZ18R DNA was incubated with *Sso*TopA in the standard reaction mixture at 95°C for 5 min, then cooled at 4°C. After addition of 10 U of T5 exonuclease, the reactions were incubated for the indicated time at 4°C. The reaction products were analyzed as described above on a 2% agarose gel.

Unlinking intact supercoiled DNA circles

Catenated DNA molecules (catenated products, CP) were from Twister Biotech, Inc. (Houston, TX, USA). These DNA catenanes consist of a 3530 bp large circular DNA (large circle, LC) linked to a 339 bp minicircle (mC) and are generated by λ–integrase-mediated site-specific recombination on the parent plasmid (PP) pMC339 (35). As controls, three different DNA topological forms—supercoiled, linearized or nicked- of these multi-linked catenanes were obtained by incubating the DNA with the restriction enzymes

BamHI or NdeI, or the nicking endonucleases Nt.BspQI or Nb.BbvCI, respectively. The superhelical density of the supercoiled multi-linked DNA was −0.07 (35,36). TopA was incubated in 10 μl TR buffer containing 10 mM $MgCl_2$ and 0.27 μg of catenated DNA at various (as indicated) temperatures for 20 min. Reactions were stopped by cooling the reaction mixture on ice for at least 10 min. A total of 0.1% SDS (final concentration) with Purple Gel Loading Dye (no SDS) (from NEB) was added before loading onto gels. The reaction products were analyzed on 1.7 or 3.5% agarose gels in TEP buffer at room temperature and run at 3 V/cm for 2–4 h. The gels were stained by incubation in TEP buffer containing 2 μg/ml ethidium bromide for 30 min and stored in water before digitalization.

Preparation of streptavidin coated capillaries

To obtain single molecule tracking results at higher temperature, glass capillaries (1.00 mm ID * 0.20 mm Wall, Vitro-Com) were coated with PEG–Biotin–streptavidin. Briefly, after sonication in 1 M KOH for 15 min, capillaries were washed with water then dried with nitrogen gas and coated with MCC primer 80/20 at 110°C (MicroChem) for 10 min, rinsed with 0.5% azide-terminated polystyrene (Sigma) and dissolved in toluene. Capillaries were then dried with nitrogen gas again and incubated overnight with 2 μM DBCO–PEG–Biotin (5 KDa, Interchim) and 2 mM DBCO–PEG (5 KDa, Interchim) dissolved in phosphate-buffered saline (PBS) buffer pH 8.0 overnight at room temperature. After being washed with PBS, capillaries were incubated for 30 min at room temperature with 0.2 mg/ml streptavidin in 10 mM Tris pH 8.0 and 500 mM NaCl. Capillaries were rinsed and then filled with reaction buffer (10 mM Hepes pH 8.0, 200 mM NaCl, 10 mM $MgCl_2$, 20 mM β-mercaptoethanol, 0.1% Tween 20 and 0.5 mg/ml bovine serum albumin (BSA)) and stored at 4°C before use.

DNA preparation for single molecule experiments

The DNA fragment used for the tethered-DNA assays (3 kb) corresponds to a part of the *Thermus aquaticus rpoC* gene (seq ID Y19223.3, from position 227 to 3190) cloned into the XbaI and SbfI sites of pUC18. The following oligonucleotide is inserted at the KpnI site of the *rpoC* gene: 5′-TGTCAGCCCGTGATATTCATTACTTCTTATCCTAA-3′. The recombinant plasmid was cut with XbaI and SbfI, gel purified and the corresponding insert DNA ligated with 1 kb biotin-labeled or digoxigenin-labeled DNA fragments. These 1 kb DNA were labeled as described previously (37).

For DNA containing a permanent 10 bp bubble, we used a 2.2 kb DNA fragment that corresponds to a part of the *T. aquaticus rpoC* gene (from position 2103 to 4125) cloned into XbaI and SbfI sites of pUC18. This DNA fragment was prepared as described above except that before the ligation with the 1 kb biotin-labeled or digoxigenin-labeled DNA fragments, the two following oligonucleotides were annealed and then inserted into the 2.2 kb DNA between the HindIII and SpeI sites: 5′-AGCT GGATACTTACAGCCATAT**CAGTTACGCC**TACTCC ATTCCATCCACTTCCTCATCAACTACCATATG-3′ and 5′-CTAGCATATGGTAGTTGATGAGGAAGTG GATGGAATGGAGTA**TCAGCCGTGT**ATATGGCT GTAAGTATCC-3′ (bases in bold correspond to the bubble region, see Supplementary Figure S6C). The labeled DNA fragments were attached first to the anti-digoxigenin-coated magnetic beads prepared as described (38), then to the streptavidin-coated capillaries, and finally placed on a temperature controlled home-built magnetic trap running the PicoTwist software suite (PicoTwist SARL, http://www.picotwist.com).

SsoTopA relaxation rate analysis during single molecule experiments

The assays were performed at 45°C in 10 mM Hepes pH 8.0, 200 mM NaCl, 10 mM $MgCl_2$, 20 mM β-mercaptoethanol, 0.1% Tween 20 and 0.5 mg/ml BSA. The 3 kb DNA was torsionally constrained and extended in the magnetic field (with a 0.45 pN tensile force). After the addition of 600 pM of *Sso*TopA, DNA molecules were negatively supercoiled by magnetic tweezers (to a superhelical density (σ) ∼ −0.04). When most of the DNA molecules were partially or totally relaxed by the enzyme, a new round of negative supercoiling was performed again on the same DNA. The number of supercoils removed was obtained from the change in extension, compared to the calibration curve for each bead (39).

To measure the processivity of *Sso*TopA (number of supercoils removed during a single burst), the change of DNA extension in each single relaxation burst was measured and then divided by the average step-size achieved from the extension versus supercoiling curve in the linear part of the calibration curve (40), where the number of supercoils relaxed is proportional to the change of DNA extension during one burst.

To analyze the relaxation rate, the lifetimes of relaxation bursts were also measured. The total velocity of one burst was then calculated using the value of a relative processivity divided by the corresponding lifetime. The probability of relaxation ($p_{r(t)}$) during a given time (t) fits with a single exponential:

$$p_{r(t)} = Ce^{\frac{-t}{\tau}}$$

where, τ is the average time and C is a constant.

SsoTopA relaxation experiment with a DNA tether containing a single-stranded region

This experiment was conducted using a similar method as for the processivity and relaxation rate analysis but with the anti-digoxigenin-covered surface as described earlier (41) and anti-digoxigenin coated magnetic beads. A 2.2 kb DNA tether containing a 10 bp mismatch bubble with biotin- and digoxigenin-labeled ends was used, in the same reaction buffer mentioned above. The DNA molecules were extended with 0.42 pN magnetic force at 35°C. Lower *Sso*TopA concentration (6 pM) was used for this experiment. The step size for *Sso*TopA relaxation (number of turns removed by the enzyme in each relaxation step) was then measured by dividing the change of DNA extension

in a single step to the relative step-size obtained from the extension versus supercoiling curve as mentioned above.

RESULTS

*Sso*TopA is a topo III

Recombinant *Sso*TopA was expressed and purified to homogeneity (Supplementary Figure S1). Temperature dependence (Supplementary Figure S2), $MgCl_2$ dependence (Supplementary Figure S3) and NaCl dependence (not shown) of *Sso*TopA activity were identical to those obtained previously (31). By following the DNA relaxation reaction over time, we observed that at 75°C, the apparent optimal temperature (see Supplementary Figure S2), *Sso*TopA partially relaxed all of the highly negatively supercoiled DNA molecules after only 30 s of incubation (Figure 1A). However, further relaxation progressed more slowly and in a step-wise manner requiring at least 16 min for complete relaxation to be achieved (Figure 1A). This activity pattern suggests a higher efficiency of *Sso*TopA on highly negatively supercoiled DNA than on partially relaxed forms. It is consistent with the fact that this reaction is driven by the supercoiling energy stored in the DNA. The step-wise relaxation, with the gradual appearance of progressively more relaxed intermediates, is indicative of a progressive loss of this energy and a distributive mechanism (Figure 1A).

By using a kinetoplast DNA (kDNA) decatenation assay, we observed that *Sso*TopA is highly efficient in decatenating DNA, even at temperatures as high as 95°C (Figure 1B). The kDNA substrate naturally contains nicks or gaps in some of the catenated molecules, which, once decatenated, lead to the appearance of open circular form. This appearance was especially evident when the reaction was performed at 75 and 80°C (Figure 1B). More surprisingly, covalently closed DNA mCs (relaxed and/or supercoiled) were also observed depending on the temperature used for incubation (Figure 1B). Predominantly negatively supercoiled mC products were observed when the reaction was performed at 85–95°C (Figure 1B). The presence of supercoiled products means that, at higher temperatures, decatenation may not have required a nicked mC, suggesting that the presence of a nick or a gap on each catenated molecule is not a prerequisite for decatenation. A type I DNA-topoisomerase, such as *Sso*TopA, only cleaves one strand of the DNA molecule. Consequently, in the absence of a nicked or a gapped DNA region, the decatenation of kDNA catalyzed by *Sso*TopA at high temperature results from two sequential single strand passage events. The first reaction would lead to a transient hemicatenane stabilizing the single-stranded DNA region and consequently promoting the second strand passage reaction, thus providing either the decatenated product or the initial substrate.

*Sso*TopA unlinks DNA at very high temperatures

To better understand the reactions carried out by *Sso*TopA above 75°C, we extended the range of temperature for analysis to as high as 100°C (Figure 2). At temperatures up to 85°C, *Sso*TopA relaxed negatively supercoiled plasmids (Figure 2B and Supplementary Figure S2). At 90°C and above, *Sso*TopA progressively converted the substrate into several fast migrating products, FI* and FI**, (Figure 2B) so named because of their apparent similarity with highly unwound species previously described (42). The appearance of these forms is not due to thermal denaturation or degradation of the DNA substrate alone, as they were not observed in the absence of enzyme (Figure 2A), nor were they observed in the presence of an inactive enzyme. Indeed, reactions lacking the magnesium cofactor essential for *Sso*TopA activity leave the DNA substrate unchanged (Supplementary Figure S3, lane 0). When the enzyme was inactivated with SDS before incubating with DNA, the FI* and FI** forms were no longer produced (Supplementary Figure S4, lane 1).

To investigate formation of the FI* and FI** forms, plasmid substrate was incubated with *Sso*TopA at 95°C over an 8 min time course, samples were removed at the time points indicated and incubated at 4°C prior to gel loading. We observed over time of incubation with *Sso*TopA the disappearance of the supercoiled DNA substrate and the appearance of FI* and FI** forms (Figure 3A). When the samples were further incubated 5 min at 25°C instead of 4°C prior to loading on the gel, the disappearance of the supercoiled DNA substrate was similar (Figure 3, compare -SC in panels A and B) while the accumulation kinetics were higher for FI* and lower for FI** (Figure 3, compare FI* and FI** in panels A and B). These observed differences reflect the conversion of FI** into FI* during the post-incubation at 25°C because the enzyme was inactivated just after the incubation at 95°C (Figure 3B). This conversion of FI** into FI* is reversible and is temperature dependent. Compared to 25°C, incubation at 65°C increased the conversion of FI** into FI* (Supplementary Figure S4, compare lanes 2 and 4). An additional heating of the samples at 95°C for 2 min before loading restored the presence of FI** with the concomitant disappearance of FI* (Supplementary Figure S4, lanes 3 and 5). In both experiments, we did not observe any linear double-stranded DNA or significant additional OC form (Figure 3, panel B and Supplementary Figure S4, compare lanes 2 and 4 with lanes 3 and 5). Therefore, no linear single-stranded form was produced during the unlinking reaction. These results indicate that the FI** corresponds to circular single-stranded DNA.

The single-stranded nature of the FI** form was further confirmed by probing its sensitivity to S1 nuclease. We observed that form FI** was almost completely degraded when incubated at 4°C overnight with 1×10^{-3} units of S1 nuclease whereas form FI* remained intact (Figure 3C). Degradation of FI* required a 10-fold higher amount of S1 nuclease (Figure 3C). The negatively supercoiled form (-SC) contains limited single-stranded regions allowing SI nuclease at high concentration to introduce a nick, leading to an increase in the OC form (Figure 3C). The differential S1 nuclease sensitivity between FI* and FI** indicates that FI** contains a larger single-stranded region than that present in FI*. The circular form of FI* and FI** was further investigated by incubating the unlinked DNA with T5 exonuclease. No degradation of the different DNA forms, including FI* or FI** DNA, was seen (Figure 3D), indicating that the FI* and FI** DNA bands do not possess free ends. FI** were circular single-stranded DNA molecules, a substrate completely degraded by S1 nuclease (Figure 3C) but resis-

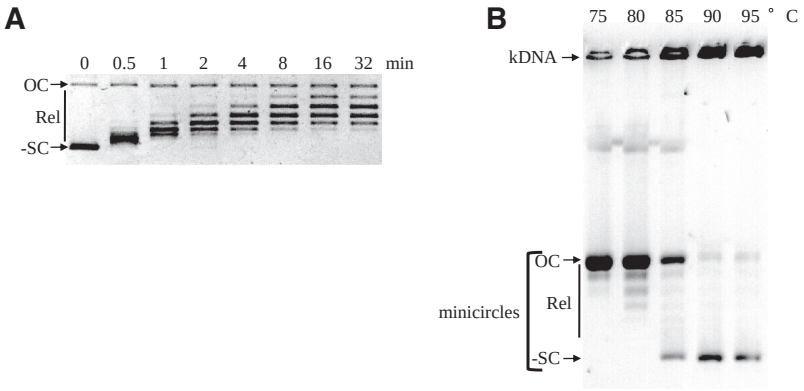

Figure 1. Activity of *Sso*TopA in bulk experiments. (**A**) For relaxation, the protein/pTZ18R DNA molar ratio used was 1:1 and the incubation time was as indicated. The reaction products were analyzed by one dimensional agarose gel electrophoresis. (**B**) Decatenation of kDNA was carried out by adding *Sso*TopA just before the incubation at the indicated temperature for 30 min in the presence of kDNA. The reactions were stopped and kDNA products were separated on a 2% agarose gel. OC indicates open circular DNA, Rel, the relaxed topoisomers and -SC the negatively supercoiled DNA for the pTZ18R plasmid (A) or the mCs (B).

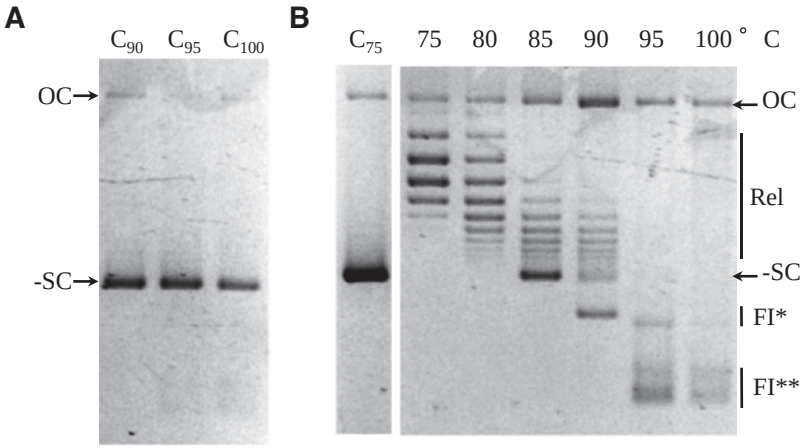

Figure 2. Activity of *Sso*TopA at very high temperatures. (**A**) The DNA controls (lanes $C_{t°c}$) were incubated in the absence of *Sso*TopA for 8 min at the indicated temperatures. (**B**) The pTZ18R substrate was incubated at the temperature indicated in the presence of *Sso*TopA (at a molar ratio of 2:1). C_{75} corresponds to the DNA control incubated at 75°C for 8 min without *Sso*TopA. The reaction products were analyzed by one dimensional agarose gel electrophoresis: OC indicates open circular DNA, Rel, the relaxed topoisomers and -SC the negatively supercoiled DNA form. FI* and FI** correspond to unlinked DNA species and were apparently similar to highly unwound species first described by Parada and Marians (42).

tant to T5 exonuclease (Figure 3D). In contrast, FI* might correspond to two circular single-stranded molecules partially annealed, a substrate less susceptible to S1 nuclease (Figure 3C). Thus, we conclude that *Sso*TopA extensively unlinks the two complementary DNA strands at temperatures ≥85°C, leading to two distinct circular single-stranded DNA (FI**). FI** can convert to FI* depending on the temperature.

*Sso*TopA catalyzes both the melting and annealing of DNA molecules

To further confirm the catalytic nature of the unlinking reaction performed by *Sso*TopA at high temperatures, we conducted a time course experiment at 95°C with a plasmid previously relaxed by *Sso*TopA at 75°C (Figure 4A, 0 min). We observed that the relaxed substrate was almost fully converted into the negatively supercoiled form within the first minute of incubation (Figure 4A, 1 min). The negatively supercoiled double-stranded DNA was subsequently converted to the two unlinked DNA forms FI* and FI** (Figure 4A, 2–8 min). After 8 min, the incubation time needed to convert all the double-stranded DNAs into forms FI* and FI**, the reaction mixture was transferred back to 75°C and the products monitored over time to assess the reversibility of the new species (Figure 4B). After just 30 s of incubation at 75°C, form FI** was almost completely converted into form FI* (Figure 4B, 0.5 min). With longer incubation times, form FI* was progressively converted into negatively supercoiled form before ultimately being relaxed (Figure 4B). To recover the covalently closed circular double-stranded DNA (cccDNA), the activity of *Sso*TopA was therefore required to restore the linking between two circular complementary DNA strands.

We can conclude that (i) *Sso*TopA is quite thermostable as it remains active even after 8 min at 95°C, (ii) *Sso*TopA unlinks the strands of a circular covalently closed double-stranded DNA at higher temperatures, leading to single-

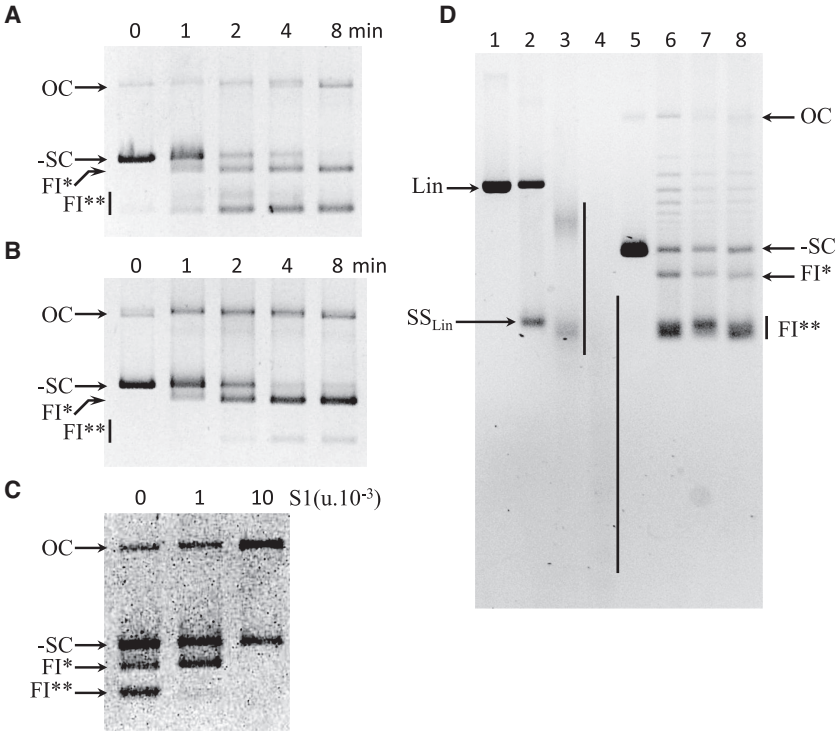

Figure 3. Analysis of FI* and FI** DNA. (**A**) Generation of FI* and FI** over time during incubation with *Sso*TopA at 95°C. After incubation at 95°C for the indicated times, samples were cooled at 4°C for 5 min, centrifuged before adding 0.1% SDS, 25 mg/ml bromophenol blue and 15% sucrose (final concentrations). The samples were further incubated for an additional 5 min at 4°C. The samples were loaded onto an agarose gel at 4°C and run at 3 V/cm for 6 h at 4°C. (**B**) Spontaneous re-annealing of single-stranded forms FI** at 25°C. The samples were treated as in (A) except that they were further incubated for an additional 5 min at 25°C instead of 4°C prior to loading on the gel. (**C**) Sensitivity of the different DNA forms to S1 nuclease. Purified pTZ18R DNA obtained after incubation with TopA at 95°C for 4 min was further incubated at 4°C overnight without (0) or with 1×10^{-3} unit or 10×10^{-3} unit of S1 nuclease. (**D**) Sensitivity of the different DNA forms to T5 exonuclease. pTZ18R was linearized by BamHI (lanes 1–4) and then heated at 95°C for 5 min (lanes 2–4). Unlinked DNA forms (FI* and FI**) were obtained after incubation of pTZ18R with *Sso*TopA at 95°C for 5 min (lanes 6–8). After incubation at 95°C the DNA was further incubated at 4°C without (lanes 1, 2 and 6) or with 10 units of T5 exonuclease for 4 h (lanes 3 and 7) or 16 h (lanes 4 and 8). The *Sso*TopA treated samples (lanes 6–8) were additionally heated at 95°C for 2 min just before loading. Lane 5 is the control DNA substrate (pTZ18R). In the different experiments (A–D), the reaction products were analyzed by one dimensional gel electrophoresis: OC indicates open circular DNA, Lin the linear double stranded DNA, SS_{Lin} the linear single-stranded DNA, -SC the negatively supercoiled DNA form and the particular FI* and FI** forms.

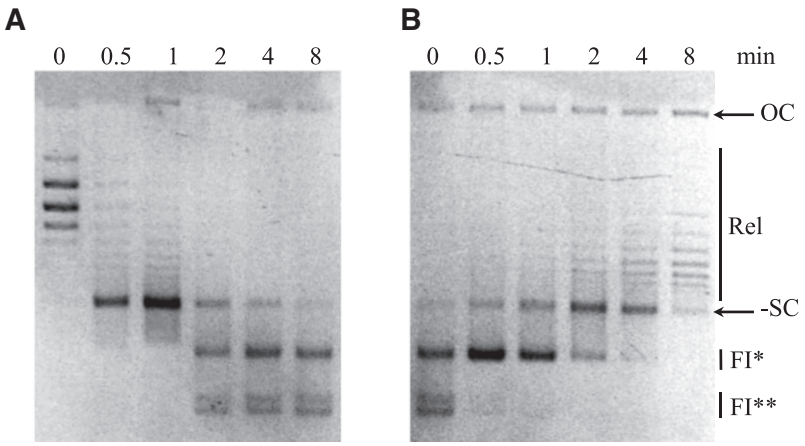

Figure 4. Reversible activity of *Sso*TopA. (**A**) Kinetics of DNA melting catalyzed by *Sso*TopA. The pTZ18R substrate relaxed by *Sso*TopA (molar ratio of 2:1) at 75°C was further incubated at 95°C in the presence of TopA for the time indicated above each corresponding lane. (**B**) Kinetics of DNA re-annealing catalyzed by TopA. The reaction mix (*Sso*TopA and resulting products obtained after 8 min at 95°C, panel (A) was further incubated at 75°C. The incubation times are indicated above each corresponding lane. The reaction products were analyzed by one dimensional agarose gel electrophoresis: OC indicates open circular (nicked) DNA, Rel, the relaxed topoisomers and -SC the negatively supercoiled DNA. FI* and FI** are the unlinked DNA species.

stranded circular DNA at a temperature as high as 95°C, (iii) *Sso*TopA promotes strands annealing at lower temperature as previously described (32), (iv) *Sso*TopA is able to increase or decrease the linking number between the two DNA strands, demonstrating that *Sso*TopA is not able to discriminate between the two possible directions during strand passage. Most importantly, we conclude that the functional *Sso*TopA is able to catalyze the production of single-stranded DNA species as well as its reverse reaction (i.e. the re-annealing of two complementary circular single-stranded molecules back to double-stranded DNA species).

Sulfolobus solfataricus TopA decatenates two covalently closed circular double-stranded DNAs

To precisely analyze the decatenation reaction catalyzed by *Sso*TopA, we used multi-linked catenated double-stranded DNA substrate (35). Briefly, from a plasmid possessing λ-integrase recombination sites (PP, Figure 5A), it is possible to produce, after integrase-mediated recombination, an LC linked to a small DNA mC (Figure 5A). Following isolation of the catenane, three supercoiled DNA forms are present in the final product, corresponding to the parent plasmid (PP_{-SC}), the catenane (CP_{-SC}) and a trace amount of decatenated (unlinked) large circle (LC_{-SC}) (Figure 5B, lanes 5 and 7). A faint band corresponding to the negatively supercoiled minicircle (mC_{-SC}) was observed after linearization of the LC by BamH1 (LC_{Lin}), the parental plasmid being linearized as well (PP_{Lin}) (Figure 5B, lane 1).

To facilitate the identification of the various bands in both the substrate and the reaction products, controls were set up with enzymes that cleave or nick at known positions on the PP, corresponding to the recognition sites on either the large plasmid or the mC component of the catenane (Figure 5A). The NdeI restriction enzyme cleaves both DNA strands within the mC sequence (Figure 5A), linearizing both the PP and the DNA mC (PP_{Lin} and mC_{Lin}, respectively) whereas the LC released from the catenated form remains supercoiled (LC_{-SC}) (Figure 5B, lane 2; Supplementary Figure S5, lane 3). The nicking endonuclease Nt.BspQI cleaves at a specific position on only one DNA strand within the DNA sequence outside of the mC sequence on the PP (see Figure 5A). The incubation of the PP with Nt.BspQI resulted in a single nick generating an open circular form (PP_{OC}) (Figure 5B, lane 6). With the catenated form (CP_{-SC}) as substrate for Nt.BspQI, the LC was nicked but the mC remained supercoiled and linked, resulting in an open circular catenated form (CP_{OC}) (Figure 5B, lane 6). Additional residual electrophoretic bands were also observed in lane 6, they correspond to different noded catenanes (i.e. catenanes with different number of crossovers), but it is difficult to definitively identify each band. The nicking endonuclease Nb.BbvCI cleaves at a specific position on only one DNA strand within the DNA sequence corresponding to the mC (see Figure 5A). The incubation with Nb.BbvCI led to nicking of the PP producing an open circular form (PP_{OC}) (Figure 5B, lane 10 and Supplementary Figure S5, lane 2). With the catenated form substrate, the mC was nicked by Nb.BbvCI but remained linked to the LC. However because of the small size of the mC, there was no significant mobility change of the corresponding catenane compared with that of intact CP_{SC} (Figure 5B, lane 10).

The decatenation of the negatively supercoiled catenated form by *Sso*TopA was performed at two different temperatures, 80°C (Figure 5B, lanes 3, 8 and 11) and 90°C (Figure 5B, lanes 4, 9 and 12), the upper temperature helping us to assign unambiguously the different DNA forms obtained. At 80°C, the catenane was unlinked and the decatenated LC was subsequently relaxed by *Sso*TopA and corresponding topoisomers were visualized after linearization of the PP and mC by NdeI (Figure 5B, lanes 3, LC_{rel}). When incubated with *Sso*TopA at 90°C, these relaxed forms migrated exactly at the same position as the negatively supercoiled LC (LC_{-SC}) in the control experiment (Figure 5B, lane 4 compared with lane 2) as we showed previously for both plasmid and kDNA substrates (Figure 2B, 85–90°C and Figure 1B, above 80°C, respectively). Similar profiles were obtained after incubation of the products with Nb.BbvC1: *Sso*TopA led to the decatenation of the linked rings into an LC and an mC (Figure 5B, lanes 11 and 12 compared with lanes 3 and 4, respectively). While the PP, catenane and decatenated LC were clearly visualized, the released mC, because of its small size was difficult to detect, except when a larger amount of DNA was used and loaded on a higher resolution gel (Supplementary Figure S5).

Importantly, by using supercoiled catenated DNA circle (CP_{-SC}), we demonstrated that *Sso*TopA decatenated the linked circles and produced topoisomers corresponding to a mixture of the relaxed forms of both the decatenated LC (LC_{Rel}) and the PP (PP_{Rel}). These topoisomers were clearly visible as individual bands at 80°C (Figure 5B, lane 8) but as a single band at 90°C (Figure 5B, lane 9), as previously mentioned for the corresponding controls (Figure 5B, lanes 4 and 12). We observed the complete disappearance of catenanes (CP_{-SC}), which were unlinked to release the LC that migrated as the supercoiled form (LP_{-SC}) as illustrated by the higher intensity of the corresponding band (Figure 5B, compare lanes 9 and 7). This complete disappearance of the catenated circles indicates that *Sso*TopA is able to decatenate two linked covalently closed circular DNAs at 80 or 90°C (Figure 5B, lanes 8 and 9). The released DNA mCs are visualized as a single band at 90°C that migrates closely to open circular mC (Supplementary Figure S5, lane 1). By incubating these DNA products with the nicking endonuclease Nb.BbvCI or the restriction enzyme NdeI after the *Sso*TopA decatenation step, the topological pattern of the mCs was simplified: the relaxed mCs were converted to either open circular or linear forms (Supplementary Figure S5, lanes 2 and 3, respectively). Hence, for the first time, by using a multi-linked catenated DNA substrate for which the main DNA species are easily attributed, we demonstrate unambiguously that *Sso*TopA decatenates circular covalently closed double-stranded DNAs.

*Sso*TopA works on single-stranded DNA

To characterize the mechanism catalyzed by *Sso*TopA, we analyzed the reaction using single-molecule manipulation. As shown for other thermophilic enzymes (43,44) including topoisomerases (45,46), *Sso*TopA is active at relatively low temperatures (31). This activity allowed us to perform single

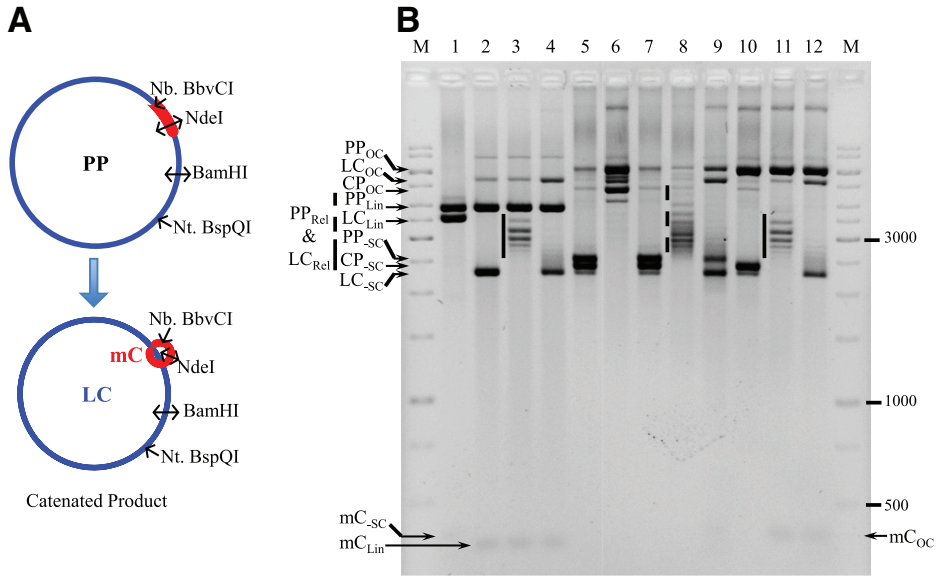

Figure 5. Decatenation of multi-linked DNA circles by *Sso*TopA. (**A**) The PP used to produce catenated molecules (CP) is schematically represented. The catenated DNA is composed of the LC (in blue color) and the mC (in red color) which are interlinked. The different enzymes used to characterize the different forms of these DNA are indicated. (**B**) The multi-linked DNA substrate (lanes 5 and 7) produced from the parent plasmid pMC339 (PP) includes two major species, the PP itself and the catenane (CP), and one minor species, the decatenated LC and mC. The multi-linked DNA substrate was incubated for 1 h at 37°C with BamHI (lane 1), NdeI (lanes 2–4), Nt.BspQI (lane 6) or Nb.BbvCI (lanes 10–12). *Sso* TopA was added in lanes 3, 4, 8, 9, 11 and 12 and incubated for 20 min at 80°C (lanes 3, 8 and 11) or 90°C (lanes 4, 9 and 12) producing relaxed DNA. The vertical plain bars correspond to the large plasmid relaxed at 80°C by TopA and the vertical dashed line corresponds to a mix of large plasmid and catenane relaxed at 80°C by *Sso*TopA. The DNA was loaded onto a 1.7% agarose gel and ran at about 2.5 V cm^{-1} for 3 h. The different DNA bands were attributed according to their size and topological forms (OC, open circular; Lin, linear; Rel, relaxed; -SC, negatively supercoiled) as deduced from the control reactions. M corresponds to the GeneRuler 1 kb ladders (ThermoFisher).

molecule assays at 45 or 35°C. In the absence of *Sso*TopA we observed a background of transient DNA extension fluctuations with a negatively supercoiled DNA substrate at 45°C with a magnetic tensile force of 0.45 pN (Supplementary Figure S6B). These fluctuations were not observed at a lower tensile force (e.g. 0.2 pN, not shown), suggesting that these transient extension changes might correspond to a reversible transition between a decrease of the plectoneme number and an introduction of a single-stranded DNA region (Supplementary Figure S6A) (47). In the absence of *Sso*TopA, these fluctuations were fairly short-lived and the DNA quickly reverted to its original extension (Supplementary Figure S6B). In the presence of *Sso*TopA, a transient extension change (corresponding approximately to one DNA helical repeat) was also observed and preceded each DNA relaxation event (Figure 6A). We hypothesized that *Sso*TopA binds and then operates on the transiently spontaneously formed single-stranded DNA region. This idea is supported by the faster relaxation velocity of *Sso*TopA on highly negatively supercoiled DNA than on partially relaxed forms in bulk experiment (Figure 1A). To test this hypothesis, we performed a similar experiment using DNA that contained a 10 bp mismatch bubble (Supplementary Figure S6C). The size of the bubble is similar to that of the transient melted region we observed (Figure 6A). At 45°C, the enzyme efficiency was dramatically increased with this DNA substrate, relative to the substrate lacking the single-stranded bubble (not shown). Therefore we lowered the enzyme concentration 100-fold and decreased the temperature down to 35°C to allow observation of individual DNA relaxation events (Figure 7A). In the presence of the permanent mismatch bubble, we did not observe the transient extension fluctuation prior to relaxation (Figure 7A and Supplementary Figure S6D). Moreover, *Sso*TopA relaxed the bubble-containing substrate at a higher rate than the fully base-paired substrate (compare Figures 7A and 6A). Indeed, with fully base-paired substrate the apparent *Sso*TopA rate is slow, 26.5 (±10) s to remove one negative supercoil (Figure 6B) compared to the maximum velocity of the *T. maritima* enzyme which is <1 s/supercoil (45). The apparent *Sso*TopA relaxation rate includes the time needed by the enzyme to bind a single-stranded DNA region. The measure of the enzyme velocity on double stranded DNA takes into account the single-stranded formation, the capture of this single-stranded DNA by *Sso*TopA, the strand passage reaction then the dissociation of the enzyme from DNA. In our experiments using DNA without bubble, this velocity is essentially dependent on the single-stranded formation frequency and in a lesser extent on the single strand capture ability. Moreover, we found that although most of the time *Sso*TopA relaxed only few supercoils per relaxation burst (Figure 6C) with an average of 2.83 supercoils/burst. The presence of a permanent bubble leads to a decrease of the *Sso*TopA processivity with an average of 1.50 supercoils relaxed/burst (Figure 7B). These results indicate that *SsoTopA* has very limited processivity contrary to the highly processive type I enzymes of *T. maritima* and *Streptomyces coelicolor* (45,48).

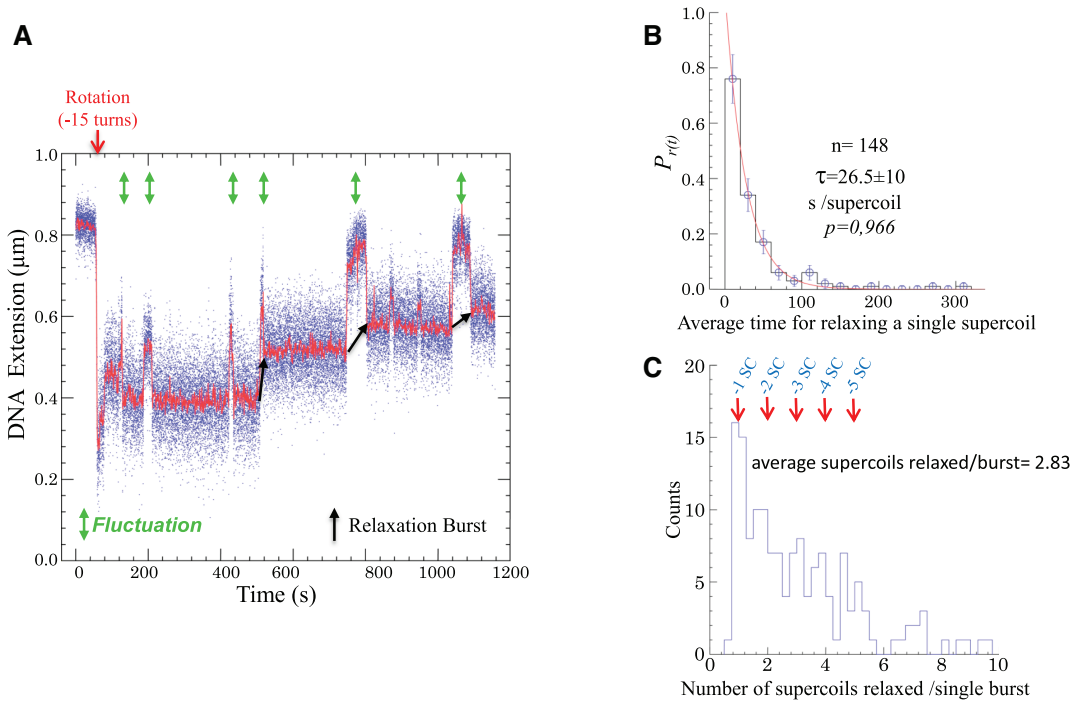

Figure 6. Relaxation activity of *Sso*TopA on single molecule. (**A**) Time-trace of a DNA extension variation at 45°C of a 3 kb DNA extended by a force of 0.45 pN in the presence of 600 pM of *Sso*TopA. The time at which the negative supercoils are added to the DNA by rotating the magnet, is indicated by a red arrow. Extension length fluctuations are indicated by green arrows and the relaxation burst by black arrows. (**B**) Histograms of the average time in second per supercoil removed. The red line is the best fit (*P*-value = 0.966) using the single exponential equation $p_{r(t)} = Ce^{\frac{-t}{\tau}}$, where τ is the average time. A total of 148 relaxation events were used in this analysis. (**C**) Histograms of the burst processivity of *Sso*TopA. The number of supercoils removed was obtained from the extension variation using, for each bead, its calibration curve (39). The periodicity of one for the supercoil removal is indicated above the peaks. A total of 148 relaxation events were used in this analysis.

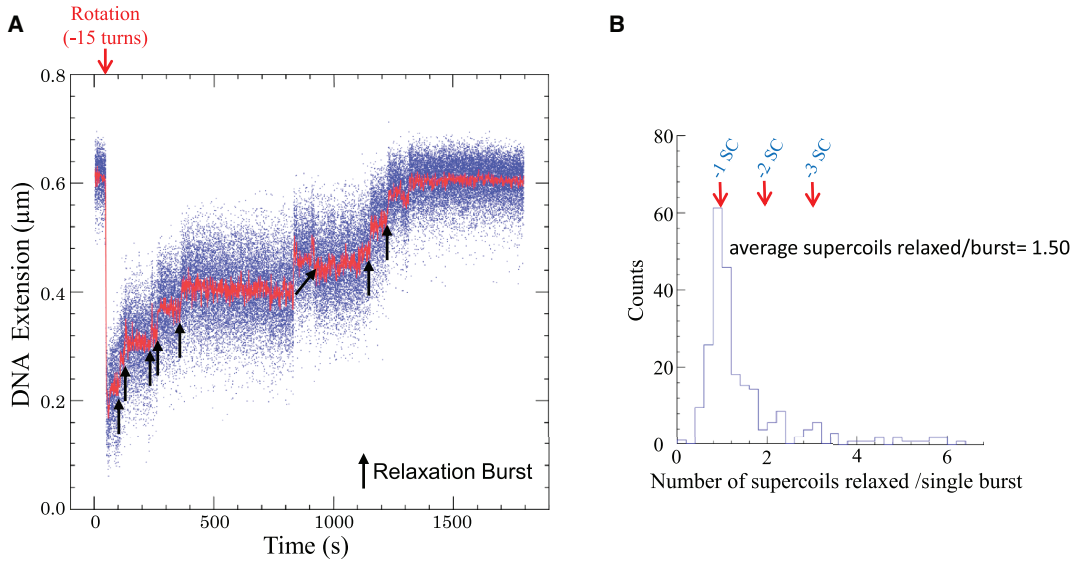

Figure 7. Relaxation activity of *Sso*TopA on single molecule containing a permanent single-stranded DNA bubble. (**A**) Time-trace of the DNA extension variation at 35°C of the 2.2 kb DNA extended by a force of 0.42 pN and in the presence of 6 pM *Sso*TopA. (**B**) Histograms of the burst processivity of *Sso*TopA on a DNA containing a bubble. The number of supercoils removed was obtained from the extension variation using the calibration curve.

DISCUSSION

The type IA topoisomerases share a common structure and are able to perform multiple activities on a variety of DNA substrates. The efficiencies of these enzymes on their various substrates, however, are different. These differences allow to further subdivide the enzymes into two groups: the processive topo I enzymes efficiently remove negative supercoils at a high rate (45,48–50) whereas the topo III enzymes are distributive, relaxing negative supercoils at a much slower rate than the topo I enzymes (9,50). Unlike topoisomerase I, topoisomerase III is able to decatenate DNA, requiring at least one of the catenated circles to have a break in one strand (9,12,51). Moreover, decatenation reaction could occur with cccDNA in the presence of an excess of helicase (14,15). Finally, topoisomerase III is also much more efficient on DNA containing a single-stranded DNA region (51).

In the present report, we show that *Sso*TopA is efficient at relaxing and unlinking DNA, both activities requiring negatively supercoiled DNA. Indeed, like a topoisomerase III, *Sso*TopA decatenates linked DNA. Thus, we prove that *Sso*TopA is a topo III, as previously suggested by a phylogenetic analysis (31). kDNA is a network of catenated DNA circles, some of which naturally contain nicks or gaps. It was, thus, impossible to determine whether *Sso*TopA could decatenate cccDNA. Precisely topologically defined multilinked catenanes were chosen to address this problem. With this substrate, we proved that *Sso*TopA decatenated two cccDNA. The decatenation reaction of cccDNA was an unexpected intrinsic property for a type I topoisomerase never reported before. This activity implies that two successive single-strand passage events should be performed on a single-stranded DNA region (cleavage, strand passage and resealing) to disentangle DNA.

Because *Sso*TopA is a type IA topoisomerase, its intrinsic activity must depend on single-stranded DNA regions for both relaxation and decatenation. Transient short-lived base-pair opening, even at temperatures below the DNA melting temperature, has been observed previously (47). Using a single molecule assay, we directly observed for the first time individual *Sso*TopA relaxation events. Indeed, *Sso*TopA uses the breathing of negatively supercoiled DNA to provide a transient single-stranded region to act upon to initiate relaxation. When a substrate engineered to contain a single-stranded DNA bubble region was used, the reaction rate increased drastically, verifying that single stranded DNA stimulates *Sso*TopA. We also observed that the stabilization of single-stranded regions by adding single strand binding proteins (SSBs) stimulates kDNA decatenation by *Sso*TopA (see Supplementary Figure S7), as observed previously for *Saccharomyces cerevisiae* topo III (14). A very recent report indicates that during DNA relaxation, *E. coli* topo I changes its conformation with a high frequency and successful strand passage events occur with a much lower frequency (52). Our single molecule experiments suggest that the rate-limiting step corresponds to the time required to trap single-stranded DNA. *Sso*TopA had previously been found to cleave and reseal single-stranded DNA oligonucleotides (32) or RNA molecules (18). Similarly, the *Nanoarchaeum equitans* hyperthermophilic enzyme, closely related to *Sso*TopA, is active on single-stranded DNA regions for dissolving hemicatenanes (22).

Unlinked DNA products were observed when the DNA substrate was incubated with *Sso*TopA at temperatures of $\geq$90°C. These DNA species have been reported during the initiation of pBR322 replication and referred to as FI* and FI** DNA (42). These two previously reported forms had similar increased electrophoretic mobility and S1 nuclease sensitivity as those we observed in the current study. For *Desulfurococcus amyloliticus* topo III such extensive unwinding was also observed but only after a long incubation time and only at very high temperatures (at least 90°C) (53). Unfortunately, the two highly unwound DNA forms observed in that study, also referred to as FI* and FI**, have not been fully characterized (53).

More recently, it has been shown that unwinding and unlinking of two complementary DNA strands can be performed by *S. cerevisiae* topo III in the presence of RPA or SSB, the eukaryotic and bacterial single-strand binding protein respectively, or Sgs1, the yeast SF2 helicase partner of topo III (14). Catenation of partially single-stranded DNA was also obtained by adding Rmi1, another partner of yeast topo III (14). It is likely that during the catenation/decatenation processes, topoisomerases III enzymes act on the single-stranded DNA region induced by these proteins. Indeed, all of these topo III partners are required for decatenation in numerous organisms and are essential to the maintenance of genome integrity (14,22,25). The unlinking feature is retained in the reaction catalyzed by *Sso*TopA except that no additional protein is required because single-stranded regions are, instead, favored by high temperature. Hence, depending on the temperature, *Sso*TopA is able either to promote or to prevent the unlinking of the two DNA strands. This observation implies that *Sso*TopA itself is not able to direct the strand passage and does not discriminate the direction of this strand passage as reported for *E. coli* ω protein (49,54), *T. maritima* topo I (45) or *N. equitans* topo III (22).

Recently, it was shown that yeast topo III partners with Sgs1 and Rmi1 or human topo IIIα partners with BLM and Rmi1 to form the dissolvasome which can resolve hemicatenanes (14,55). This complex decatenates kDNA, just as we observed for *Sso*TopA. Moreover, *N. equitans*, topo III is able to form or unlink hemicatenanes on its own (22) but it cannot be excluded that *Neq*Topo III possesses a true decatenation activity as its orthologous *Sso*TopA. Indeed, the decatenation activity that we observed for *Sso*TopA, could be a general property extended to all the topoisomerases III enzymes, either alone or in association with a SF2 helicase and proteins containing oligonucleotide-binding domain (OB fold).

*Sso*TopA is a topo III able to manipulate a wide variety of substrates, at least *in vitro*. It is obvious that single-stranded DNA regions required for the enzyme activity can be spontaneously formed *in vivo* due to the wide temperature range at which *Sulfolobus* cells divide (46,56). Considering that *Sso*TopA is fully competent to decatenate DNA, *Sso*TopA is licensed for, at least, the decatenation of hemicatenanes generated during replication, as reported for its homologue from *N. equitans* (22). Therefore, *Sso*TopA could be a relevant candidate to participate in chromosome segregation

in *Sulfolobus*. This possibility is strengthened by the phenotype of the *topA* mutant obtained in *S. islandicus* (slow growth and defects in cell-cycle control), which strongly suggests that TopA plays a major role in resolving DNA entanglements during the cell cycle and in particular during the chromosome segregation step (57). Alternatively, TopoVI, the unique type II topoisomerase of *Sulfolobus* cells, may perform this action.

*Sso*TopA can perform a closely related decatenation reaction on knotted RNA suggesting another potential role of the enzyme in DNA transcription by acting on R-loops, as recently proposed (18). Finally, as demonstrated in this work, *Sso*TopA alone is unable to influence the direction of DNA strand transfer. Proteins known to associate with *Sso*TopA, such as Hel112 or SSB, could promote or limit the choice between the different possible reactions, as previously suggested (33). The action of other proteins could modulate *Sso*TopA activity, even without a direct interaction, but only by acting on DNA as proposed for topo III enzymes from other organisms (14,22). Thus, during the segregation process, the proteins involved in the chromosome tracking would allow *Sso*TopA to modulate the direction of strand transfer. To date, the importance of the different activities assumed by *Sso*TopA in DNA metabolism processes remains to be more fully characterized *in vivo*. Comparison of these activities catalyzed by the topoisomerase III enzymes throughout the three domains of life and organisms living in different conditions, especially those living at high temperature, will help us to understand their importance in the genomic stability and evolution.

SUPPLEMENTARY DATA

Supplementary Data are available at NAR Online.

ACKNOWLEDGEMENTS

We are grateful to Shuang Wang for providing us the DNA substrate containing a single-stranded DNA bubble used in the single molecule experiments and Jean-François Riou for helpful discussions.

FUNDING

Centre National de la Recherche Scientifique; National Institutes of Health [R56 AI054830, R01 GM115501 to L.Z., in part]. Funding for open access charge: Laboratory Grants.
Conflict of interest statement. None declared.

REFERENCES

1. Champoux,J.J. (2001) DNA topoisomerases: structure, function, and mechanism. *Annu. Rev. Biochem.*, **70**, 369–413.
2. Wang,J.C. (2002) Cellular roles of dna topoisomerases: a molecular perspective. *Nat. Rev. Mol. Cell Biol.*, **3**, 430–440.
3. Duguet,M., Serre,M.-C. and Bouthier de La Tour,C. (2006) A universal type IA topoisomerase fold. *J. Mol. Biol.*, **359**, 805–812.
4. Viard,T. and Bouthier de La Tour,C. (2007) Type IA topoisomerases: a simple puzzle? *Biochimie*, **89**, 456–467.
5. Tse-Dinh,Y.C. (1998) Bacterial and archeal type I topoisomerases. *Biochim. Biophys. Acta*, **1400**, 19–27.
6. Viard,T., Lamour,V., Duguet,M. and Bouthier de la Tour,C. (2001) Hyperthermophilic topoisomerase I from Thermotoga maritima. A very efficient enzyme that functions independently of zinc binding. *J. Biol. Chem.*, **276**, 46495–46503.
7. Wang,J.C. (1971) Interaction between DNA and an Escherichia coli protein omega. *J. Mol. Biol.*, **55**, 523–533.
8. Zechiedrich,E.L., Khodursky,A.B., Bachellier,S., Schneider,R., Chen,D., Lilley,D.M. and Cozzarelli,N.R. (2000) Roles of topoisomerases in maintaining steady-state DNA supercoiling in Escherichia coli. *J. Biol. Chem.*, **275**, 8103–8113.
9. DiGate,R.J. and Marians,K.J. (1988) Identification of a potent decatenating enzyme from Escherichia coli. *J. Biol. Chem.*, **263**, 13366–13373.
10. DiGate,R.J. and Marians,K.J. (1989) Molecular cloning and DNA sequence analysis of Escherichia coli topB, the gene encoding topoisomerase III. *J. Biol. Chem.*, **264**, 17924–17930.
11. Wallis,J.W., Chrebet,G., Brodsky,G., Rolfe,M. and Rothstein,R. (1989) A hyper-recombination mutation in S-Cerevisiae identifies a novel eukaryotic topoisomerase. *Cell*, **58**, 409–419.
12. Hiasa,H., DiGate,R.J. and Marians,K.J. (1994) Decatenating activity of Escherichia coli DNA gyrase and topoisomerases I and III during oriC and pBR322 DNA replication in vitro. *J. Biol. Chem.*, **269**, 2093–2099.
13. Nurse,P., Levine,C., Hassing,H. and Marians,K.J. (2003) Topoisomerase III can serve as the cellular decatenase in Escherichia coli. *J. Biol. Chem.*, **278**, 8653–8660.
14. Cejka,P., Plank,J.L., Dombrowski,C.C. and Kowalczykowski,S.C. (2012) Decatenation of DNA by the S. cerevisiae Sgs1-Top3-Rmi1 and RPA complex: a mechanism for disentangling chromosomes. *Mol. Cell*, **47**, 886–896.
15. Harmon,F.G., DiGate,R.J. and Kowalczykowski,S.C. (1999) RecQ helicase and topoisomerase III comprise a novel DNA strand passage function: a conserved mechanism for control of DNA recombination. *Mol. Cell*, **3**, 611–620.
16. Wang,H., Di Gate,R.J. and Seeman,N.C. (1996) An RNA topoisomerase. *Proc. Natl. Acad. Sci. U.S.A.*, **93**, 9477–9482.
17. Xu,D., Shen,W., Guo,R., Xue,Y., Peng,W., Sima,J., Yang,J., Sharov,A., Srikantan,S., Yang,J. *et al.* (2013) Top3β is an RNA topoisomerase that works with fragile X syndrome protein to promote synapse formation. *Nat. Neurosci.*, **16**, 1238–1247.
18. Ahmad,M., Xue,Y., Lee,S.K., Martindale,J.L., Shen,W., Li,W., Zou,S., Ciaramella,M., Debat,H., Nadal,M. *et al.* (2016) RNA topoisomerase is prevalent in all domains of life and associates with polyribosomes in animals. *Nucleic Acids Res.*, **44**, 6335–6349.
19. Wu,L. and Hickson,I.D. (2003) The Bloom's syndrome helicase suppresses crossing over during homologous recombination. *Nature*, **426**, 870–874.
20. Plank,J.L. and Hsieh,T.-S. (2006) A novel, topologically constrained DNA molecule containing a double Holliday junction: design, synthesis, and initial biochemical characterization. *J. Biol. Chem.*, **281**, 17510–17516.
21. Yang,J., Bachrati,C.Z., Ou,J., Hickson,I.D. and Brown,G.W. (2010) Human topoisomerase IIIalpha is a single-stranded DNA decatenase that is stimulated by BLM and RMI1 *J. Biol. Chem.*, **285**, 21426–21436.
22. Lee,S.-H., Siaw,G.E.-L., Willcox,S., Griffith,J.D. and Hsieh,T.-S. (2013) Synthesis and dissolution of hemicatenanes by type IA DNA topoisomerases. *Proc. Natl. Acad. Sci. U.S.A.*, **110**, E3587–E3594.
23. Fasching,C.L., Cejka,P., Kowalczykowski,S.C. and Heyer,W.-D. (2015) Top3-Rmi1 dissolve Rad51-mediated D Loops by a topoisomerase-based mechanism. *Mol. Cell*, **57**, 595–606.
24. Usongo,V. and Drolet,M. (2014) Roles of type 1A topoisomerases in genome maintenance in Escherichia coli. *PLoS Genet.*, **10**, e1004543.
25. Bizard,A.H. and Hickson,I.D. (2014) The dissolution of double Holliday junctions. *Cold Spring Harb. Perspect. Biol.*, **6**, a016477.
26. Bocquet,N., Bizard,A.H., Abdulrahman,W., Larsen,N.B., Faty,M., Cavadini,S., Bunker,R.D., Kowalczykowski,S.C., Cejka,P., Hickson,I.D. *et al.* (2014) Structural and mechanistic insight into Holliday-junction dissolution by Topoisomerase IIIα and RMI1. *Nat. Struct. Mol. Biol.*, **21**, 261–268.
27. Forterre,P. (2002) A hot story from comparative genomics: reverse gyrase is the only hyperthermophile-specific protein. *Trends Genet.*, **18**, 236–237.

28. Nadal,M. (2007) Reverse gyrase: an insight into the role of DNA-topoisomerases. *Biochimie*, **89**, 447–455.
29. Jaxel,C., Bouthier de la Tour,C., Duguet,M. and Nadal,M. (1996) Reverse gyrase gene from Sulfolobus shibatae B12: gene structure, transcription unit and comparative sequence analysis of the two domains. *Nucleic Acids Res.*, **24**, 4668–4675.
30. She,Q.Q., Singh,R.K.R., Confalonieri,F.F., Zivanovic,Y.Y., Allard,G.G., Awayez,M.J.M., Chan-Weiher,C.C.C., Clausen,I.G.I., Curtis,B.A.B., De Moors,A.A. *et al.* (2001) The complete genome of the crenarchaeon Sulfolobus solfataricus P2. *Proc. Natl. Acad. Sci. U.S.A.*, **98**, 7835–7840.
31. Dai,P., Wang,Y., Ye,R., Chen,L. and Huang,L. (2003) DNA topoisomerase III from the hyperthermophilic archaeon Sulfolobus solfataricus with specific DNA cleavage activity. *J. Bacteriol.*, **185**, 5500–5507.
32. Chen,L. and Huang,L. (2006) Oligonucleotide cleavage and rejoining by topoisomerase III from the hyperthermophilic archaeon Sulfolobus solfataricus: temperature dependence and strand annealing-promoted DNA religation. *Mol. Microbiol.*, **60**, 783–794.
33. Valenti,A., De Felice,M., Perugino,G., Bizard,A., Nadal,M., Rossi,M. and Ciaramella,M. (2012) Synergic and opposing activities of thermophilic RecQ-like helicase and topoisomerase 3 proteins in holliday junction processing and replication fork stabilization. *J. Biol. Chem.*, **287**, 30282–30295.
34. Bizard,A., Garnier,F. and Nadal,M. (2011) TopR2, the second reverse gyrase of sulfolobus solfataricus, exhibits unusual properties. *J. Mol. Biol.*, **408**, 839–849.
35. Fogg,J.M., Kolmakova,N., Rees,I., Magonov,S., Hansma,H., Perona,J.J. and Zechiedrich,E.L. (2006) Exploring writhe in supercoiled minicircle DNA. *J. Phys. Condens. Matter*, **18**, S145–S159.
36. Zechiedrich,E.L., Khodursky,A.B. and Cozzarelli,N.R. (1997) Topoisomerase IV, not gyrase, decatenates products of site-specific recombination in Escherichia coli. *Genes Dev.*, **11**, 2580–2592.
37. Revyakin,A., Liu,C., Ebright,R.H. and Strick,T.R. (2006) Abortive initiation and productive initiation by RNA polymerase involve DNA scrunching. *Science*, **314**, 1139–1143.
38. Duboc,C., Fan,J., Graves,E.T. and Strick,T.R. (2017) Preparation of DNA substrates and functionalized glass surfaces for correlative nanomanipulation and colocalization (NanoCOSM) of single molecules. *Methods Enzymol.*, **582**, 275–296.
39. Strick,T.R., Allemand,J.-F., Bensimon,D., Bensimon,A. and Croquette,V. (1996) The elasticity of a single supercoiled DNA molecule. *Science*, **271**, 1835–1837.
40. Lionnet,T., Allemand,J.-F., Revyakin,A., Strick,T.R., Saleh,O.A., Bensimon,D. and Croquette,V. (2012) Single-molecule studies using magnetic traps. *Cold Spring Harb. Protoc.*, **2012**, 34–49.
41. Fan,J., Leroux-Coyau,M., Savery,N.J. and Strick,T.R. (2016) Reconstruction of bacterial transcription-coupled repair at single-molecule resolution. *Nature*, **536**, 234–237.
42. Parada,C.A. and Marians,K.J. (1989) Transcriptional activation of pBR322 DNA can lead to duplex DNA unwinding catalyzed by the Escherichia coli preprimosome. *J. Biol. Chem.*, **264**, 15120–15129.
43. Lin,H.-K.H., Chase,S.F.S., Laue,T.M.T., Jen-Jacobson,L.L. and Trakselis,M.A.M. (2012) Differential temperature-dependent multimeric assemblies of replication and repair polymerases on DNA increase processivity. *Biochemistry*, **51**, 7367–7382.
44. Choi,J.-Y., Eoff,R.L., Pence,M.G., Wang,J., Martin,M.V., Kim,E.-J., Folkmann,L.M. and Guengerich,F.P. (2011) Roles of the four DNA polymerases of the crenarchaeon Sulfolobus solfataricus and accessory proteins in DNA replication. *J. Biol. Chem.*, **286**, 31180–31193.
45. Dekker,N.H., Viard,T., Bouthier de la Tour,C., Duguet,M., Bensimon,D. and Croquette,V. (2003) Thermophilic topoisomerase I on a single DNA molecule. *J. Mol. Biol.*, **329**, 271–282.
46. Couturier,M., Bizard,A.H., Garnier,F. and Nadal,M. (2014) Insight into the cellular involvement of the two reverse gyrases from the hyperthermophilic archaeon Sulfolobus solfataricus. *BMC Mol. Biol.*, **15**, 18.
47. Phelps,C., Lee,W., Jose,D., Hippel von,P.H. and Marcus,A.H. (2013) Single-molecule FRET and linear dichroism studies of DNA breathing and helicase binding at replication fork junctions. *Proc. Natl. Acad. Sci. U.S.A.*, **110**, 17320–17325.
48. Szafran,M.J., Strick,T., Strzałka,A., Zakrzewska-Czerwińska,J. and Jakimowicz,D. (2014) A highly processive topoisomerase I: studies at the single-molecule level. *Nucleic Acids Res.*, **42**, 7935–7946.
49. Dekker,N.H., Rybenkov,V.V., Duguet,M., Crisona,N.J., Cozzarelli,N.R., Bensimon,D. and Croquette,V. (2002) The mechanism of type IA topoisomerases. *Proc. Natl. Acad. Sci. U.S.A.*, **99**, 12126–12131.
50. Terekhova,K., Gunn,K.H., Marko,J.F. and Mondragón,A. (2012) Bacterial topoisomerase I and topoisomerase III relax supercoiled DNA via distinct pathways. *Nucleic Acids Res.*, **40**, 10432–10440.
51. Terekhova,K., Marko,J.F. and Mondragón,A. (2014) Single-molecule analysis uncovers the difference between the kinetics of DNA decatenation by bacterial topoisomerases I and III. *Nucleic Acids Res.*, **42**, 11657–11667.
52. Gunn,K.H., Marko,J.F. and Mondragón,A. (2017) An orthogonal single-molecule experiment reveals multiple-attempt dynamics of type IA topoisomerases. *Nat. Struct. Mol. Biol.*, **24**, 484–490.
53. Slesarev,A.I., Zaitzev,D.A., Kopylov,V.M., Stetter,K.O. and Kozyavkin,S.A. (1991) DNA topoisomerase III from extremely thermophilic archaebacteria. ATP-independent type I topoisomerase from Desulfurococcus amylolyticus drives extensive unwinding of closed circular DNA at high temperature. *J. Biol. Chem.*, **266**, 12321–12328.
54. Kirkegaard,K. and Wang,J.C. (1985) Bacterial-DNA topoisomerase-i can relax positively supercoiled DNA containing a single-stranded loop. *J. Mol. Biol.*, **185**, 625–637.
55. Yang,J., Bachrati,C.Z., Hickson,I.D. and Brown,G.W. (2012) BLM and RMI1 alleviate RPA inhibition of TopoIIIα decatenase activity. *PLoS One*, **7**, e41208.
56. Hjort,K. and Bernander,R. (1999) Changes in cell size and DNA content in sulfolobus cultures during dilution and temperature shift experiments. *J. Bacteriol.*, **181**, 5669–5675.
57. Li,X., Guo,L., Deng,L., Feng,D., Ren,Y., Chu,Y., She,Q. and Huang,L. (2011) Deletion of the topoisomerase III gene in the hyperthermophilic archaeon Sulfolobus islandicus results in slow growth and defects in cell cycle control. *J. Genet. Genomics*, **38**, 253–259.

TopA, the *Sulfolobus solfataricus* topoisomerase III, is a decatenase.

Anna H. Bizard[1,†], Xi Yang[2,†], Hélène Débat[1,2], Jonathan M. Fog[43], Lynn Zechiedrich[3], Terence R. Strick[2], Florence Garnier[1,2] and Marc Nadal[1,2]*

SUPPLEMENTARY DATA

Figure legends

Figure S1. Purification of *S. solfataricus* recombinant TopA. Coomassie-stained SDS-PAGE of the purified enzyme. Approximately 1 μg of the protein was loaded onto the gel.

Figure S2. Activity of *Sso*TopA as a function of temperature. TopA was incubated 8 min with a protein/pTZ18R DNA molar ratio of 2:1 in the standard conditions and at the temperature indicated above each corresponding lane. The DNA control (C) was incubated for 8 min at 75 °C in the absence of TopA. The reaction was performed at 100 mM of NaCl. The reaction products were analysed by one dimensional gel electrophoresis: OC indicates open circular (nicked) DNA, Rel, the relaxed topoisomers and -SC the negatively supercoiled DNA.

Figure S3. Activity of *Sso*TopA as a function of the magnesium concentration. TopA was incubated 30 min at 75°C with a protein/pTZ18R DNA molar ratio of 1:1 in the standard conditions with the concentration of $MgCl_2$ indicated above. The reaction products were analysed by one dimensional gel electrophoresis: OC indicates open circular (nicked) DNA, Rel, the relaxed topoisomers and -SC the negatively supercoiled DNA.

Figure S4. Annealing properties of the FI** produced by *Sso*TopA. SsoTopA was incubated with pTZ18R DNA (molar ratio of 1:1) for 5 min at 95°C in the standard conditions with 15 mM $MgCl_2$. After incubation, the samples were quickly cooled and kept at 4°C except when indicated and finally 0.5% SDS (final concentration) was added (lanes 2-5). SDS was added before the incubation as a control (lane 1). An additional incubation at 65°C for 15 min was realized for lanes 4 and 5. For all the samples, 25 mg/ml bromophenol blue, and 15% sucrose (final concentrations) were added. Samples corresponding to lanes 2 and 4 were further equilibrated at room temperature for 15 min while samples corresponding to lanes 3 and 4 were incubated 2 min at 95°C just prior loading. The reaction products were analysed by agarose gel electrophoresis (2%) in TEP buffer. OC indicates open circular (nicked) DNA and -SC the negatively supercoiled DNA and the particular FI* and FI** forms.

Figure S5. Decatenation of multi-linked DNA circles by *Sso*TopA. 600 ng of the multi-linked DNA substrate was incubated with *Sso*TopA for 20 min at 90 °C then cooled at 4°C (lane 1). The samples were further incubated for 30 min at 37°C in the presence of Nb.BbvCI (lane 2) or NdeI (lane 3). The panel B is a zoom of the squared zone from panel A. The DNAs ran in a 2% agarose gel at about 2.5 $V.cm^{-1}$ for 3 hours. The different DNA bands were attributed according to their size and topological forms : PP corresponds to the parental plasmid, LC to the decatenated large circle, and mC to the minicircle while OC is the open circular form, Lin the linear, Rel the relaxed and –SC the negatively supercoiled. M corresponds to the GeneRuler 1kb ladders.

Figure S6. DNA extension fluctuation in the absence of *Sso*TopA. (A) Schematic representation of the single molecule assay using magnetic tweezers explaining the

occurrence of DNA extension fluctuation. (B) Time-trace of the 3 kb DNA extension variation at 45 °C at an extended force of 0.45 pN in the absence of *Sso*TopA (control of the figure 6). The variation of extension is indicated as “fluctuation” in green. (C) Same extension fluctuation using the DNA containing the permanent single-stranded bubble region. (D) Corresponding time-trace of the DNA extension variation without *Sso*TopA (control of Figure 7).

Figure S7. Decatenation of kDNA by TopA of *S. solfataricus*. (A) TopA is added (0.5 ng) just before the incubation at indicated temperature for 30 min. (B) TopA (0.5 ng) is incubated at 85°C for 30 min in the presence of the indicated amount of SSB protein (ng). The lane T corresponds to kDNA incubated without TopA. The reactions were stopped and kDNA products were separated by a 2% agarose gel electrophoresis.

Supplementary Figure S1

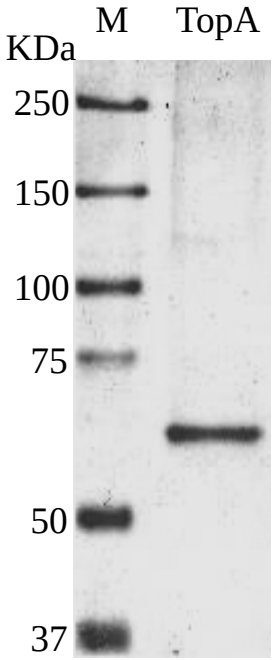

Supplementary Figure S2

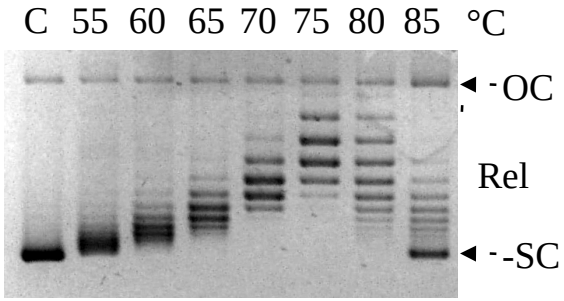

Supplementary Figure S3

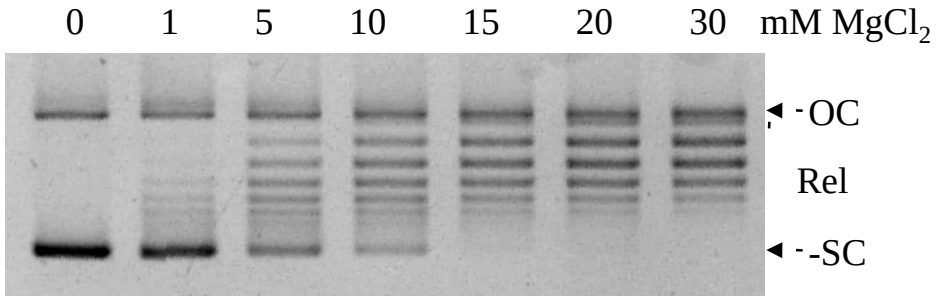

Supplementary Figure S4

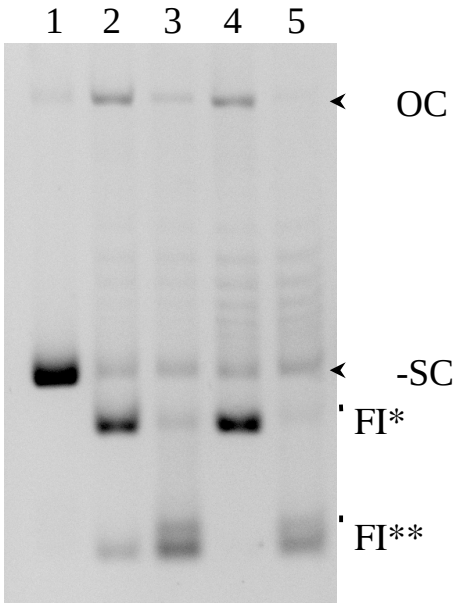

Supplementary Figure S5

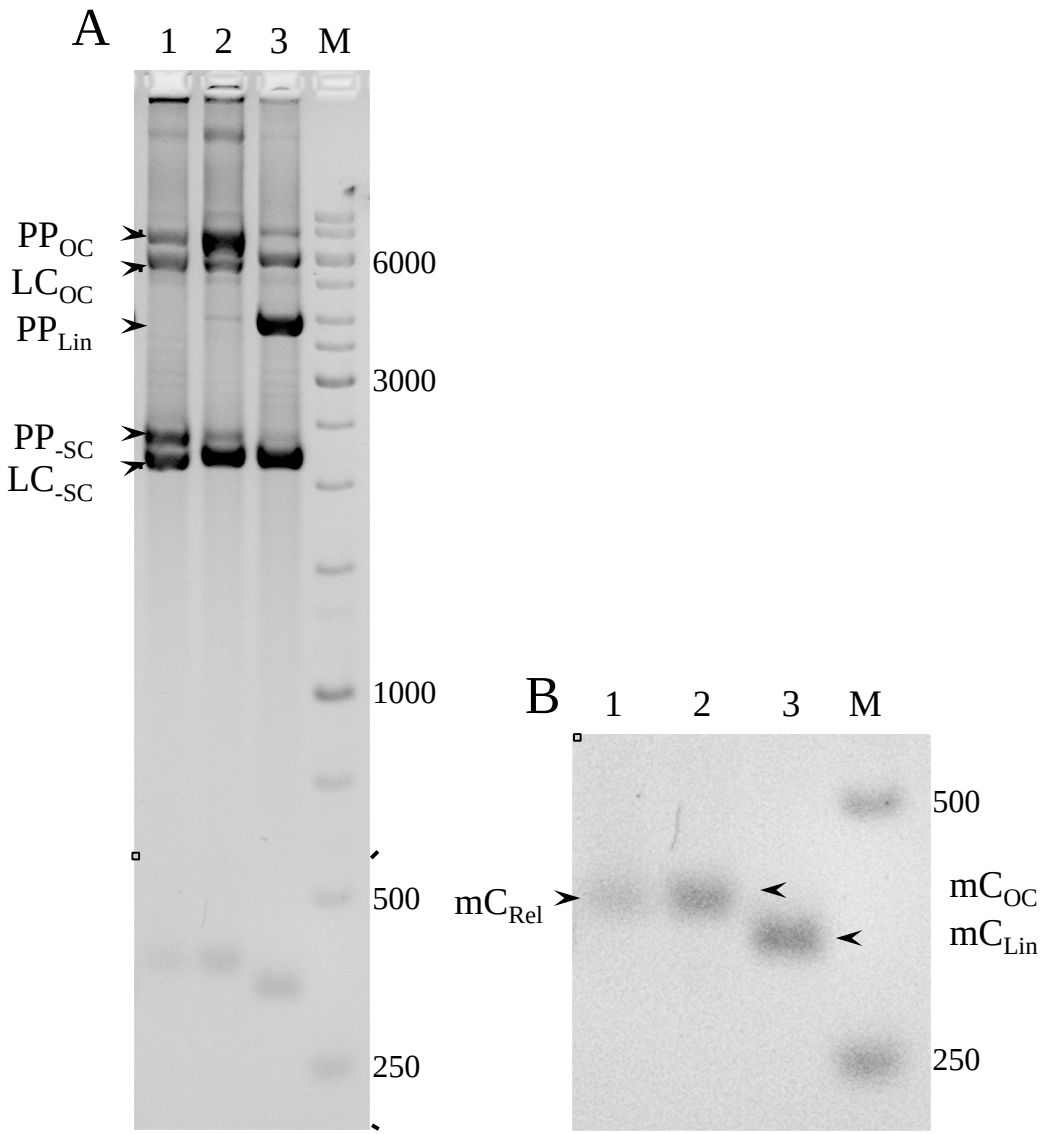

Supplementary Figure S6

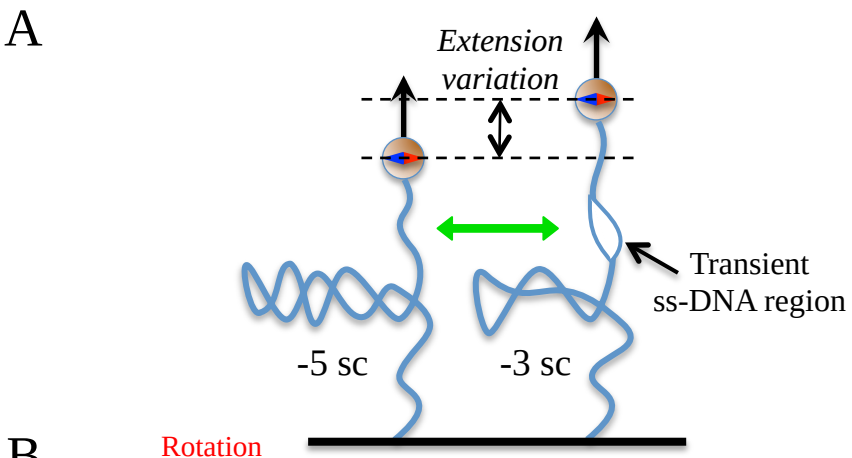

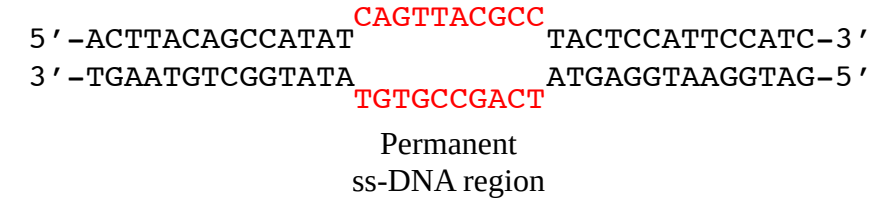

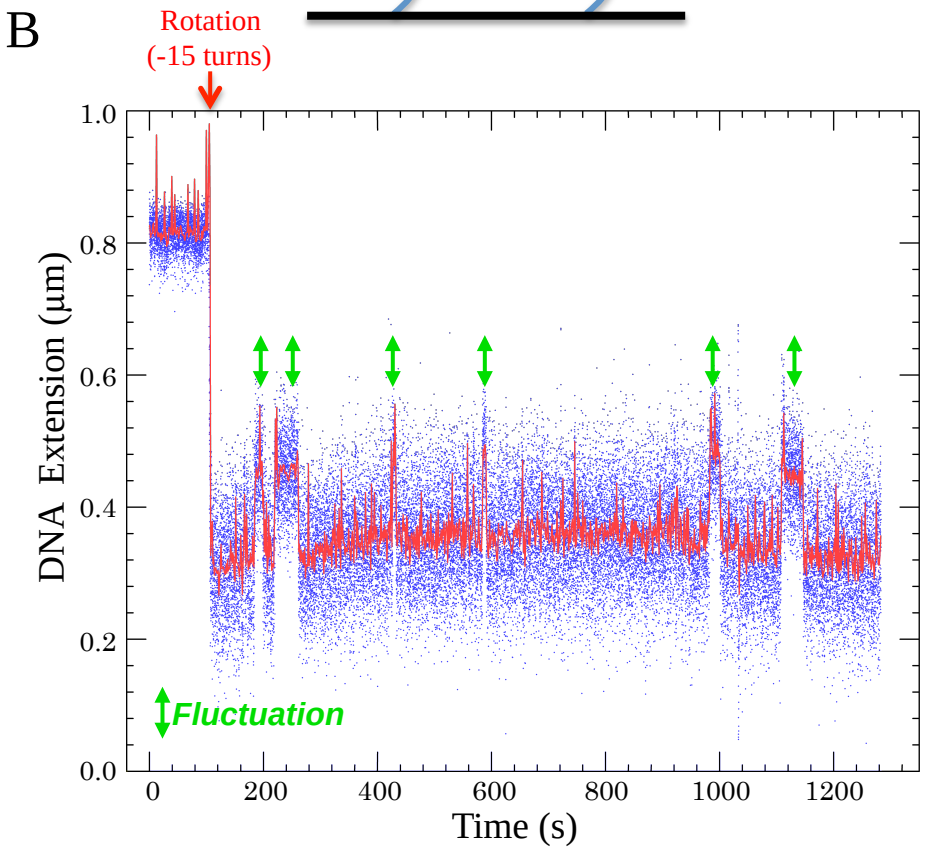

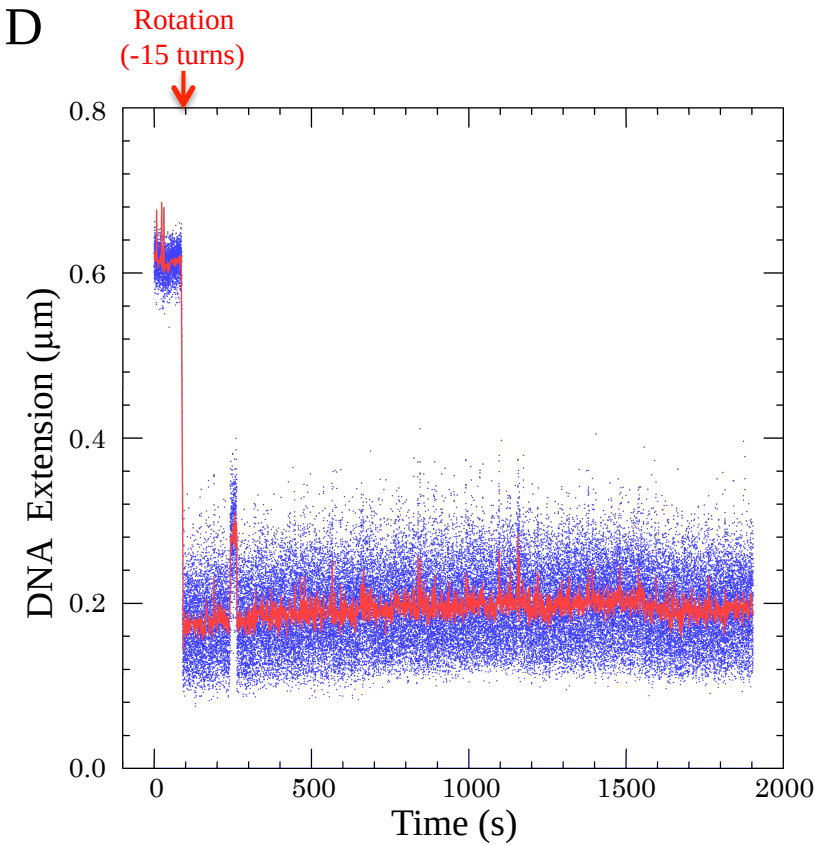

Figure S7

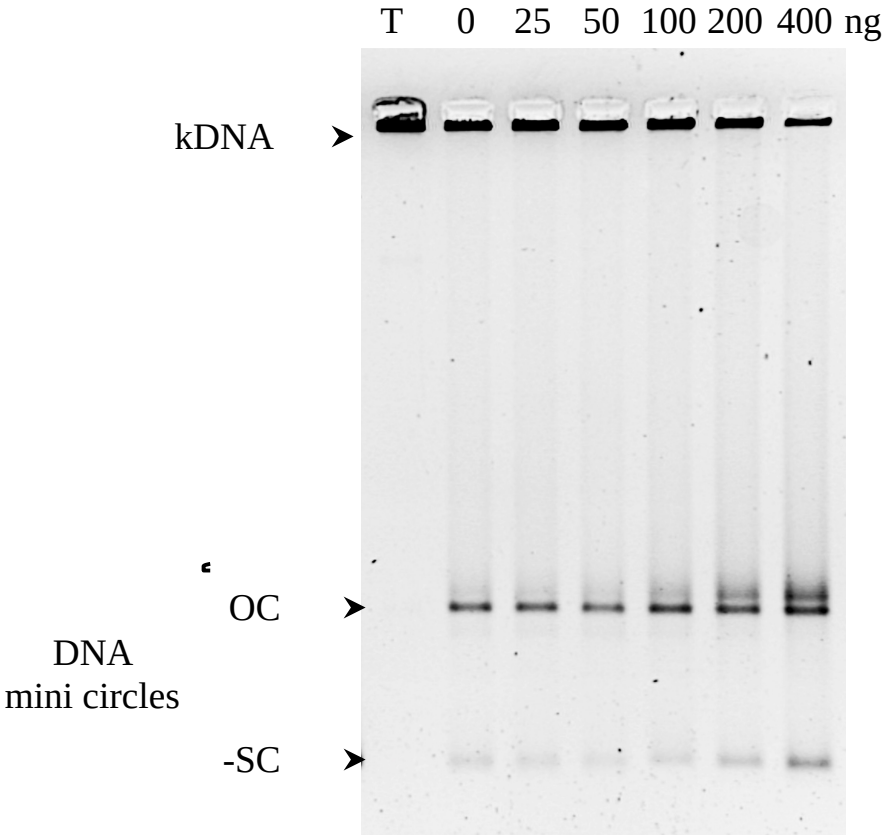

Discussion

1. RG mechanism: helicase-topoisomerase coordination

As described previously, RG combines an SF2 helicase and a classical Top IA in one polypeptide. Dissection of this chimeric molecular motor helps to understand its unique helicase-topoisomerase coupling. In this chapter, enzymatic feathers of an isolated RG helicase/Top IA domain is described and followed by a discussion of their interplay in solution. Finally, an RG mechanistic model on DNA positive supercoiling is proposed.

1.1 ATP cycle of an isolated RG helicase domain

The helicase domain of RG (see introduction Fig 3.2) belongs to the DEAD-box helicase family (within the SF2 category). Members of this family, such as eIF4A, unwind RNA duplexes as an ATP-dependent molecular switch (Pause, 1993), in which the two RecA-folds alternate between an open and a closed conformations (Story & Abelson, 2001; Theissen *et al.*, 2008; Peck & Herschhlag, 1999; Henn *et al.*, 2008; Liu & Jankowsky, 2008; Andreou & Klostermeier, 2013). Single-molecule FRET allowed researchers to observe structural transitions of an isolated RG helicase domain (RG-HC) in an ATP cycle, and these transitions are similar to that of a classical DEAD-box helicase (Fig 1.1) (del Toro Duany *et al.*, 2011). In the nucleotide-free state, RG-HC of *T. maritima* is presented as an open conformation in which the two RecA-folds, H1 and H2 (see introduction Fig 3.2 for structural information), keep away from each other and no ATP binding site forms in the helicase cleft between them. ATP binding (mimicked by binding AMPPNP) switches RG-HC to the closed-form in which H1 and H2 approach toward each other to generate the ATP binding pocket. The ATP pre-hydrolysis and post-hydrolysis states of RG-HC were obtained by binding ADP-BeF_x/ADP-MgF_x, in which the helicase cleft

closes in the pre-hydrolysis state and opens during post-hydrolysis. The Pi releasing state was achieved by binding ADP and the helicase cleft keeps open in this state (del Toro Duany *et al.*, 2011).

On the other hand, the affinity of RG-HC to three types of DNA (ssDNA, dsDNA and ss/dsDNA junction) was also found varying in different nucleotide states (Fig 1.1) (del Toro Duany *et al.,* 2008; Ganguly *et al.,* 2010). RG-HC exhibits a higher affinity for ss/dsDNA junction in the absence of ATP while prefers dsDNA in the ATP-bound state. In the pre-hydrolysis state, it favors all three types of DNA but a slightly higher affinity for the ss/dsDNA junction. Its preference converts to ssDNA in the post-hydrolysis and Pi release stages (del Toro Duany et al., 2011).

Combining RG-HC transitions in structure and DNA affinity unveils a significant coupling between its protein conformation and dsDNA binding: RG-HC couples its open-form (in the NTP-free/hydrolyzed state) to low dsDNA affinity and transition to the closed-form (NTP-bound state) greatly promotes its dsDNA binding. This feature of RG-HC indicates its potential manner in DNA unwinding (low dsDNA affinity) and rewinding (high dsDNA affinity) in the catalytic cycle.

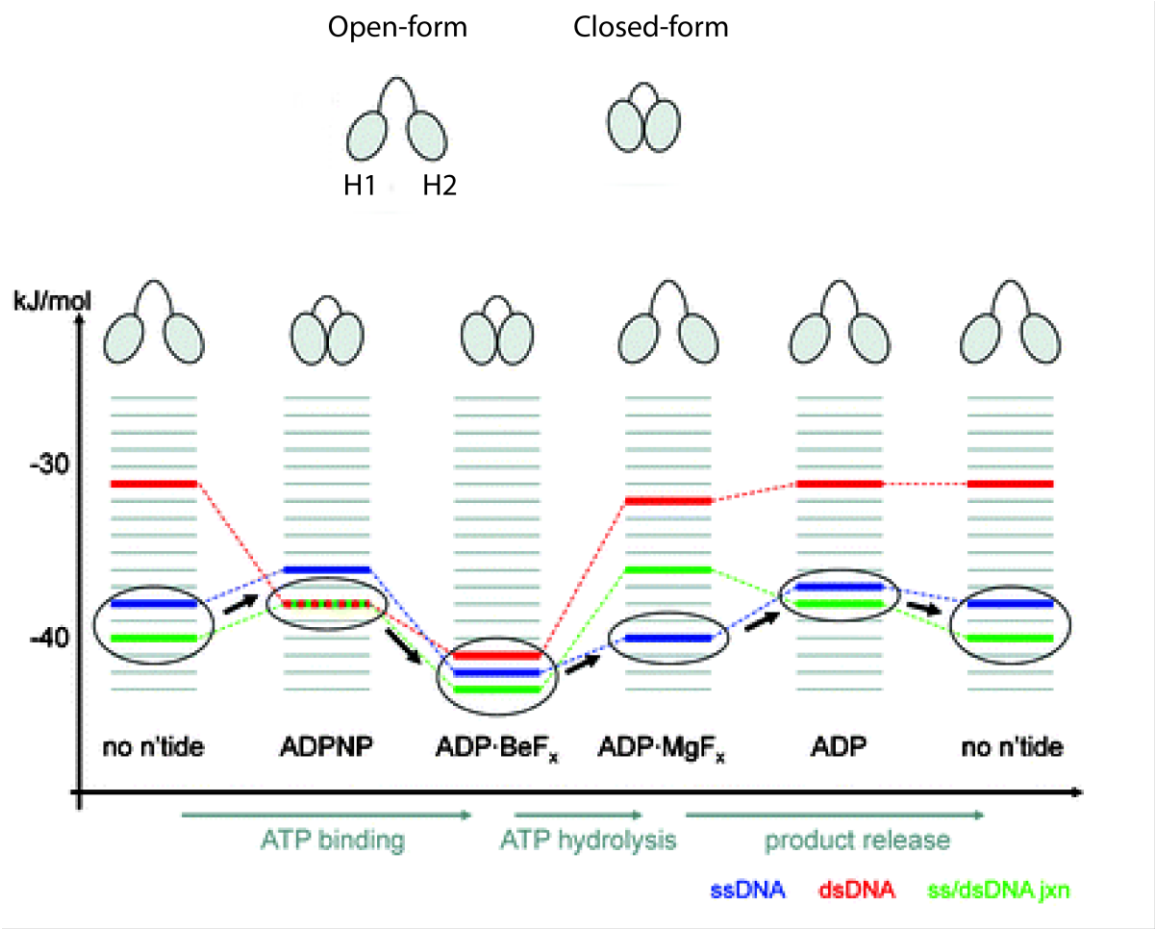

Figure 1.1 Catalytic cycle of an isolated RG helicase. Conformational alternation of an isolated RG helicase domain (RG-HC) in an ATP cycle is observed in a single-molecule FRET experiment and aligned with the binding preference of three types of DNA substrates in different stages. ADPNP (AMP-PNP) is applied for the enzyme to mimic an ATP binding state. ADP-BeF_x, ADP-MgF_x and ADP are used to achieve the pre-hydrolysis, post-hydrolysis and the Pi release states. Blue, red and green lines indicate the levels of RG-HC affinity (presented by values of binding enthalpy) with ssDNA, dsDNA and ss/ds DNA junction (del Toro Duany *et al.*, 2011).

1.2 Interplay between individual domains of RG

To look into how an isolated RG helicase domain (RG-HC) interplays with a topoisomerase domain (RG-TOP), researchers first investigated their individual functionalities and then mixed them in solution. Results show that RG-TOP alone still

maintains its capability as a classical Top IA to remove DNA negative supercoils, while RG-HC loses its DNA unwinding ability (Déclais *et al.*, 2000). This phenomenon was also verified in the study of a naturally split RG from *Nanoarqueum equitans* (Capp *et al.*, 2010). When mixed in solution, RG-HC and RG-TOP interact with each other and re-generate the ability to positively supercoil DNA (Declais *et al.*, 2000; Valenti *et al.*, 2008; Capp *et al.*, 2010). All these results above indicate that physical interaction (other than the peptide bond) in RG mutually regulates its two functional domains. Moreover, this interaction was proposed to be achieved through the latch, a protein insertion in the RG H2 domain (see introduction Fig 3.2). Indeed, the potential interaction between the latch and the domain III of top IA (see introduction Fig 3.1) was reported by a structural study of *Archaeoglobus fulgidus* RG. (Rudolph *et al.*, 2012). The significance of the latch in RG catalysis had also been proved: deletion of the latch totally disrupted RG's DNA overwinding activity (Ganguly *et al.*, 2010) and reduced its ssDNA binding affinity which is important for DNA unwinding (Ganguly *et al.*, 2013). In conclusion, the interplay between helicase and topoisomerase domains of RG achieves unique DNA positive supercoiling activity beyond their individual capabilities.

1.3 Stepwise depiction of RG catalytic cycle

Based on all the evidence and inferences discussed above, a step-by-step depiction of an RG catalytic cycle is proposed below (Fig 1.2).

Stage 1: RG initial DNA binding.

RG binds on DNA and unwinds (or stabilizes) a 20-bp ssDNA bubble. Identical amplitude between RG unwinding (on a negatively supercoiled DNA) and rewinding (on a positively supercoiled DNA) shows that its initial binding does not include noticeable DNA bending or wrapping.

In addition, as RG-induced DNA nicking has also been observed in our single-molecule experiment (introducing 0.1% SDS in the reaction buffer led to an abrupt relaxation on RG-bound DNA, data not shown), we suggest that DNA cleavage and resealing by RG topoisomerase domain may start from initial DNA binding and dynamically occur throughout the catalytic cycle.

Stage 2: ATP binding.

Both our single-molecule experiment on RG and the single-molecule FRET assay on RG-HC (Fig 1.1) (del Toro Duany *et al.*, 2011) reveal a significant change in protein/DNA conformation upon AMP-PNP binding. When RG-HC binds AMP-PNP, its helicase cleft closes and dsDNA affinity increases, indicating a rewinding effect of its bound ssDNA. This matches our observation of the 10-bp DNA partial retwisting due to RG binding AMP-PNP. Therefore, both the behaviors of RG and RG-HC on binding AMP-PNP suggest that nucleotide-induced helicase closure in RG leads to DNA rewinding.

Concerning the direct helicase-Top IA coupling in RG, especially TopR2, one helicase conformation should couple one top IA conformation. For a classical Top IA, two protein configurations, gate-closed and gate-open (see introduction 3.1.1 for definition of a “gate”), have been observed in single-molecule assays (Gunn *et al.,* 2017; Mills *et al.,* 2018) and they take place frequently and are regarded as the enzyme’s attempts to obtain a strand-passage (Gunn *et al.*, 2017). Previous studies also suggested that gate opening and gate closure together allow a Top IA to re-organize the ssDNA strands and then conduct a strand-passage (Viard & de la Tour, 2007). Therefore, two conformations of Top IA domain can be coupled with two conformations of the helicase domain. Besides, considering the position of the latch (see Fig 1.2 and introduction Fig 3.2) which attaches the two domains of RG, its movement upon helicase closure could have a potential effect on the topoisomerase to drag domain III away from domain I, thus open the Top IA gate.

Altogether, I suggest that ATP binding-induced RG helicase closure promotes the conformational change of the Top IA domain from gate-closure to gate-opening, re-organizing DNA before a unidirectional strand passage.

Stage 3 & 4: ATP hydrolysis and Pi release.

To complete the catalytic cycle from Stage 2, RG must then: (1) pass the intact ssDNA strand through the cleaved counterpart, (2) re-ligate the broken DNA ends and (3) reform the initial protein-DNA configuration. These steps together enable RG to increase a unit of DNA linking number and re-generate the initial 20-bp DNA-unwinding for the next turnover.

These goals can be achieved via further conformational changes in RG, including the helicase re-opening induced by ATP hydrolysis/Pi releasing (discussed in 1.1) and its coordinated Top IA gate-closure. The latter directs the intact ssDNA towards the cleaved DNA ends and lock the topological change via strand re-ligation. On the other hand, the re-unwinding of the re-twisted 10-bp DNA can be promoted by the helicase re-opening in this stage. The newly generated DNA overtwisting (ΔLk +1) may diffuse along the DNA long axis to release the locally increased torque.

Thus, the gate opening and closure, a complete turnover of a classical Top IA to perform a DNA strand passage, are here in RG coupled with the ATP binding/hydrolysis-induced helicase closure/opening, to achieve a unidirectional strand passage, crucial for RG positive supercoiling.

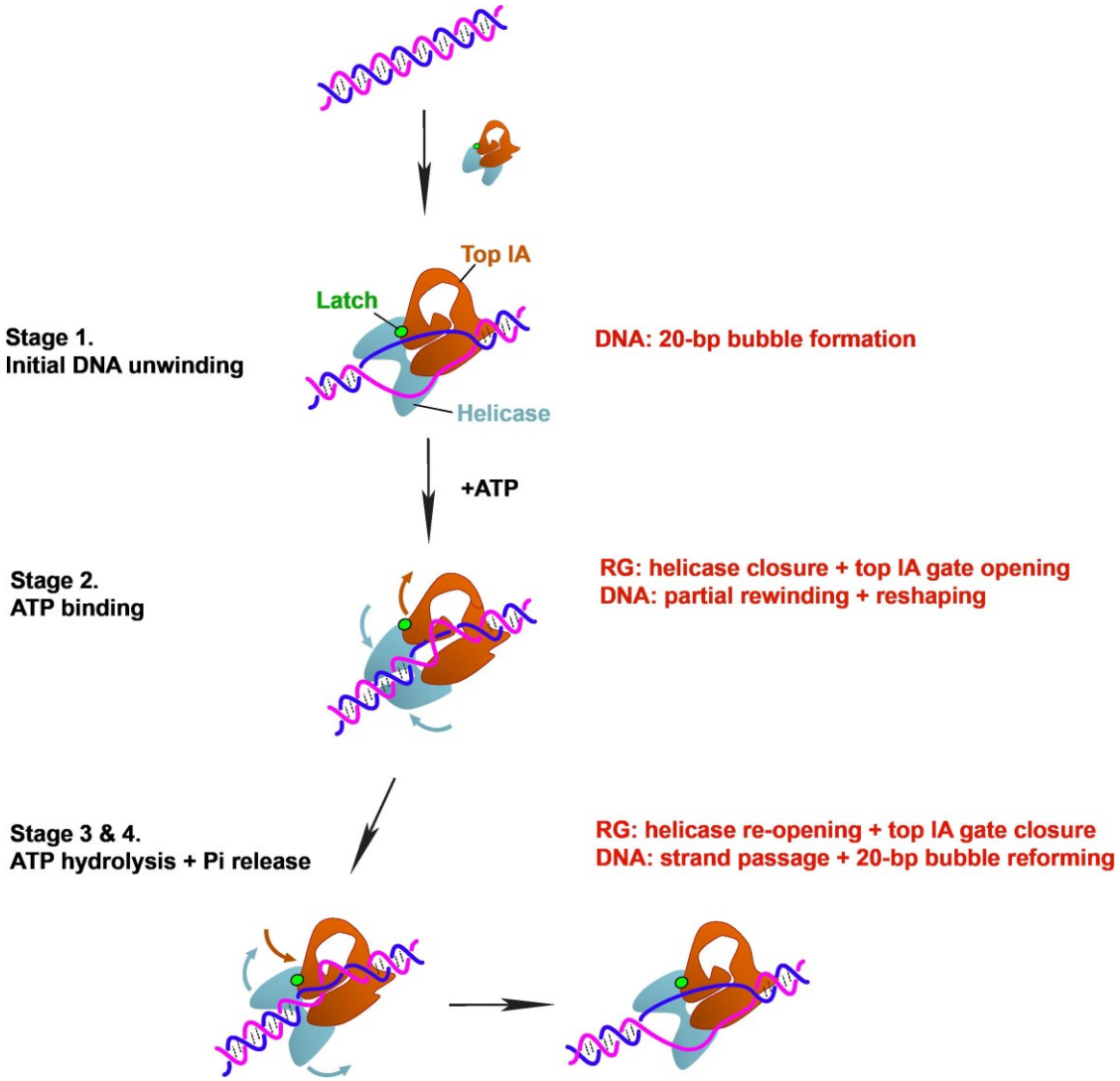

Figure 1.2 Mechanistic model of an RG ATP cycle. Initial RG DNA unwinding generates a 20-bp DNA bubble (stage 1). ATP association switches the RG helicase domain from an open to a closed conformation, and the helicase-topoisomerase coupling through the latch leads to a synchronized gate-opening in the top IA domain to re-shapes the ssDNA before strand passage (stage 2). Structural transitions in RG, including the helicase re-opening and top IA gate-closure, take place during ATP hydrolysis/Pi release, leading to a directional DNA strand passage and regeneration of the initial 20-bp DNA bubble (stage 3 and 4).

2 Cooperating with helicase achieves Topo III's requirement for ssDNA

Topo III enzymes have been found in all domains of life interacting with their RecQ-like helicase partners, such as RecQ in *E. coli*, Sgs1 in yeast, Hel112 in *Sulfolobus* and BLM and WRM in human (Garnier *et al.*, 2018). Studies show that partnership with a RecQ helicase enhances the activity of Topo III. For example, in the presence of RecQ and SSB proteins, *E. coli* Topo III can efficiently catenate covalently closed circular DNA without a nick or an ssDNA region (Harmon *et al.*, 1999). In eukaryotes, similarly, Top3 cooperates with RecQ and promoted by single-strand binding protein RPA to decatenate genomic DNA, and their activity is further stimulated by a special regulatory protein Rmi1. The Top3-RecQ-Rmi1 complex is reported to dissolute double Holliday junctions (Cejka *et al., 2010;* Cejka *et al., 2012;* Bocquet *et al., 2014*).

Topo III collaborates with RecQ in a way that the latter utilizes ATP to unwind dsDNA (then stabilized by SSBs) and feeds the former with ssDNA to perform strand-passage reactions (Fig 1.3) (Harmon *et al.*, 2003). Although the activity of Topo III relies on RecQ, they both work independently during collaboration. This cooperative manner provides an opportunity for DNA intermolecular tangling: when an unwound ssDNA region generated by RecQ and SSB encounters a foreign DNA molecule, Topo III has a chance to tangle them up via strand-passage reaction (Fig 1.3a). On the other hand, this joint effort can also introduce supercoils to a covalently closed circular DNA when it occurs intramolecularly: as local unwinding by RecQ and SSBs generates positively supercoils the rest of the DNA, Topo III binding and removal of positive supercoils lead to a negatively supercoiled DNA (Fig 1.3b) (Harmon *et al.*, 2003; Kirkegaard & Wang, 1985).

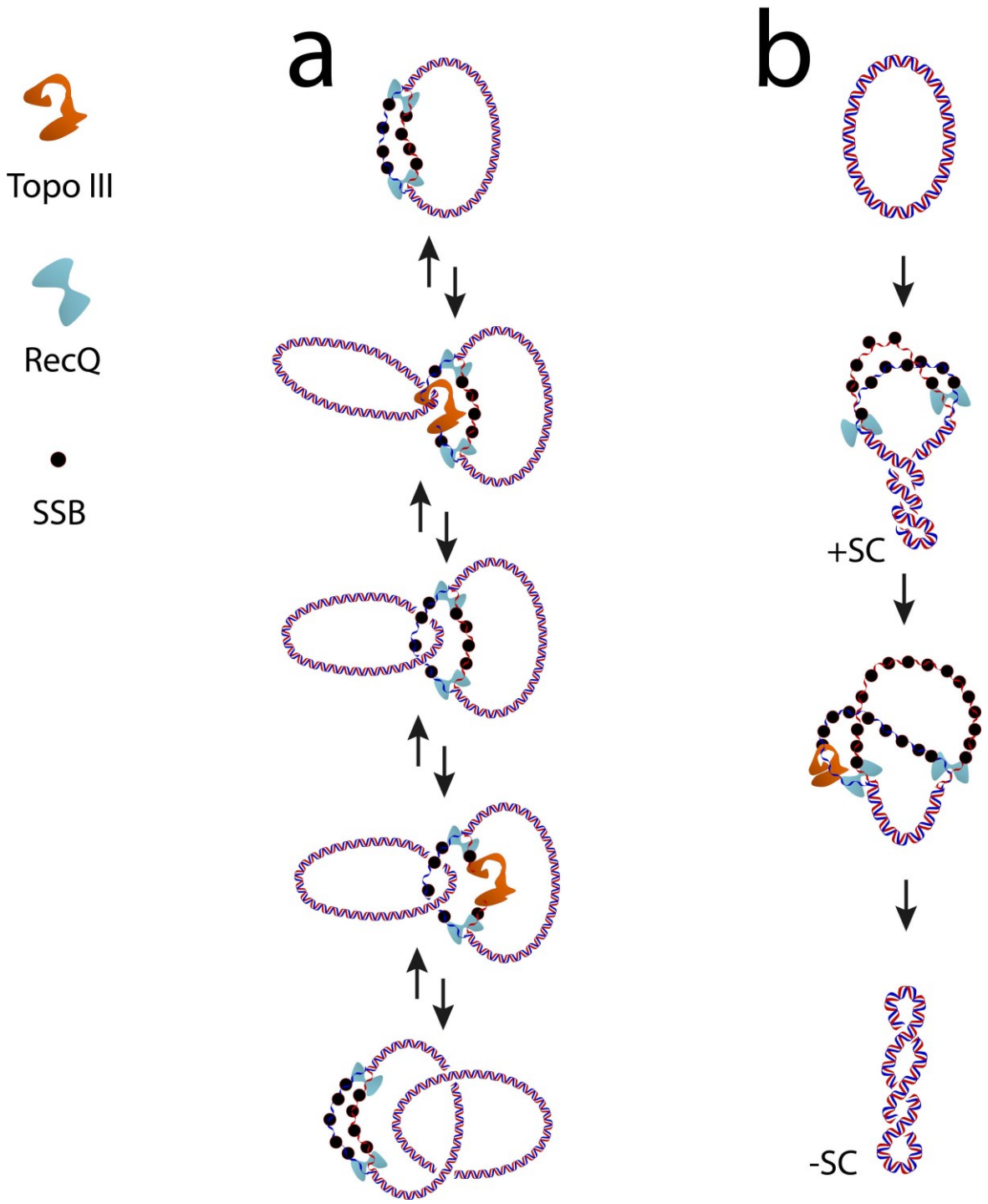

Figure 1.3 Mechanisms of RecQ-Topo III cooperation. RecQ unwinds a circular dsDNA and SSB proteins stabilize the unwound region. Topo III binds on the ssDNA and (a) performs intermolecular strand-passage reactions to fully tangle a foreign DNA circle; (b) conducts strand-passage intramolecularly to remove DNA positive supercoils and obtain an overall underwound DNA product.

Cooperations of Topo III with other helicases, in addition to RecQ, have also been found (Garnier *et al.*, 2018), including a recently reported partnership between human Top3A and PICH (see Introduction 3.3.2) (Bizard *et al.*, 2018). Both mechanisms of RecQ-Topo III and PICH-Topo III cooperations are reminiscent of the classic “twin-model” (Liu & Wang, 1987; Wu *et al.*, 1988), in which Topo I and Gyrase bind on and relax the negatively/positively supercoiled DNA region generated by the translocation of an RNA polymerase. All of these examples suggest that the helicase-topoisomerase partnership can be universal during cellular transactions.

*S.so*Topo III, however, can efficiently unlink two covalently closed circular double-stranded DNA by its own at high temperature (Bizard *et al.*, 2018). This exception shows the effect of DNA melting under high thermal energy to substitute the DNA unwinding activity of helicase and SSBs, which further demonstrates that ssDNA is the functional basis for a Top IA enzyme.

Regarding RG, although it contains both RecQ and Top IA, no DNA catenation/decatenation activity has been observed so far both in previous publications (Shibata *et al.*, 1987) and our unpublished results. This could be explained by RG’s DNA unwinding amplitude and its stringent regulation of DNA strand passage. Firstly, RG only unwinds 20-bp DNA and the unwound DNA is probably constrained by the enzyme thus hardly accessible for a foreign DNA molecule to obtain an intermolecular linkage. Also, rigorous coupling in RG catalysis, especially TopR2, only allows the right ssDNA strand with a right orientation to pass through the gate, which further raises the threshold to tangle a foreign DNA. It can be interesting to investigate the catenation activity by mixing isolated and uncoupled RG helicase and top IA domains with SSB proteins to compare with RecQ-Topo III-SSB complex.

3 Direct helicase-topoisomerase coupling regulates strand-passage of RG to increase DNA linking number

As described above, the rigorous helicase-topoisomerase coupling in RG allows this chimera to exclusively increase DNA linking number via strands passage. Two requirements are considered crucial for achieving a unidirection in RG supercoiling:

(1) The presence of an ssDNA region:

Imagine performing a strand passage on a right-handed DNA double helix, it only decreases linking number on the DNA. Thus, an unwound ssDNA region is a prerequisite to increase DNA linking number on a B-form DNA, and the ssDNA strands have to be re-oriented before strand passage. It also explains why a DNA bubble is crucial to all the Top IA enzymes. As for RG, stabilizing an ssDNA bubble is especially important for its positive DNA supercoiling, as double-strand DNA melting is not energetically favored on an overwound DNA.

(2) Re-organization of ssDNA for strand passage:

Re-organization of the ssDNA strands is equally crucial to a directional strand passage. For a classical Top IA, the ssDNA conformation during strand passage is regulated by the supercoiling state on the DNA so the enzyme relaxes both negative and positive DNA supercoils on a DNA bubble. For RG, especially TopR2, the unidirectional DNA strand passage is highly coordinated with the protein conformational change upon NTP binding/hydrolysis.

It is worth noting that many RG family members manipulate DNA topology in the absence of ATP. For example, *S.so*TopR1 can relax negatively supercoiled DNA (Bizard *et al.*, 2011) and *A. fulgidus* RG can remove positive supercoils on DNA containing a bubble (Hsieh & Plank, 2006). While in terms of *S.so*TopR2, no catalysis achieves without NTP, either on a negatively supercoiled DNA (Bizard *et al.*, 2011) or a positively supercoiled DNA containing a bubble (data not shown). It indicates a

divergence among RG family concerning the strength of the helicase-Top IA coupling.

4 Understanding Top IA mechanisms through the perspective of thermodynamics

The intricate behaviors and relationships among the topoisomerase family, such as their selectivity in DNA supercoiling and their discrepancies in DNA catenation/decatenation activity, often prevent people from clearly understanding their mechanisms. Essential principles such as laws of thermodynamics provide perspectives to obtain a universal rule of these molecular motors. According to the second law of thermodynamics, an isolated reaction system spontaneously reaches its thermodynamic equilibrium. In terms of DNA topology, a group of DNA topoisomers in solution tend to reach a topological equilibrium in supercoiling, catenation or knotting and can be accelerated by certain types of topoisomerases. Catalysis of an NTP-independent topoisomerase will finally facilitate its DNA substrates to achieve thermodynamic equilibrium; while NTP-consuming enzymes introduce external energy into the reaction system to shift the topological equilibrium to a new “steady state” (Rybenkov *et al.*, 1997).

4.1 Thermodynamic rule in DNA catenation

In terms of DNA tangling, random cyclization of a group of linear DNA should reach an equilibrium point of catenation and knotting due to their thermal fluctuation (Bates & Maxwell, 2005; Wang & Davidson, 1966). The tendency of catenation/decatenation in macroscopy is decided by the concentration of DNA substrates which determine the frequency of molecular collision. For example, when adding PEG in the reaction system to increase the apparent concentration of the circular DNA substrates, the steady-state of RecQ-Topo III catalysis shifted towards DNA catenation (Harmon *et al.*, 2003).

In order to study the catalytic effect of topoisomerases on DNA catenation, researchers first found a way to measure the equilibrium fraction of DNA catenanes achieved via thermal fluctuation. They mixed linear DNA duplexes containing cohesive ends with a group of open circular DNA in solution and the former randomly self-cyclize. When reached thermal equilibrium, fractions of all the DNA topological isoforms (including catenanes and knots) can be measured by running an agarose gel. They then compared steady-state fractions of DNA catenanes catalyzed by different topoisomerases with that generated under thermal fluctuation. As expected, only topoisomerases consuming NTP can shift the fraction of DNA catenanes in the product away from thermal equilibrium. For example, *E. coli* Topo IV, in the presence of ATP, lowered the fraction of DNA catenanes 80 times from thermal equilibrium; while *E. coli* Topo III, which does not utilize NTP, catalyzed DNA substrates to the thermal equilibrium (Rybenkov *et al.*, 1997).

4.2 Thermodynamic effects in DNA supercoiling

Studies of NTP-independent topoisomerases, such as classical Top IAs, show that the direction included in their supercoiling activity is determined by the torsional state on the DNA. For example, although Top IAs are known for their activity in reducing negatively supercoiled DNA, the introduction of an ssDNA bubble also allows them to relax positive DNA supercoils (Kirkegaard & Wang 1985; Plank et al., 2005; Terekhova et al., 2012). Thus, Top IAs only reduce the torsional energy on a DNA to achieve a low-entropy equilibrium state in the reaction system.

On the contrary, when providing NTP-consuming topoisomerases (*eg.*, RG and Gyrase) with ATP, they can increase DNA supercoiling levels against torque. For example, RG consumes ATP to increase DNA linking number on either a B-DNA or a DNA containing a mismatched bubble (Ogawa *et al.*, 2015). Similarly, DNA gyrase utilizes energy in ATP to generate negative DNA supercoils via DNA-duplex cleavage and passage (Wang, 1996). However, in the absence of ATP, as mentioned before, many RG family members behave like a classical Top IA that relaxes negatively supercoiled DNA (Bizard *et al.*, 2011) and also remove positive supercoils in the presence of a DNA bubble (Hsieh & Plank, 2006). This phenomenon also indicates

the requirement of external energy to modify the equilibrium state in DNA supercoiling.

Interestingly, when comparing the DNA supercoiling activity between a RecQ-Topo III complex and an RG, the former generates negative supercoils on a relaxed DNA circle (Fig 1.3) (Harmon et al., 2003) while the latter only positively supercoil DNA. This difference indicates their major discrepancy in a cooperative relationship. As the topo III strand-passage reaction is not directly coupled by RecQ, it can relax the positive DNA supercoils (generated by RecQ unwinding) thus obtains an overall negatively supercoiled DNA product; as the Top IA domain in RG is structurally coordinated with the helicase domain, it only performs unidirectional strand passage to increase DNA linking number.

References

Abdurashidova, G., Radulescu, S., Sandoval, O., Zahariev, S., Danailov, M. B., Demidovich, A., ... & Falaschi, A. (2007). Functional interactions of DNA topoisomerases with a human replication origin. *The EMBO journal*, *26*(4), 998-1009.

Adachi, Y., Luke, M., & Laemmli, U. K. (1991). Chromosome assembly in vitro: topoisomerase II is required for condensation. *Cell*, *64*(1), 137-148.

Aguilera, A. (2002). The connection between transcription and genomic instability. *The EMBO journal*, *21*(3), 195-201.

Ahumada, A., & Tse-Dinh, Y. C. (1998). The Zn (II) Binding Motifs ofE. coliDNA Topoisomerase I Is Part of a High-Affinity DNA Binding Domain. *Biochemical and biophysical research communications*, *251*(2), 509-514.

Amor-Guéret, M., & Riou, J. F. (2012). Topoisomerases and Carcinogenesis: Topoisomerase IIIα and BLM. In *DNA Topoisomerases and Cancer* (pp. 155-173). Springer, New York, NY.

Andreou, A. Z., & Klostermeier, D. (2013). The DEAD-box helicase eIF4A: paradigm or the odd one out?. *RNA biology*, *10*(1), 19-32.

Arnott, S., & Hukins, D. W. L. (1972). Optimised parameters for A-DNA and B-DNA. *Biochemical and biophysical research communications*, *47*(6), 1504-1509.

Ashour, M. E., Atteya, R., & El-Khamisy, S. F. (2015). Topoisomerase-mediated chromosomal break repair: an emerging player in many games. *Nature Reviews Cancer*, *15*(3), 137.

Axelrod, D. (1981). Cell-substrate contacts illuminated by total internal reflection fluorescence. *The Journal of cell biology*, *89*(1), 141-145.

Baranello, L., Wojtowicz, D., Cui, K., Devaiah, B. N., Chung, H. J., Chan-Salis, K. Y., ... & Piotrowski, J. (2016). RNA polymerase II regulates topoisomerase 1 activity to favor efficient transcription. *Cell*, *165*(2), 357-371.

Basu, A., Schoeffler, A. J., Berger, J. M., & Bryant, Z. (2012). ATP binding controls distinct structural transitions of Escherichia coli DNA gyrase in complex with DNA. *Nature Structural and Molecular Biology*, *19*(5), 538.

Bates, A. D., & Maxwell, A. (2005). *DNA topology*. Oxford University Press, USA.

Bauer, W., & Vinograd, J. (1968). The interaction of closed circular DNA with intercalative dyes: I. The superhelix density of SV40 DNA in the presence and absence of dye. *Journal of molecular biology*, *33*(1), 141-171.

Baumann, C., Körner, R., Hofmann, K., & Nigg, E. A. (2007). PICH, a centromere-associated SNF2 family ATPase, is regulated by Plk1 and required for the spindle checkpoint. *Cell*, *128*(1), 101-114.

Baxter, J., & Diffley, J. F. (2008). Topoisomerase II inactivation prevents the completion of DNA replication in budding yeast. *Molecular cell*, *30*(6), 790-802.

Baxter, J., Sen, N., Martínez, V. L., De Carandini, M. M., Schvartzman, J. B., Diffley, J. F. X., & Aragon, L. (2011). Positive supercoiling of mitotic DNA drives decatenation by topoisomerase II in eukaryotes. *Science*, *331*(6022), 1328-1332.

Bell, S. D., Jaxel, C., Nadal, M., Kosa, P. F., & Jackson, S. P. (1998). Temperature, template topology, and factor requirements of archaeal transcription. *Proceedings of the National Academy of Sciences*, *95*(26), 15218-15222.

Berg JM, Tymoczko JL, Stryer L (2002): Biochemistry, 5th ed., Freeman WH and Co., New York; pp: 205-206.

Bergerat, A., de Massy, B., Gadelle, D., Varoutas, P. C., Nicolas, A., & Forterre, P. (1997). An atypical topoisomerase II from Archaea with implications for meiotic recombination. *Nature*, *386*(6623), 414.

Bergerat, A., Gadelle, D., & Forterre, P. (1994). Purification of a DNA topoisomerase II from the hyperthermophilic archaeon Sulfolobus shibatae. A thermostable enzyme with both bacterial and eucaryal features. *Journal of Biological Chemistry*, *269*(44), 27663-27669.

Bhat, M. A., Philp, A. V., Glover, D. M., & Bellen, H. J. (1996). Chromatid segregation at anaphase requires the barren product, a novel chromosome-associated protein that interacts with Topoisomerase II. *Cell*, *87*(6), 1103-1114.

Biebricher, A., Hirano, S., Enzlin, J. H., Wiechens, N., Streicher, W. W., Huttner, D., ... & Peterman, E. (2013). PICH: a DNA translocase specially adapted for processing anaphase bridge DNA. *Molecular cell*, *51*(5), 691-701.

Bizard, A. H., Allemand, J. F., Hassenkam, T., Paramasivam, M., Sarlós, K., Singh, M. I., & Hickson, I. D. (2019). PICH and TOP3A cooperate to induce positive DNA supercoiling. *Nature structural & molecular biology*, 1.

Bizard, A. H., Yang, X., Débat, H., Fogg, J. M., Zechiedrich, L., Strick, T. R., ... & Nadal, M. (2018). TopA, the Sulfolobus solfataricus topoisomerase III, is a decatenase. *Nucleic acids research*, *46*(2), 861-872.

Bizard, A., Garnier, F., & Nadal, M. (2011). TopR2, the second reverse gyrase of Sulfolobus solfataricus, exhibits unusual properties. *Journal of molecular biology*, *408*(5), 839-849.

Blot, N., Mavathur, R., Geertz, M., Travers, A., & Muskhelishvili, G. (2006). Homeostatic regulation of supercoiling sensitivity coordinates transcription of the bacterial genome. *EMBO reports*, *7*(7), 710-715.

Bocquet, N., Bizard, A. H., Abdulrahman, W., Larsen, N. B., Faty, M., Cavadini, S., ... & Thomä, N. H. (2014). Structural and mechanistic insight into Holliday-junction dissolution by topoisomerase IIIα and RMI1. *Nature structural & molecular biology*, *21*(3), 261.

Bowater, R., Aboul-Ela, F., & Lilley, D. M. (1992). [5] Two-dimensional gel electrophoresis of circular DNA topoisomers. In *Methods in enzymology* (Vol. 212, pp. 105-120). Academic Press.

Brick, K., Pratto, F., Sun, C. Y., Camerini-Otero, R. D., & Petukhova, G. (2018). Analysis of meiotic double-strand break initiation in mammals. In *Methods in Enzymology* (Vol. 601, pp. 391-418). Academic Press.

Brosh Jr, R. M. (2013). DNA helicases involved in DNA repair and their roles in cancer. *Nature Reviews Cancer*, *13*(8), 542.

Buck, D. (2009). DNA topology. *Applications of knot theory (Proc. Sympos. Appl. Math., 66, Amer. Math. Soc., 2009)*, 47-79.

Byrd, A. K., & Raney, K. D. (2012). Superfamily 2 helicases. *Frontiers in bioscience (Landmark edition)*, *17*, 2070.

Capp,C., Qian,Y., Sage,H., Huber,H. and Hsieh,T.-S. (2010) Separate and combined biochemical activities of the subunits of a naturally split reverse gyrase. Journal of Biological Chemistry, 285, 39637–39645.

Carter, S. D., & Sjögren, C. (2012). The SMC complexes, DNA and chromosome topology: right or knot?. Critical reviews in biochemistry and molecular biology, 47(1), 1-16.

Cejka, P., Plank, J. L., Bachrati, C. Z., Hickson, I. D., & Kowalczykowski, S. C. (2010). Rmi1 stimulates decatenation of double Holliday junctions during dissolution by Sgs1–Top3. *Nature structural & molecular biology, 17*(11), 1377.

Cejka, P., Plank, J. L., Dombrowski, C. C., & Kowalczykowski, S. C. (2012). Decatenation of DNA by the S. cerevisiae Sgs1-Top3-Rmi1 and RPA complex: a mechanism for disentangling chromosomes. *Molecular cell*, *47*(6), 886-896.

Chan, K. L., North, P. S., & Hickson, I. D. (2007). BLM is required for faithful chromosome segregation and its localization defines a class of ultrafine anaphase bridges. *The EMBO journal*, *26*(14), 3397-3409.

Charbonnier, F. R. A. N. C. K., & Forterre, P. A. T. R. I. C. K. (1994). Comparison of plasmid DNA topology among mesophilic and thermophilic eubacteria and archaebacteria. *Journal of bacteriology*, *176*(5), 1251-1259.

Charvin, G., Bensimon, D., & Croquette, V. (2003). Single-molecule study of DNA unlinking by eukaryotic and prokaryotic type-II topoisomerases. Proceedings of the National Academy of Sciences, 100(17), 9820-9825.

Chen, S. H., Plank, J. L., Willcox, S., Griffith, J. D., & Hsieh, T. S. (2014). Top3α is required during the convergent migration step of double Holliday junction dissolution. *PloS one*, *9*(1), e83582.

Cheng, B., Zhu, C. X., Ji, C., Ahumada, A., & Tse-Dinh, Y. C. (2003). Direct interaction between Escherichia coli RNA polymerase and the zinc ribbon domains of DNA topoisomerase I. *Journal of Biological Chemistry*, *278*(33), 30705-30710.

Corless, S., & Gilbert, N. (2016). Effects of DNA supercoiling on chromatin architecture. Biophysical reviews, 8(3), 245-258.

Corless, S., & Gilbert, N. (2017). Investigating DNA supercoiling in eukaryotic genomes. Briefings in functional genomics, 16(6), 379-389.

Couturier, M., Bizard, A. H., Garnier, F., & Nadal, M. (2014). Insight into the cellular involvement of the two reverse gyrases from the hyperthermophilic archaeon Sulfolobus solfataricus. *BMC molecular biology*, *15*(1), 18.

Déclais, A. C., Marsault, J., Confalonieri, F., de La Tour, C. B., & Duguet, M. (2000). Reverse gyrase, the two domains intimately cooperate to promote positive supercoiling. *Journal of Biological Chemistry*, *275*(26), 19498-19504.

Dekker, N. H., Rybenkov, V. V., Duguet, M., Crisona, N. J., Cozzarelli, N. R., Bensimon, D., & Croquette, V. (2002). The mechanism of type IA topoisomerases. Proceedings of the National Academy of Sciences, 99(19), 12126-12131.

Dekker, N. H., Viard, T., de La Tour, C. B., Duguet, M., Bensimon, D., & Croquette, V. (2003). Thermophilic topoisomerase I on a single DNA molecule. *Journal of molecular biology*, *329*(2), 271-282.

del Toro Duany, Y., & Klostermeier, D. (2011). Nucleotide-driven conformational changes in the reverse gyrase helicase-like domain couple the nucleotide cycle to DNA processing. *Physical Chemistry Chemical Physics*, *13*(21), 10009-10019.

del Toro Duany, Y., Ganguly, A., & Klostermeier, D. (2014). Differential contributions of the latch in Thermotoga maritima reverse gyrase to the binding of single-stranded DNA before and after ATP hydrolysis. *Biological chemistry*, *395*(1), 83-93.

del Toro Duany, Y., Jungblut, S. P., Schmidt, A. S., & Klostermeier, D. (2008). The reverse gyrase helicase-like domain is a nucleotide-dependent switch that is attenuated by the topoisomerase domain. Nucleic acids research, 36(18), 5882-5895.

del Toro Duany, Y., Klostermeier, D., & Rudolph, M. G. (2011). The conformational flexibility of the helicase-like domain from Thermotoga maritima reverse gyrase is restricted by the topoisomerase domain. *Biochemistry*, *50*(26), 5816-5823.

Dewar, J. M., & Walter, J. C. (2017). Mechanisms of DNA replication termination. *Nature Reviews Molecular Cell Biology*, *18*(8), 507.

DiGate, R. J., & Marians, K. J. (1988). Identification of a potent decatenating enzyme from Escherichia coli. *Journal of Biological Chemistry*, *263*(26), 13366-13373.

Drolet, M., Bi, X., & Liu, L. F. (1994). Hypernegative supercoiling of the DNA template during transcription elongation in vitro. *Journal of Biological Chemistry*, *269*(3), 2068-2074.

Duguet, M., Serre, M. C., & de La Tour, C. B. (2006). A universal type IA topoisomerase fold. *Journal of molecular biology*, 359(3), 805-812.

Ellis, N. A., Groden, J., Ye, T. Z., Straughen, J., Lennon, D. J., Ciocci, S., ... & German, J. (1995). The Bloom's syndrome gene product is homologous to RecQ helicases. *Cell*, *83*(4), 655-666.

Forterre, P. (2002). A hot story from comparative genomics: reverse gyrase is the only hyperthermophile-specific protein. *Trends in Genetics*, *18*(5), 236-237.

Forterre, P., Mirambeau, G., Jaxel, C., Nadal, M., & Duguet, M. (1985). High positive supercoiling in vitro catalyzed by an ATP and polyethylene glycol-stimulated topoisomerase from Sulfolobus acidocaldarius. *The EMBO journal*, *4*(8), 2123-2128.

Fuller, F. B. (1978). Decomposition of the linking number of a closed ribbon: a problem from molecular biology. *Proceedings of the National Academy of Sciences of the United States of America*, *75*(8), 3557.

Gadelle, D., Krupovic, M., Raymann, K., Mayer, C., & Forterre, P. (2014). DNA topoisomerase VIII: a novel subfamily of type IIB topoisomerases encoded by free or integrated plasmids in Archaea and Bacteria. *Nucleic acids research*, *42*(13), 8578-8591.

Gaertner, B., & Zeitlinger, J. (2014). RNA polymerase II pausing during development. *Development*, *141*(6), 1179-1183.

Ganguly, A., del Toro Duany, Y., & Klostermeier, D. (2013). Reverse gyrase transiently unwinds double-stranded DNA in an ATP-dependent reaction. *Journal of molecular biology*, *425*(1), 32-40.

Ganguly, A., del Toro Duany, Y., Rudolph, M. G., & Klostermeier, D. (2010). The latch modulates nucleotide and DNA binding to the helicase-like domain of Thermotoga maritima reverse gyrase and is required for positive DNA supercoiling. *Nucleic acids research*, *39*(5), 1789-1800.

Garnier, F., Debat, H., & Nadal, M. (2018). Type IA DNA topoisomerases: A universal core and multiple activities. In *DNA Topoisomerases* (pp. 1-20). Humana Press, New York, NY.

Gore, J., Bryant, Z., Stone, M. D., Nöllmann, M., Cozzarelli, N. R., & Bustamante, C. (2006). Mechanochemical analysis of DNA gyrase using rotor bead tracking. *Nature*, *439*(7072), 100.

Graves, E. T., Duboc, C., Fan, J., Stransky, F., Leroux-Coyau, M., & Strick, T. R. (2015). A dynamic DNA-repair complex observed by correlative single-molecule nanomanipulation and fluorescence. *Nature structural & molecular biology*, *22*(6), 452.

Griswold, A. (2008). Genome packaging in prokaryotes: The circular chromosome of E. coli. *Nature Education*, *1*(1), 57.

Goulaouic, H., Roulon, T., Flamand, O., Grondard, L., Lavelle, F., & Riou, J. F. (1999). Purification and characterization of human DNA topoisomerase IIIα. *Nucleic acids research, 27*(12), 2443-2450.

Gubaev, A., & Klostermeier, D. (2014). Reprint of “the mechanism of negative DNA supercoiling: a cascade of DNA-induced conformational changes prepares gyrase for strand passage”. *DNA repair*, *20*, 130-141.

Gunn, K. H., Marko, J. F., & Mondragón, A. (2017). An orthogonal single-molecule experiment reveals multiple-attempt dynamics of type IA topoisomerases. *Nature structural & molecular biology*, *24*(5), 484.

Harmon, F. G., Brockman, J. P., & Kowalczykowski, S. C. (2003). RecQ helicase stimulates both DNA catenation and changes in DNA topology by topoisomerase III. *Journal of Biological Chemistry*, *278*(43), 42668-42678.

Harmon, F. G., DiGate, R. J., & Kowalczykowski, S. C. (1999). RecQ helicase and topoisomerase III comprise a novel DNA strand passage function: a conserved mechanism for control of DNA recombination. *Molecular cell*, *3*(5), 611-620.

Hayama, R., & Marians, K. J. (2010). Physical and functional interaction between the condensin MukB and the decatenase topoisomerase IV in Escherichia coli. *Proceedings of the National Academy of Sciences*, *107*(44), 18826-18831.

Henn, A., Cao, W., Hackney, D. D., & Enrique, M. (2008). The ATPase cycle mechanism of the DEAD-box rRNA helicase, DbpA. *Journal of molecular biology*, *377*(1), 193-205.

Hiasa, H., & Marians, K. J. (1994). Topoisomerase III, but not topoisomerase I, can support nascent chain elongation during theta-type DNA replication. *Journal of Biological Chemistry*, *269*(51), 32655-32659.

Hiasa, H., & Marians, K. J. (1994). Topoisomerase IV can support oriC DNA replication in vitro. *Journal of Biological Chemistry*, *269*(23), 16371-16375.

Hiasa, H., DiGate, R. J., & Marians, K. J. (1994). Decatenating activity of Escherichia coli DNA gyrase and topoisomerases I and III during oriC and pBR322 DNA replication in vitro. *Journal of Biological Chemistry*, *269*(3), 2093-2099.

Hickson, I. D., & Mankouri, H. W. (2011). Processing of homologous recombination repair intermediates by the Sgs1-Top3-Rmi1 and Mus81-Mms4 complexes. *Cell cycle*, *10*(18), 3078-3085.

Howan, K., Monnet, J., Fan, J., & Strick, T. R. (2014). Stopped in its tracks: the RNA polymerase molecular motor as a robust sensor of DNA damage. *DNA repair*, *20*, 49-57.

Howan, K., Smith, A. J., Westblade, L. F., Joly, N., Grange, W., Zorman, S., ... & Strick, T. R. (2012). Initiation of transcription-coupled repair characterized at single-molecule resolution. Nature, 490(7420), 431.

Hsieh, T. S., & Plank, J. L. (2006). Reverse Gyrase Functions as a DNA Renaturase annealing of complementary single-stranded circles and positive supercoiling of a bubble substrate. *Journal of Biological Chemistry*, *281*(9), 5640-5647.

Jaxel, C., de la Tour, C. B., Duguet, M., & Nadal, M. (1996). Reverse gyrase gene from Sulfolobus shibatae B12: gene structure, transcription unit and comparative sequence analysis of the two domains. *Nucleic acids research*, *24*(23), 4668-4675.

Johnson, R. C., Johnson, L. M., Schmidt, J. W., & Gardner, J. F. (2005). Major nucleoid proteins in the structure and function of the Escherichia coli chromosome. In *The Bacterial Chromosome* (pp. 65-132). American Society of Microbiology.

Joshi, R. S., Pina, B., & Roca, J. (2012). Topoisomerase II is required for the production of long Pol II gene transcripts in yeast. *Nucleic acids research*, *40*(16), 7907-7915.

Kaguni, J. M., & Kornberg, A. (1984). Topoisomerase I confers specificity in enzymatic replication of the Escherichia coli chromosomal origin. *Journal of Biological Chemistry*, *259*(13), 8578-8583.

Keller, W. (1975). Determination of the number of superhelical turns in simian virus 40 DNA by gel electrophoresis. *Proceedings of the National Academy of Sciences*, *72*(12), 4876-4880.

Kirkegaard, K., & Wang, J. C. (1985). Bacterial DNA topoisomerase I can relax positively supercoiled DNA containing a single-stranded loop. Journal of molecular biology, 185(3), 625-637.

Koster, D. A., Croquette, V., Dekker, C., Shuman, S., & Dekker, N. H. (2005). Friction and torque govern the relaxation of DNA supercoils by eukaryotic topoisomerase IB. Nature, 434(7033), 671.

Koster, D. A., Palle, K., Bot, E. S., Bjornsti, M. A., & Dekker, N. H. (2007). Antitumour drugs impede DNA uncoiling by topoisomerase I. Nature, 448(7150), 213.

Kouzine, F., Levens, D., & Baranello, L. (2014). DNA topology and transcription. *Nucleus*, *5*(3), 195-202.

Kschonsak, M., & Haering, C. H. (2015). Shaping mitotic chromosomes: From classical concepts to molecular mechanisms. *BioEssays*, *37*(7), 755-766.

Lamour, V., Hoermann, L., Jeltsch, J. M., Oudet, P., & Moras, D. (2002). An Open Conformation of the Thermus thermophilusGyrase B ATP-binding Domain. *Journal of Biological Chemistry, 277*(21), 18947-18953.

Langridge, R., Wilson, H. R., Hooper, C. W., Wilkins, M. H., & Hamilton, L. D. (1960). The molecular configuration of deoxyribonucleic acid: I. X-ray diffraction study of a crystalline form of the lithium salt. *Journal of Molecular Biology*, *2*(1), 19-IN11.

Li, J., Liu, J., Zhou, J., & Xiang, H. (2011). Functional evaluation of four putative DNA-binding regions in Thermoanaerobacter tengcongensis reverse gyrase. *Extremophiles*, *15*(2), 281-291.

Li, Z., Mondragón, A., Hiasa, H., Marians, K. J., & DiGate, R. J. (2000). Identification of a unique domain essential for Escherichia coli DNA topoisomerase III-catalysed decatenation of replication intermediates. *Molecular microbiology*, *35*(4), 888-895.

Lionnet, T., Allemand, J. F., Revyakin, A., Strick, T. R., Saleh, O. A., Bensimon, D., & Croquette, V. (2012). Single-molecule studies using magnetic traps. *Cold Spring Harbor Protocols*, *2012*(1), pdb-top067488.

Liu, F., Putnam, A., & Jankowsky, E. (2008). ATP hydrolysis is required for DEAD-box protein recycling but not for duplex unwinding. *Proceedings of the National Academy of Sciences*, *105*(51), 20209-20214.

Liu, L. F., & Wang, J. C. (1987). Supercoiling of the DNA template during transcription. Proceedings of the National Academy of Sciences, 84(20), 7024-7027.

Ljungman, M., & Hanawalt, P. C. (1996). The anti-cancer drug camptothecin inhibits elongation but stimulates initiation of RNA polymerase II transcription. *Carcinogenesis*, *17*(1), 31-36.

López-García, P. (1999). DNA supercoiling and temperature adaptation: A clue to early diversification of life?. *Journal of molecular evolution*, *49*(4), 439-452.

Lulchev, P., & Klostermeier, D. (2014). Reverse gyrase—recent advances and current mechanistic understanding of positive DNA supercoiling. *Nucleic acids research*, *42*(13), 8200-8213.

Maeshima, K., & Laemmli, U. K. (2003). A two-step scaffolding model for mitotic chromosome assembly. *Developmental cell*, *4*(4), 467-480.

Marko, J. F., Siggia, E. D., Smith, S., & Bustamante, C. (1994). Entropic elasticity of λ-phage DNA. *Science*, *265*, 1599-1600.

Matoba, K., Mayanagi, K., Nakasu, S., Kikuchi, A., & Morikawa, K. (2002). Three-dimensional electron microscopy of the reverse gyrase from Sulfolobus tokodaii. *Biochemical and biophysical research communications*, *297*(4), 749-755.

Mayer, A., Landry, H. M., & Churchman, L. S. (2017). Pause & go: from the discovery of RNA polymerase pausing to its functional implications. *Current opinion in cell biology*, *46*, 72-80.

Merino, A., Madden, K. R., Lane, W. S., Champoux, J. J., & Reinberg, D. (1993). DNA topoisomerase I is involved in both repression and activation of transcription. *Nature*, *365*(6443), 227.

Mills, M., Tse-Dinh, Y. C., & Neuman, K. C. (2018). Direct observation of topoisomerase IA gate dynamics. *Nature structural & molecular biology*, *25*(12), 1111.

Mirkin, S. M. (2001). DNA topology: fundamentals. *e LS*.

Nadal, M. (2007). Reverse gyrase: an insight into the role of DNA-topoisomerases. *Biochimie*, *89*(4), 447-455.

Nadal, M., Jaxel, C., Portemer, C., Forterre, P., Mirambeau, G., & Duguet, M. (1988). Reverse gyrase of Sulfolobus: purification to homogeneity and characterization. *Biochemistry*, *27*(26), 9102-9108.

Nadal, M., Mirambeau, G., Forterre, P., Reiter, W. D., & Duguet, M. (1986). Positively supercoiled DNA in a virus-like particle of an archaebacterium. *Nature*, *321*(6067), 256.

Napoli, A., Valenti, A., Salerno, V., Nadal, M., Garnier, F., Rossi, M., & Ciaramella, M. (2004). Reverse gyrase recruitment to DNA after UV light irradiation in Sulfolobus solfataricus. *Journal of Biological Chemistry*, *279*(32), 33192-33198.

Nurse, P., Levine, C., Hassing, H., & Marians, K. J. (2003). Topoisomerase III can serve as the cellular decatenase in Escherichia coli. *Journal of Biological Chemistry*, *278*(10), 8653-8660.

Ogawa, T., Yogo, K., Furuike, S., Sutoh, K., Kikuchi, A., & Kinosita, K. (2015). Direct observation of DNA overwinding by reverse gyrase. *Proceedings of the National Academy of Sciences*, *112*(24), 7495-7500.

Papillon, J., Menetret, J. F., Batisse, C., Helye, R., Schultz, P., Potier, N., & Lamour, V. (2013). Structural insight into negative DNA supercoiling by DNA gyrase, a bacterial type 2A DNA topoisomerase. *Nucleic acids research, 41*(16), 7815-7827.

Pause, A. R. N. I. M., Méthot, N. A. T. H. A. L. I. E., & Sonenberg, N. A. H. U. M. (1993). The HRIGRXXR region of the DEAD box RNA helicase eukaryotic translation initiation factor 4A is required for RNA binding and ATP hydrolysis. *Molecular and cellular biology*, *13*(11), 6789-6798.

Peck, L. J., & Wang, J. C. (1983). Energetics of B-to-Z transition in DNA. *Proceedings of the National Academy of Sciences*, *80*(20), 6206-6210.

Peck, M. L., & Herschlag, D. (1999). Effects of oligonucleotide length and atomic composition on stimulation of the ATPase activity of translation initiation factor eIF4A. *Rna*, *5*(9), 1210-1221.

Perez-Cheeks, B. A., Lee, C., Hayama, R., & Marians, K. J. (2012). A role for topoisomerase III in Escherichia coli chromosome segregation. *Molecular microbiology*, *86*(4), 1007-1022.

Perugino, G., Valenti, A., D'amaro, A., Rossi, M., & Ciaramella, M. (2009). Reverse gyrase and genome stability in hyperthermophilic organisms.

Plank, J. L., Chu, S. H., Pohlhaus, J. R., Wilson-Sali, T., & Hsieh, T. S. (2005). Drosophila melanogaster topoisomerase IIIα preferentially relaxes a positively or negatively supercoiled bubble substrate and is essential during development. *Journal of Biological Chemistry*, *280*(5), 3564-3573.

Plank, J. L., Wu, J., & Hsieh, T. S. (2006). Topoisomerase IIIα and Bloom's helicase can resolve a mobile double Holliday junction substrate through convergent branch migration. *Proceedings of the National Academy of Sciences*, *103*(30), 11118-11123.

Pommier, Y., Leo, E., Zhang, H., & Marchand, C. (2010). DNA topoisomerases and their poisoning by anticancer and antibacterial drugs. *Chemistry & biology, 17*(5), 421-433.

Pommier, Y., Sun, Y., Shar-yin, N. H., & Nitiss, J. L. (2016). Roles of eukaryotic topoisomerases in transcription, replication and genomic stability. *Nature reviews Molecular cell biology*, *17*(11), 703.

Pray, L. "Discovery of DNA structure and function: Watson and Crick." Nature Education 1.1 (2008): 100.

Pray, L. (2008) Eukaryotic genome complexity. Nature Education 1(1):96.

Qi, H., Menzel, R., & Tse-Dinh, Y. C. (1999). Increased thermosensitivity associated with topoisomerase I deletion and promoter mutations in Escherichia coli. *FEMS microbiology letters*, *178*(1), 141-146.

Revyakin, A., Liu, C., Ebright, R. H., & Strick, T. R. (2006). Abortive initiation and productive initiation by RNA polymerase involve DNA scrunching. *Science*, *314*(5802), 1139-1143.

Riera, A., Barbon, M., Noguchi, Y., Reuter, L. M., Schneider, S., & Speck, C. (2017). From structure to mechanism—understanding initiation of DNA replication. *Genes & development*, *31*(11), 1073-1088.

Rodríguez, A. C., & Stock, D. (2002). Crystal structure of reverse gyrase: insights into the positive supercoiling of DNA. *The EMBO journal*, *21*(3), 418-426.

Rudolph, M. G., del Toro Duany, Y., Jungblut, S. P., Ganguly, A., & Klostermeier, D. (2012). Crystal structures of Thermotoga maritima reverse gyrase: inferences for the mechanism of positive DNA supercoiling. *Nucleic acids research*, *41*(2), 1058-1070.

Rybenkov, V. V., Ullsperger, C., Vologodskii, A. V., & Cozzarelli, N. R. (1997). Simplification of DNA topology below equilibrium values by type II topoisomerases. *Science*, *277*(5326), 690-693.

Santos-Pereira, J. M., & Aguilera, A. (2015). R loops: new modulators of genome dynamics and function. *Nature Reviews Genetics*, *16*(10), 583.

Shibata, T., Nakasu, S., Yasui, K., & Kikuchi, A. (1987). Intrinsic DNA-dependent ATPase activity of reverse gyrase. *Journal of Biological Chemistry, 262*(22), 10419-10421.

Shindo, H., Iwaki, T., Ieda, R., Kurumizaka, H., Ueguchi, C., Mizuno, T., ... & Kuboniwa, H. (1995). Solution structure of the DNA binding domain of a nucleoid-associated protein, H-NS, from Escherichia coli. *FEBS letters*, *360*(2), 125-131.

Sordet, O., Nakamura, A. J., Redon, C. E., & Pommier, Y. (2010). DNA double-strand breaks and ATM activation by transcription-blocking DNA lesions. *Cell Cycle*, *9*(2), 274-278.

Stennett, E. M., Ciuba, M. A., Lin, S., & Levitus, M. (2015). Demystifying PIFE: the photophysics behind the protein-induced fluorescence enhancement phenomenon in Cy3. *The journal of physical chemistry letters*, *6*(10), 1819-1823.

Story, R. M., Li, H., & Abelson, J. N. (2001). Crystal structure of a DEAD box protein from the hyperthermophile Methanococcus jannaschii. *Proceedings of the National Academy of Sciences*, *98*(4), 1465-1470.

Strick, T. R., Allemand, J. F., Bensimon, D., Bensimon, A., & Croquette, V. (1996). The elasticity of a single supercoiled DNA molecule. *Science*, *271*(5257), 1835-1837.

Strick, T. R., Croquette, V., & Bensimon, D. (2000). Single-molecule analysis of DNA uncoiling by a type II topoisomerase. Nature, 404(6780), 901.

Suresh, G., & Priyakumar, U. D. (2014). DNA–RNA hybrid duplexes with decreasing pyrimidine content in the DNA strand provide structural snapshots for the A-to B-form conformational transition of nucleic acids. *Physical Chemistry Chemical Physics*, *16*(34), 18148-18155.

Swinger, K. K., & Rice, P. A. (2004). IHF and HU: flexible architects of bent DNA. *Current opinion in structural biology*, *14*(1), 28-35.

Szafran, M. J., Strick, T., Strzałka, A., Zakrzewska-Czerwińska, J., & Jakimowicz, D. (2014). A highly processive topoisomerase I: studies at the single-molecule level. *Nucleic acids research*, *42*(12), 7935-7946.

Tan, K., Zhou, Q., Cheng, B., Zhang, Z., Joachimiak, A., & Tse-Dinh, Y. C. (2015). Structural basis for suppression of hypernegative DNA supercoiling by E. coli topoisomerase I. *Nucleic acids research*, *43*(22), 11031-11046.

Taneja, B., Patel, A., Slesarev, A., & Mondragón, A. (2006). Structure of the N-terminal fragment of topoisomerase V reveals a new family of topoisomerases. *The EMBO journal*, *25*(2), 398-408.

Temime‐Smaali, N., Guittat, L., Wenner, T., Bayart, E., Douarre, C., Gomez, D., ... & Riou, J. F. (2008). Topoisomerase IIIα is required for normal proliferation and telomere stability in alternative lengthening of telomeres. *The EMBO journal, 27*(10), 1513-1524.

Terekhova, K., Gunn, K. H., Marko, J. F., & Mondragon, A. (2012). Bacterial topoisomerase I and topoisomerase III relax supercoiled DNA via distinct pathways. *Nucleic acids research*, *40*(20), 10432-10440.

Terekhova, K., Marko, J. F., & Mondragón, A. (2014). Single-molecule analysis uncovers the difference between the kinetics of DNA decatenation by bacterial topoisomerases I and III. *Nucleic acids research*, *42*(18), 11657-11667.

Theissen, B., Karow, A. R., Köhler, J., Gubaev, A., & Klostermeier, D. (2008). Cooperative binding of ATP and RNA induces a closed conformation in a DEAD box RNA helicase. *Proceedings of the National Academy of Sciences*, *105*(2), 548-553.

Uemura, T., Ohkura, H., Adachi, Y., Morino, K., Shiozaki, K., & Yanagida, M. (1987). DNA topoisomerase II is required for condensation and separation of mitotic chromosomes in S. pombe. *Cell*, *50*(6), 917-925.

Uhlmann, F. (2016). SMC complexes: from DNA to chromosomes. *Nature Reviews Molecular Cell Biology*, *17*(7), 399.

Ussery, D. W. (2002). DNA Structure: A-, B-and Z-DNA Helix Families. Encyclopedia of Life Sciences.

Valenti, A., Perugino, G., D'amaro, A., Cacace, A., Napoli, A., Rossi, M., & Ciaramella, M. (2008). Dissection of reverse gyrase activities: insight into the evolution of a thermostable molecular machine. *Nucleic acids research*, *36*(14), 4587-4597.

Valenti, A., Perugino, G., Nohmi, T., Rossi, M., & Ciaramella, M. (2009). Inhibition of translesion DNA polymerase by archaeal reverse gyrase. *Nucleic acids research*, *37*(13), 4287-4295.

Valenti,A., De Felice,M., Perugino,G., Bizard,A., Nadal,M., Rossi,M. and Ciaramella,M. (2012) Synergic and Opposing Activities of Thermophilic RecQ-like Helicase and Topoisomerase 3 Proteins in Holliday Junction Processing and Replication Fork Stabilization. J Biol Chem, 287, 30282–30295.

Valjavec-Gratian, M., Henderson, T. A., & Hill, T. M. (2005). Tus-mediated arrest of DNA replication in Escherichia coli is modulated by DNA supercoiling. *Molecular microbiology*, *58*(3), 758-773.

Viard, T., & de la Tour, C. B. (2007). Type IA topoisomerases: a simple puzzle?. *Biochimie*, *89*(4), 456-467.

Viard, T., Cossard, R., Duguet, M., & de La Tour, C. B. (2004). Thermotoga maritima-Escherichia coli chimeric topoisomerases. Answers about involvement of the carboxyl-terminal domain in DNA topoisomerase I-mediated catalysis. *Journal of Biological Chemistry*, *279*(29), 30073-30080.

Viard, T., Lamour, V., Duguet, M., & de La Tour, C. B. (2001). Hyperthermophilic topoisomerase I from Thermotoga maritima. A very efficient enzyme that functions independently of zinc binding. *Journal of Biological Chemistry*, *276*(49), 46495-46503.

Vos, S. M., Tretter, E. M., Schmidt, B. H., & Berger, J. M. (2011). All tangled up: how cells direct, manage and exploit topoisomerase function. *Nature reviews Molecular cell biology*, *12*(12), 827.

Wang, A. H. J., Quigley, G. J., Kolpak, F. J., Crawford, J. L., Van Boom, J. H., van der Marel, G., & Rich, A. (1979). Molecular structure of a left-handed double helical DNA fragment at atomic resolution. *Nature*, *282*(5740), 680.

Wang, J. C. (1971). Interaction between DNA and an Escherichia coli protein ω. *Journal of molecular biology*, *55*(3), 523-IN16.

Wang, J. C. (1996). DNA topoisomerases. *Annual review of biochemistry, 65*(1), 635-692.

Wang, J. C. (2009). *Untangling the double helix: DNA entanglement and the action of the DNA topoisomerases* (Vol. 225). Cold Spring Harbor, NY: Cold Spring Harbor Laboratory Press.

Wang, J. C., & Davidson, N. (1966). On the probability of ring closure of lambda DNA. *Journal of molecular biology, 19*(2), 469-482.

Wendorff, T. J., & Berger, J. M. (2018). Topoisomerase VI senses and exploits both DNA crossings and bends to facilitate strand passage. *eLife*, *7*, e31724.

Whelan, D. R., Hiscox, T. J., Rood, J. I., Bambery, K. R., McNaughton, D., & Wood, B. R. (2014). Detection of an en masse and reversible B-to A-DNA conformational transition in prokaryotes in response to desiccation. *Journal of the Royal Society Interface*, *11*(97), 20140454.

White, J. H., & Bauer, W. R. (1987). Superhelical DNA with local substructures: A generalization of the topological constraint in terms of the intersection number and the ladder-like correspondence surface. *Journal of molecular biology*, *195*(1), 205-213.

Williamson, L. M., & Lees-Miller, S. P. (2010). Estrogen receptor α-mediated transcription induces cell cycle-dependent DNA double-strand breaks. *Carcinogenesis*, *32*(3), 279-285.

Witz, G., & Stasiak, A. (2009). DNA supercoiling and its role in DNA decatenation and unknotting. *Nucleic acids research*, *38*(7), 2119-2133.

Wood, B. R. (2016). The importance of hydration and DNA conformation in interpreting infrared spectra of cells and tissues. Chemical Society Reviews, 45(7), 1980-1998.

Wright, W. D., Shah, S. S., & Heyer, W. D. (2018). Homologous recombination and the repair of DNA double-strand breaks. *Journal of Biological Chemistry*, *293*(27), 10524-10535.

Wu, H. Y., Shyy, S., Wang, J. C., & Liu, L. F. (1988). Transcription generates positively and negatively supercoiled domains in the template. Cell, 53(3), 433-440.

Wu, L., & Hickson, I. D. (2001). RecQ helicases and topoisomerases: components of a conserved complex for the regulation of genetic recombination. *Cellular and Molecular Life Sciences CMLS*, *58*(7), 894-901.

Wu, L., & Hickson, I. D. (2003). The Bloom's syndrome helicase suppresses crossing over during homologous recombination. *Nature*, *426*(6968), 870.

Yang, X., Li, W., Prescott, E. D., Burden, S. J., & Wang, J. C. (2000). DNA topoisomerase IIβ and neural development. *Science*, *287*(5450), 131-134.

Zechiedrich, E. L., & Cozzarelli, N. R. (1995). Roles of topoisomerase IV and DNA gyrase in DNA unlinking during replication in Escherichia coli. *Genes & development*, *9*(22), 2859-2869.

Zechiedrich, E. L., Khodursky, A. B., Bachellier, S., Schneider, R., Chen, D., Lilley, D. M., & Cozzarelli, N. R. (2000). Roles of topoisomerases in maintaining steady-state DNA supercoiling in Escherichia coli. *Journal of Biological Chemistry*, *275*(11), 8103-8113.

Zhang, Z., Cheng, B., & Tse-Dinh, Y. C. (2011). Crystal structure of a covalent intermediate in DNA cleavage and rejoining by Escherichia coli DNA topoisomerase I. *Proceedings of the National Academy of Sciences*, *108*(17), 6939-6944.

Zhou, Q., Li, T., & Price, D. H. (2012). RNA polymerase II elongation control. *Annual review of biochemistry*, 81, 119-143.

Acknowledgments

I would first like to thank my supervisor Dr. M. Nadal and Lab leader Dr. T.R. Strick for their invaluable guidance on my research project. My Ph.D. projects are based on their cooperation to study DNA topoisomerases by using single-molecule assays. I learned a lot from their wide knowledge of both research background and methodology, and benefited from their brilliant ideas and proposals to solve my research problems. Dr. Nadal read my thesis manuscript carefully and provided me plenty of useful suggestions.

I would also like to thank all the lab members for all of their assistance and collaboration.

I would like to thank the China Scholarship Council for its financial support.

Finally, I would like to thank my parents for their selfless love and support since my birth.